Università degli Studi di Ferrara

DOCTORAL COURSE IN
"Earth and Marine Sciences" (EMAS)

CYCLE XXXII

DIRECTOR Prof. Massimo COLTORTI

INNOVATIVE REA TOOLS FOR SEABED MAPPING

Scientific/Disciplinary Sector (SDS) GEO-02

Candidate

Dott. Maurizio Demarte

Supervisor

Prof. Roberta Ivaldi

Prof. Paolo Ciavola

Years 2016/2019

Università degli Studi di Ferrara

DOCTORAL COURSE IN
"Earth and Marine Sciences" (EMAS)

CYCLE XXXII

DIRECTOR Prof. Massimo COLTORTI

INNOVATIVE REA TOOLS FOR SEABED MAPPING

Scientific/Disciplinary Sector (SDS) GEO-02

Candidate

Dott. Maurizio Demarte

_____
(signature)

Supervisor

Prof. Roberta Ivaldi

_____
(signature)

Prof. Paolo Ciavola

_____
(signature)

Years 2016/2019

Summary

List of figures

List of tables

Introduction

The acronym REA (Rapid Environmental Assessment) outlines the ability of acquiring environmental information and, subsequently, processing and valorising in the shortest possible timeframe, in order to comply with specific demands that require minimal intervention times.
There are different events that can relate to such critical conditions. In the marine sector, REA interventions are contemplated when there is the need to characterize areas which are the location of marine incidents, sites for emergency operations following natural disaster or for the direct and indirect consequences of incidents. The methodology varies depending on the distance from the coast and on whether there are sites of natural or cultural interest nearby; however, such sites are almost always present in coastal areas or in shallow water.
Therefore, in such terms, the REA activity can then be conducted in the open sea and regards numeric data models for circulation or transportation of materials, lost substances and the search for objects on the seabed. Furthermore, it can also be applied to the coastline, thus to the Shallow Waters, where the activities that requires the usage of REA can range from environmental/humanitarian emergencies to exceptional events, activities which are all characterized by the need for a quick intervention (Bush et al, 1999; Kelly, 2005 – http://www.unhcr.org). Hence, the Rapid Environmental Assessment is expressed in the ability to react immediately to certain events, often basing the operations on very limited data and gaining a strategic importance under various points of view, sometimes anticipating even the stages of planning and management of the subsequent actions.
The dynamicity of the marine environment, whether it is coastal or in open sea, requires an equally dynamic response in the overall evaluation of the case. It is of primary importance to standardize the executive methodologies during data acquisition, processing and, above all, in the restitution of the final product, especially for what concerns formatting, unit of measurement and reported information. The marine environment, naturally dynamic, complex and fragile, has many peculiarities. It is a system which is necessarily sensitive to the variation of natural processes, but also to the increasing of anthropic pressure, such as the change in the usage of the littoral area, the reduction of the resources, the destabilization of the ecosystems and, finally, the growing phenomenon of tourism and the relative industrialization that is involved in the process.
The marine environment, according to what has been outlined so far, highlights all the complexities of a REA and underlines since the very beginning the need for a multidisciplinary approach, which has to be pinpointed in time alongside a study of the specific context. In all of this, the spatial and temporal variability in the parameters of interest is so high that the absence of a standardization in the acquisition process or, nonetheless, the lack of certifications for the equipment in use, would endanger and void the complex work of data collection and, consequently, the final result. The conducted study is aimed to research methodologies of data collection, no matter if they are purely geophysical or geospatial, exploring new frontiers in terms of vectors and instrumentation to utilise, but also exploring different methods of planning for the various stages of the project. For such activity, the formative periods among different academic institutions have been very helpful, just

like the availability of new vectors and technologically advanced solutions provided by the partners of the Arctic marine geophysical campaign High North17 (Ivaldi et al. 2017), part of the program HIGH NORTH, the Italian Navy multidisciplinary research program, started in 2017 and carry-on in 2018 and 2019.

The combined integration of different disciplines and equipment was particularly interesting in order to return a mapping of the entire investigated volume, achieving a three-dimensional mapping from the atmosphere, through the surface and water column, till the seabed and the first substrate. The equipment of interest was focused on autonomous instruments, both underwater and aerial, upon the development of the new potentialities of the acoustic tools, alongside the study of semi-automatic methodologies for the characterization of the seafloor and, finally, upon a valorization of the historical information from the available Multibeam Echo Sounder data.

Such activities require a constant updating of the instrumentation, which is not only devoted to maximize the potentiality and the field of intervention, but also and especially to limit the timing for data acquisition, processing, analysis and for returning the final product.

Therefore, the development of Maritime REA are crucial towards the efficacy of the decisional process with particular acquisition techniques and methodologies, in support to institutions and authorities that need to approve and decide policies in the immediate term.

1. Conceptualization of Rapid Environmental Assessment (REA)

1.1. Generality

The Rapid Environmental Assessment procedure is addressed to provide a quick and sufficiently accurate response in support to various activities that can take place in any sector of the marine, oceanic, coastal and port environment. Such tasks aim at responding efficiently to operative evaluation requests in situations where the available information is often very limited. Thus, REA assumes a strategic importance, especially for what concerns the temporal evaluation of the response time.

The above-mentioned notion of "sufficiently accurate" will be examined more in detail later in the dissertation, and it will be shown that it acts as the discriminatory element to assess the efficiency of a project, survey or research within a limited time-frame.

REA was conceived as an instrument to quickly evaluate and manage environmental issues at their initial stages. REA operations are run according to a succession of data analysis, based on a semi-quantitative approach. REA's process and structure take into account that whoever will be in charge of responding to the calamity/natural event may not necessarily be a specialist, often has little time to conduct detailed researches and, very frequently, has a limited equipment (Asian Development Bank, 2003; Kelly, 2005).

In this context, REA is a very compatible instrument with a dynamic, complex, vulnerable and fragile system such as the marine-coastal environment. The knowledge and the observation of phenomenon that take place in a limited time-frame, require a multidisciplinary approach based upon high-quality data, which have to be acquired with extreme accuracy through standardized methodologies, following a suitable elaboration process. Hence, it is possible to see why quick evaluation strategies in support to operations and emergency management in a marine context get so much attention.

Different techniques are present in the literature to characterize and monitor the littoral dynamics and the coastal area (Ivaldi et al., 2009; kasalos and Chayes, 1983; Monterale-Gavazz et al., 2017). These zones highlight the need to develop cognitive tools for rapid environmental assessment, particularly in conditions of exceptional events, natural disaster or human interventions.

Indeed, operating in this environment generates the need to develop fact-finding tools for rapid environmental evaluation within particular conditions, such as a coastal sector impacted by an extraordinary event, beach erosion or subject to anthropic interventions with particular support actions.

1.2. REA activity and procedure

REA is a combination of instruments that permit to identify, define and, finally, prioritize the interventions in the eventuality that human lives or the environment are threatened

and, generally, in an optic to minimize the effects of a calamity (Asian Development Bank, 2003).

Taking what has been outlined above into consideration, a quick REA type characterization will need to be:

- easy to enact and quick in its execution;
- thought and designed for the usage in the event of natural, technological and/or geo/political emergencies;
- be quick and efficient in sharing the available environmental information, in particular towards the designed authorities responsible of deploying countermeasures in regards to the occurred events.

Decisions will have to be taken in a quickly manner and, very often, waiting for more detailed information or for an accurate assessment of the situation will not be an option. Hence, decisions will have to be taken drawing upon data that is considered to be "sufficiently accurate", following a time/benefit review. (Demarte et al., 2009).

REA procedure

In case of a calamitous event, where the intervention will have to be coordinated at civil protection level, with the involvement of several entities and ministers, the organization of a REA analysis will have to be very clear to the concerned people. Generally, there are be 4 main phases and each one of them will have tasks that will have to be accomplished in a coordinated manner (Kelly, 2005).

In detail, the 4 phases will consist in Organization Level Assessment, Community Level Assessment, Consolidation and Analysis and Green Review of Relief Procurement.

Organization Level Assessment : the organization will have to assess the situation focusing on the environmental issues, trying to adopt the widest possible scope. For example, it will be necessary to investigate the event taking into consideration the point of view of the government, the process to action the rescue services, the reconstruction plan and, finally, the return to the original conditions.

In the same way, it will be crucial to coordinate the support of Non Governative Organizations (NGO) involved in the first aid. This phase is divided into 5 different tasks, each one of which will be explored in detail.

Task 1: Context statement, a briefing on the environmental situation, the anthropic elements in the site and on the impact that the calamity had on the area.

Task 2: Factors influencing environmental impacts, namely an analysis of the social, cultural economical and geographical factors that can have either a direct or an indirect impact on the population.

Task 3: Environmental Threats of Disasters, the consequences of the event will undergo through a review, assessing the short-term impact on sustainment sources (such as agriculture, tourism, etc.) or the loss of routes of communication.

Task 4: Unmet Basic Needs, representing the analysis and the evaluation of the primary needs of the affected population.

Task 5: Negative Environmental Consequences of Relief Activities, which aims at individuating those potential interventions that might have negative consequences on the environment (e.g. the use of too much plastic without the presence of an adequate collection and recycling system).

Community Level Assessment: the organization will have to identify the priorities of the rescue services for what concerns the affected population, in order to minimize the disruptions and optimize the rescue operations. Information to achieve and support such objectives will be collected either through the population on site or through secondary sources.

Consolidation and Analysis: in this phase, the coordination of the REA activity will need to analyse and consolidate the data acquired in the two previous phases. The objective will be to prioritize the intervention activity and compile a succession of measures that, on one hand, considers the findings of the 5 previous tasks and, on the other hand, valorizes the needs (or the perception of the needs) of the community. Such needs can be, for example, preventing further life-threatening situations, the wellbeing of the community whilst respecting the environment.

Green Review of Relief Procurement, this last phase is perhaps the most delicate one. Its aim is to incentive and support a "green" management of the rescue operations (e.g. the reduction of waste produced by the rescuers, taking care the energy efficiency of rescue ships and equipment). Moreover, it is necessary to be careful about the commodities brought by the rescue services. For example, the infrastructure facility, which are necessary for the first phase of interventions, can easily become an unsustainable activity in the future, under both an environmental and an economical point of view.

Specialistic Geographical, Meteorological and OCeanographic (Geo-MetOc) support to the REA activities following natural calamities

REA interventions aimed at characterizing an area after a natural disaster are contextualized giving priority to the first phase, for organizational assessment, as outlined in the previous paragraph. The Geo-MetOc process, supporting the REA activities, will contextualize the ongoing environmental situation, provide an analysis to identify the changes brought by the event and a further analysis to understand the consequences of such changes and variations (Demarte et al., 2009; Bush et al., 1999).

All of these actions are part of the first three tasks belonging to the first phase of intervention. Remaining in a marine environment, there are several cases in which Geo-MetOc support has been relevant to support REA activities, the most recent one is the partial sinking of the cruise ship Concordia, owned by the Costa company, which was transporting 4228 people on 13th January 2012. Immediately after the accident and the arrival of the first rescuers, strategic actions to characterize the area were being planned. In particular, the potential areas of particular sensitivity were individuated, mapped with an integrated High Resolution survey with MBES (Figure 1 and Figure 2) and a research was subsequently undertaken in order to locate features anomalies. Furthermore, different

oceanographic models for polluting elements (Figure 3) were activate, in order to study the possible trajectory of eventual leaks of oil, lubricants and hydrocarbons.

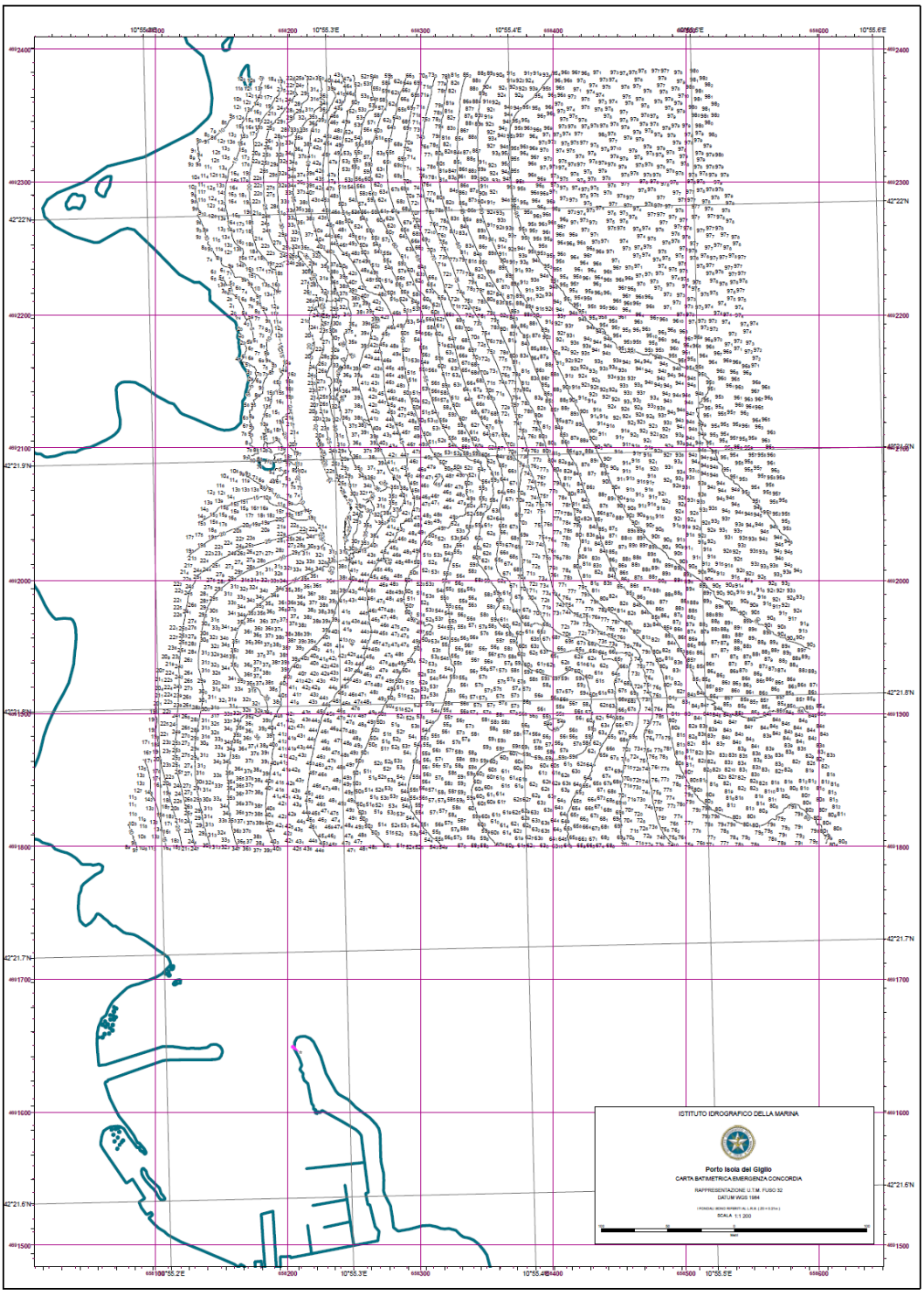

Figure 1 Example of REA activity – Porto Isola del Giglio – Bathymetric chart – Costa Concordia Emergency (from Italian Hydrographic Office)

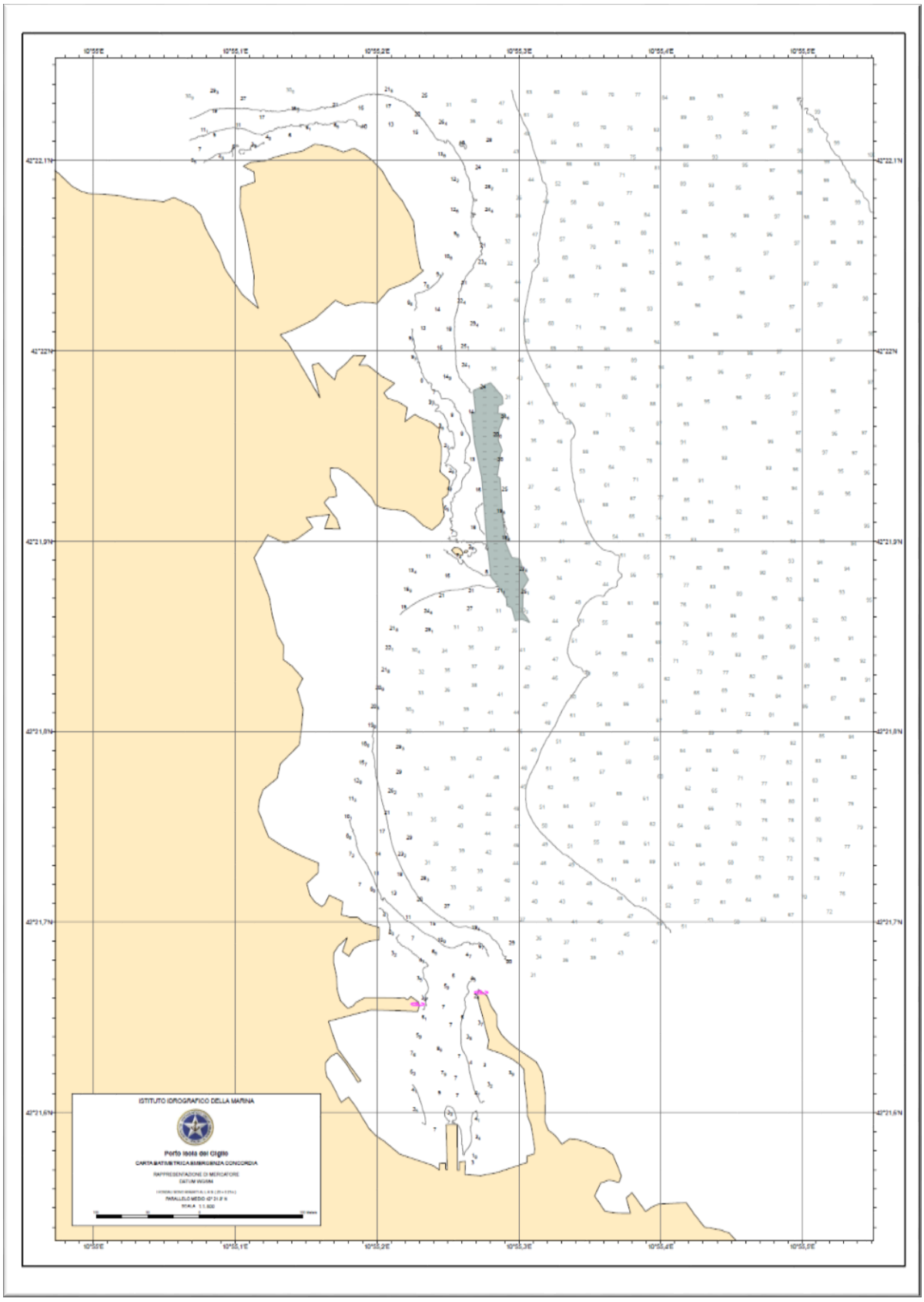

Figure 2 Example of REA activity – Porto Isola del Giglio – Bathymetric chart – Costa Concordia Emergency (from Italian Hydrographic Office)

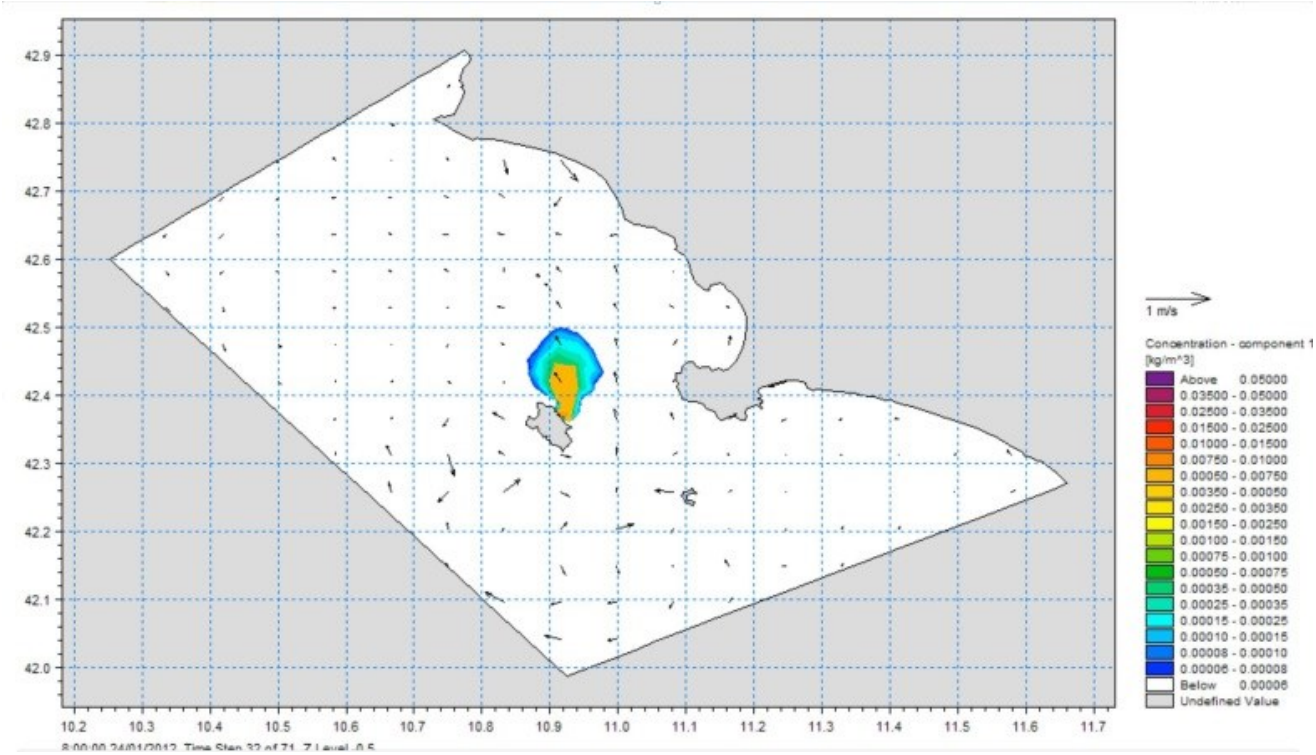

Figure 3 Example of REA activity - Costa Concordia - oil spill simulation

1.3. Concept of REA in the geopolitical, humanitarian and military interventions

The evolution in the global strategic scene, particularly within the Mediterranean Sea and the Indian Ocean, has seen the participation of military forces in support to emergencies related to political instabilities over the past years. Furthermore, such emergencies have taken place outside normal work areas and, additionally, with a limited temporal notice.

The REA activities in response to geo-strategical needs, international crises or humanitarian operations have been often undertaken in new or less known operative contexts, devoting particular attention to the environmental factor.

Hence, the Geo-MetOc support to rescue vehicles and ships (which are usually aeronaval) has been re-evaluated and in terms of knowledge of the intervention area and for the exploitation of the environmental conditions. This is particularly true for what concerns the littoral areas, where the issues brought by the open sea are accentuated by the strong variability imposed by shallow water and coastal areas.

Thus, a prompt and accurate knowledge of the Geo-MetOc kind of information, enables the coordinator of the rescue activities to have a higher degree of flexibility and efficiency in the management of the resources. This implicates remarkable advantages for what concerns the interactions with both environmental elements and enemy forces, this last one providing that the operations take place in a hostile area. The activity of environmental data acquisition and the subsequent evaluation of such data translated in impact matrixes on the operations is thus defined REA. Hence, the cell of support that ensures the

performance of the REA activity has the role of producing or collaborating to the production of a picture that represents, at the highest possible definition, the environmental situation that interests the operative area, with the aim of supporting the wide range of means and assets available.
It is important to remember that the timing factor plays a crucial role in the definition of "sufficiently accurate" to allow the performance of the planned activity (Kelly, 2005; NATO MILOC handbook, 2014).

Operative concept of REA activity

In operations like the above-mentioned one, the planning and the organization of a process of pre-set activities is essential to successfully accomplish the operations.
Again, the time factor plays a fundamental role in the REA activities, either it is of support/rescue consequently to natural/anthropic disasters or it is aimed to evacuate the population from a critical area or to provide a prompt intervention.
Thus, the elements that characterize an operational REA activity are the following:

- a quick and integrated environmental characterization
- the deployment of cutting-edge technological solutions
- the coordination of the activities, with a major effort aimed at data collection and at the verification of the information stream.

The activation of a REA cell for a Geo-MetOc support can derive from different circumstances. Some of them can be triggered by geopolitical instabilities or by periods antecedent to international crises. Generally, the activation criterion and the deployment methodology is mainly based on the phases:

- data acquisition: this phase includes, depending on the intervention's timescale, different methods. The first step will be consulting databases and a recent bibliography, provided there is enough time for that. Remote acquisitions (satellite, aerial, naval, underwater vectors, including unmanned vehicles) and, in some cases, for hostile areas with a lack of information, specialist personnel undercover are deployed;
- analysis and data processing for the generation of operational products: the area's assets are not always able to host assets with complex computing capacity or, regardless, to host specialized staff. Hence, data assimilation, analysis, modelling and data fusion will be managed from ground-based specialized personnel, in a condition of relative comfort. Data transmission capacity has a strategic importance in this instance (Demarte et al., 2008; Ivaldi et al., 2009)
- dissemination of operational products: the final user of the finished product of a REA cell can be either a set of multiple operative cells/units or a single complex unit focused on the scene of action in an operative control room. In both cases, the product, following certain rigorous scientific canons, will have to be wisely packaged in an intelligible and user-friendly manner, in order to make it accessible also for a staff that does not have technical skills. Furthermore, it will have to be easily transposable element on different platforms used for its representation.

1.4. Organization of the REA support

In the following paragraph, it will be shown what the REA organization is and to who are distributed the various tasks that were outlined during the explanation of the methodological approach. An organization for a naval activity has been selected as a case study, bearing in mind that the same organization is used, with different terminology, for civil protection or humanitarian assistance, both in and out the national borders

The REA organization within a national environment is constituted by

- REA Coordination Centre (REA-CC), which is responsible for:
  - coordinating assets, instrumentation, and personal for data collection needed for REA activity;
  - coordinating the acquisition, the elaboration and the exchange of data and products
  - coordinating the support units Geo-MetOc on the sites of the departments involved
  - inputting the validated products in safe data sharing networks.
- REA Support Centre (REA-SC), which comprises all the national operative authorities that are involved in the valorisation and in the processing of environmental data (geographic, meteorological and oceanographic data). They are in charge of:
  - gathering the observed data;
  - run the high definition numerical models for the elaboration of major scale forecasts;
  - they are the developers and the primary users of specialistic software, named TDA (Tactical Decision Aids), deployed on the field by the final users to help in the interpretation of the information or to valorise in a standardised manner different environmental variables. Generally, in such instances, thanks to known impact matrixes, quick and easy readable traffic light maps are produced (Figure 4);

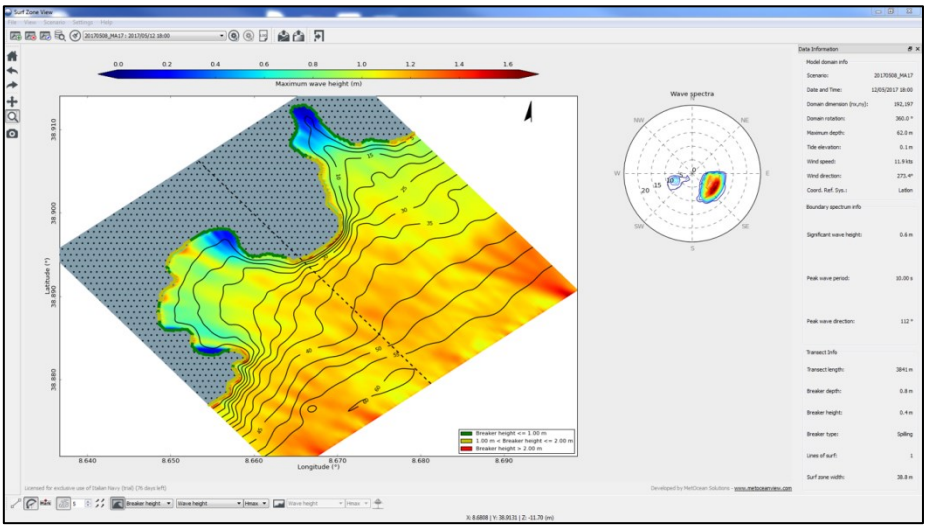

Figure 4 Example of breaking wave traffic light information and maximum wave - (Surf Zone Tactical Decision Aid).

  - they combine the observations and the elaboration of the models in specific "packages", diversified for the different needs of each activity;

- they interface with the REA-CC for the dissemination of the packages through WPN networks.

Net Centric: it ensures the dissemination of the information at the sites of action and in the operative rooms, providing the decision makers with the environmental situation of the area of interest.

Within a national context, the organizational structure for a REA kind of activity can be schematized by putting at the centre the REA Coordination Centre, which is responsible for coordinating the activities of data collection, dispatching and reception of elaborated data and, finally, for wrapping the data packages/environmental information, tailored on the needs of the final user (Figure 5).

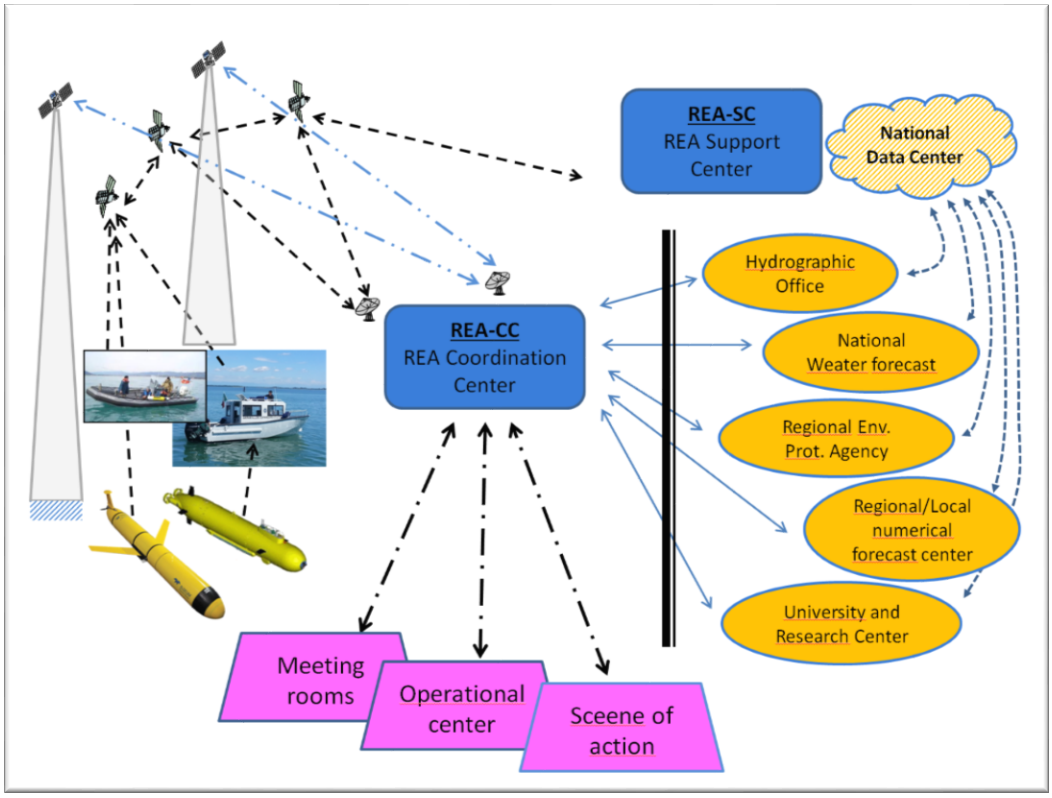

Figure 5 REA scheme organization (from NATO - MCM-051-00, 2000)

2. Acoustic 3D mapping

2.1. Acoustic seafloor mapping overview

While the primary usage of a sonar in a marine environment was aimed at determining the water depth, the necessity to localize and acquire images of the seabed brought to the developments of the Side Scan Sonar (SSS). Such system is capable to map even smaller objects on the seabed, providing their location and classification. The studies regarding the acoustic transducer, the development of the piezoelectric materials and the designing of the arrays, shortly led to the ability of transmitting a sequence of impulses, fan-shaped, through a relatively wide area of the seabed. At the very beginning, the major issue faced by this technology were the analogical recorders on thermal paper. The first SSS systems would produce a width-modulated image drawing on the signal of acoustic return, varying in function of the time of transit all the way down to the seabed. These first recording were not calibrated, though generally they would include a loss compensation due to the geometrical diffusion. The analysis of the image was often difficult for what concerned the seabed. while the evaluation of the geometrical shapes turned out to be easier. In fact, the identification of objects or natural/anthropic structures, was particularly facilitated by the instrument which would “fly” close to the seabed. This concept, called shadow-graph, has been successfully used for several years, to identify smaller objects (e.g. mines) (Fish and Carr, 2001), and it is still used to locate objects laying on the seabed. The first studies were focusing on the high-frequency SSS systems, specifically used to get the maximum spatial resolution on the seabed, which is necessary for the determination of the smaller objects, hence limiting the extension of the search area. As a countermeasure, SSS for deep surveys were developed, also because the necessity of surveying deep sea and larger objects arised. These newer SSS were equipped by low-frequency transmitter and towed by the ship (Spiess, 1980; Tyce, 1986). Originally, the development was pushed by the advancements in the military sector, but subsequently, marine geology studies contributed to the birth of such technology, allowing the identification and the mapping, on a larger scale, of consistent geological structures. (Rusby and Somers, 1977; Kasalos and Chayes, 1983). The progresses in the electrical field and the developments in the designing of the acoustic transducer in the capability of analysis of the acoustic signal, in the precision of the positioning in the navigation, in the graphic representation of the results, the spatial resolution and the wide range of acoustic instrumentation and multi-frequences capability led to finished products with higher resolutions. Products with the capability of compensating the backscatter images produced by the SSS more appropriately, in regards to the geometrical distortions and to the production of mosaic images (composed georeferenced images of the backscatter). Therefore, the acoustic images began to offer a more realistic and coherent overview of the seabed, extending the usage of the backscatter’s data to geological, engineering and environmental studies, where information about the seabed would be fundamental. The relationship between

backscatter and typology of seabed, derived by the SSS, depends on the acquisition of the ground truth and by the personal expertise of the technician who will compare the acoustic response with the samples. In the best scenario, such studies used to be qualitative, as the backscatter returned by the SSS was not calibrated in regards to the inbound and outbound signals (relative or absolute value), and it would assume that the seabed was flat and homogenous. However, despite these limitations, it was possible to gain much precious information by the different signals, the medium levels of backscatter and by the possibility of isolating regions with a different texture (in the stage of image study). Alongside the above-mentioned improvements, there have been different techniques that have radically changed the nature of seabed mapping. The usage of more arrays of sonar transducer with lateral scan and interferometric elaboration or phase measurement furthermore allowed to determine the bathymetry alongside the backscatter.

The major change arrived with the new century, when the MultiBeam Echo Sounder (MBES) became a widespread instrumentation expert/technician. The MBES transmits with the same geometry of a SSS, but it is able to receive the seafloor backscatter's return signal from a series of narrow formed beams and thus allows the determination of both depth across the swath and the recording of the backscatter time series at known angles across the swath. With the introduction of MBES and the ability to measure the backscatter as a function of true angle of insonification across the seafloor came a new recogniction of the potential to use backscatter measurements as a means to remotely characterize the properties of the seafloor. An improved theoretical understanding of the interaction of sound with the seafloor (Jackson and Richardson, 2007) indicated the angular dependence of backscatter as a key parameter in identifying seafloor type and opened the door to more quantitative analyses of MBES backscatter (Hughes et al., 1997; Fonseca and Mayer, 2007; Lurton, et al., 2010). Further software and hardware improvements of the MBES, such as a better compensation of the ship's movement, a higher spatial and angular resolution and, most importantly, a greater bandwidth, were the pillars to efficiently face the quantitative side of the backscatter. Thus, a quantitative approach has a great usage in any field of marine searching and for military, geological, engineering and environmental applications. The guidelines of this PhD research have now been outlined. With such premises, we start to analyze the backscatter signal and the MBES data, in order to fully understand the nature of the data produced by our sensing system, and relate them with a robust seafloor characterization (Lurton and Lamarque, 2015).

2.2. Underwater acoustic principles

This section will cover the basic elements of sound generation and propagation of the underwater sound. We are going to introduce the physical phenomena causing seafloor backscatter measured with echosounders, then, from the sonar equation and definition of terms, relevant for echosounding, we arrive to describe how the echosounding system works and, finally, the physical causes of seafloor acoustic scattering.

The fundamental principle of sonar measurement is related to the propagation of acoustic waves in water. The first effect of propagation is the range of the signal's amplitude, due to the geometric effects and also to the absorption; it is a determining factor in the propagation of acoustic waves, limiting their range, mainly at high frequencies. The estimation of propagation defects is an important factor in the evaluation of the sonar systems performances. This is the way in which the propagation of a signal is often accompanied by a series of multiple paths generated by unwanted reflections on sea surface and seabed interfaces. The celerity of acoustic waves varies spatially in the ocean, especially with depth, due to temperature and pressure constraints. The paths of the sound waves are thus deviated, depending on the variations in celerity encountered, and naturally it complicates the modeling and interpretation of the spatial structure of the sound field. The simplest and most efficient modeling technique uses geometric acoustics, which relates the local values of the direction and celerity of wave propagation (Snell-Descartes law).

The acoustic waves comes from the propagation of a mechanical perturbation. Local compressions and dilatations are transmitted from one point to the surrounding points, by means of the elastic properties of the propagation medium. From one point to another, this perturbation will spread far from its source. The rate of propagation of this perturbation in the medium is called *celerity of sound* or simply *celerity* (Weber and Lurton, 2015).

If the propagation (Figure 6) takes place only along a spatial dimension x, it can be written for a perturbation s (x, t) the conditions [1]:

$$s\,(x_1, t_1) = s(x_2, t_2) = s(x_3, t_3) = \cdots = s(x_n, t_n) \qquad [1]$$

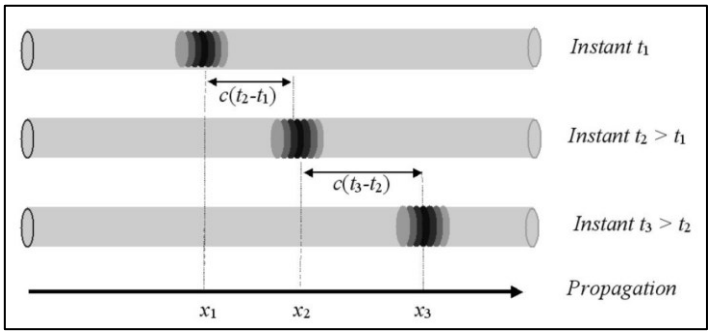

Figure 6 One-dimensional propagation of a localized overpressure in a cylindrical waveguide, as function of time (from Lurton, 2010)

The observation times t_1, t_2, ... are connected to the positions x_1, x_2, ... and to the propagation celerity c [2],

$$\begin{cases} x_2 - x_1 = c\,(t_2 - t_1) \\ x_3 - x_2 = c\,(t_3 - t_2) \\ \qquad\qquad \dots \\ x_n - x_{n-1} = c\,(t_n - t_{n-1}) \end{cases} \qquad [2]$$

The mechanical properties of this mean support the local value of the celerity of sound. The acoustic wave is characterized by the amplitude of the local movement of each particle in the propagation medium around its equilibrium position; from the velocity of the fluid corresponding to this movement and from the resulting acoustic pressure, which is the variation, around the average hydrostatic pressure, caused by the compressions - local dilatations, imposed by the particular movement (Lurton, 2010).

The velocity of propagation of an acoustic wave [3] is determined by the characteristics of the local propagation medium: the density and the modulus of elasticity E (or, for a fluid, its inverse quantity the compressibility X):

$$\mathrm{c} = \sqrt{\frac{\mathrm{E}}{\rho}} = \sqrt{\frac{1}{\mathrm{X}\rho}} \qquad [3]$$

In sea water, the celerity of the acoustic wave is close to c=1500 m/s function of pressure, salinity and temperature.

The density of sea water is approximately ρ=1025 kg/m^3 on average, depending on the same physical parameters.

In a marine sediment the density range is between 1200 and 2000 kg/m^3. In a sediment saturated with water (where velocity is proportional to the celerity of sound of interstitial water), the sound speed typically ranges between 1500 and 2000 m/s.

The acoustic signals usually vibrate around their quite positions. The frequencies used in underwater acoustics vary approximately from 10Hz to 1MHz, depending on the application (i.e. periods from 0.1s to 1µs). The wavelength is the spatial correspondent of the periodicity of time T. It is the elementary spacing between two points in the middle, undergoing the same state of vibration with a delay of T, or displacement of 2π. Said differently [4], this is the distance made by the wave during a period of the signal with speed c.

$$\lambda = cT = \frac{c}{f} \qquad [4]$$

For a sound speed of 1500 m/s, the underwater acoustic wavelengths will be 150m at 10Hz, 1.5m at 1kHz and 0.0015m at 1MHz.

Underlying the propagation of sound is a number of basic equations of physics (Ulrick, 1983). The “sonar equation” is an estimation of the expected signal-to-noise ratios for sonar (SOund Navigation And Ranging) systems.

The signal-to-noise ratio determines whether or not a sonar will be able to detect a signal in the presence of background noise (natural or anthropic).

It takes into account different parameters as source level, sound spreading, sound absorption, reflection losses, ambient noise, and receiver characteristics. The sonar parameters represent the diverse effects in underwater sound propagation and can be divided as follows (Lurton X., 2010):

- Instrumental:
  - SL (Source Level) – in underwater dB one meter from the souse
  - NL (Self-Noise Level)
  - DI (Directivity Index)
  - DT (Detection Threshold).
- Medium:
  - TL (Transmission Loss)
  - RL (Reverberation Level)
  - NL (Ambient Noice Level)
- Target:
  - TS (Target Strength)
  - SL (Target Source Level)

The relationship between sonar parameters, the effect of medium, the equipment and target, are described by the sonar equation.

If SL is produced by the transducer at unit distance on its axis. SL-TL will be the source level once it reaches the target, the source level reduced by the transmission loss TL - traveling toward the target, due to spreading and absorption, the reduction in signal intensity is called transmission loss - TL.

The intensity of the echo, one meter from the target, relative to the intensity of the sound hitting the target is called the target strength - TS, given in decibel.

The target strength, TS [5], is used to describe how much of the sound wave is redirected, relative to how much got to the target in the first place:

$$TS = 10\log_{10}\left[\frac{I_S}{I_i}\right] \qquad [5]$$

Where I_i is the incident intensity at the target and I_s is the scattered intensity in the direction of the receiver and at a reference distance of 1m from the target. In general, the scattered intensity depends on the characteristics of the target as well as the sound wave itself. For a given target, I_s can change depending on the sonar frequency, the orientation between the target and both the incident and reflected wave, the length of the sonar pulse, and other property of acoustic projector, receiver, and target.

SL-TL + TS –TL will be the echo level EL, which returns to the transducer, the source level reduced by the transmission loss TL, reflected by the target strength and reduced again by the transmission loss TL. Thus the echo level at the transducer is SL – 2TL + TS.

The echo level will be further affected by the background effect. It can be considered as noice or reverberation. In case of noise, NL is isotropic noise.

NL – DI is isotropic noise reduced by the directivity index DI of the transducer acting as the receiver. In the case of reverberation, NL – DI will be replaced by an equivalent plane-wave reverberation level RL. At the transducer terminals, the echo-to-noise ratio is thus (SL – 2TL + TS) – (NL – DI). The detection threshold DT (Figure 7) equal the signal-to-noise ratio when the target is just being detected.

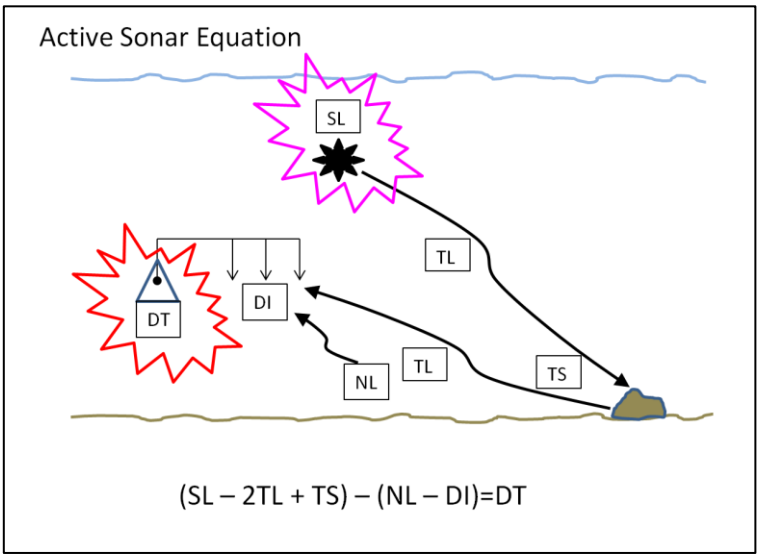

Figure 7 Detection Threshold: the detection threshold DT is equal to the signal–to–noise ratio when the target is just being detected (SL – 2TL + TS) – (NL – DI) = DT.

Another form of the active sonar equation [6] with a more convenient arrangement is:

$$SL - 2TL + TS = NL - DI + DT \qquad [6]$$

After interacting with the seafloor, a portion of the scattered wave propagates back toward the target (backscatter), experiencing the same type of spreading and absorption losses as on the way to the target. The received intensity can be described as an echo from the target, which in decibel notation is referred to as the echo level, EL (Ulrick, 1983; Lurton, 2010).

The echo level quantifies the sound-wave that we are typically interested in measuring. However, the target echo is not the only sound-wave to be received. When we measure the echo level, we are often confounded by unwanted acoustic waves, that we refer to globally as noise:

- ambient noise (ship traffic, bursting bubbles under breaking waves, marine animals);
- self-noise (platform, sonar it-self);

- reverberation (sound wave projected that scatters from objects we are not interested in).

It is assumed here that the echo level is sufficiently so that noise level is negligible (Ulrick, 1983). While it is useful to think of the sonar equation in terms of the echo level observed at the receiver, the quantity relevant to acoustic backscatter from the seafloor is the target strength (TS) which includes a combination of effects related to the sonar and to the target. The nature of this combination is dependent on the morphological characteristics of the target (size, shape and material) and characteristics of the sonar (mainly frequency and angular orientation).

The simplest TS scenario is that of a discrete target (i.e. small compared with the sonar beam and pulse length). It is often the case that the targets extent throughout a volume defined by the sonar beam and pulse length. For example, if the echo was returned from a large aggregation of fish or gas bubbles, in the water origin from an hydrothermal activity, then TS could be considered as the incoherent sum of the individual echoes from the fishes present inside an instantaneously active volume (Lurton and Lamarche, 2015).

The target acts as secondary source retransmitting the acoustic wave. The TS is the ratio between the intensity sent by the target back to towards the transmitter and the incident intensity. It is therefore the relative amount of energy sent back by the target towards the sonar. It depends on the physical nature of the target towards the sonar. It depends on the physical nature of the target, its external (angle and frequency). The intensity EL (Echo Level) [7] of the echo received by the sonar system after backscattering is:

$$EL = SL - 2TL + TS \qquad [7]$$

where SL is the level transmitted by the source, TL is the transmission loss (counted twice, one in the way in, once in the way back).

Two types of target can be envisaged. First there are target with dimensions small enough to be completely insonified by the sonar beam and signal. They behave as points: their strength is an intrinsic strength, independent of the distance to the sonar or its characteristics. On the contrary, other targets may be too large to be insonified completely at once by the same beam (e.g. seabed surface, large fish shools, etc.). The strengths of these large targets depend on their geometric intersection with the sound beam. The TS is no longer a point value but uses the insonified space (surface or volume), associated with a surface or volume backscatter coefficient (Lurton, 2010).

2.3. Backatter basic concept

An acoustic wave that propagates in the ocean and impact with obstacles in the same column of water (fish, plankton, bubbles, submarines) or within the limits of the medium (bottom and surface of the sea), return some echoes of the transmitted signal to the sonar system. These echoes will either be expected (if the obstacle is the desired goal) or

undesirable (if they interfere with the useful signal). In all cases, understanding their properties is essential for the proper functioning of the sonar system: because they must be received in the best possible conditions, they must be reduced or filtered as much as possible, or, finally, for data post-processing in order to recover physically significant information.

Several distinct physical processes are contributing to the formation of underwater acoustic echoes. The geometric propagation and the description of the multipath are associated with the well-known and rather intuitive reflection of aerial interfaces: the incident wave is reflected in a direction symmetrical to its direction of arrival (similar light in a mirror), with a loss of amplitude. The study of reflection phenomena is therefore particularly useful for submarine acoustic systems in which the transmitter and the receiver are distinct (data transmitters, multistatic sonar or seismic systems) and/or for configurations in which the propagation between the sonar and the objective is inclined to generate more echoes (when the propagation paths are close to the horizontal).

Contrary to reflections from the bottom and the surface, different types of echoes are generated by local obstacles in the water column or in the interfaces. Based on their shape and size, these irregularities spread acoustic energy in all directions and are therefore more likely to influence the signals received in any configuration. The dispersion of acoustic energy towards the sonar is called backscattering. The operating principle of most sonar systems is based on backscattered echoes.

The concept of reverberation, used in the active sonar context, summarizes all the returns of the signal echoes towards the sonar system, coming from other sources than the desired target (Ulrik, 1983; Jackson and Richardson, 2007; Lurton, 2010).

The reverberation of the surface and the background (contour effects due to the back scatter of the sound from the roughness of the interface) are traditionally distinct from the reverberation of the volume (effects of the volume in the water column, due to the dispersion of fish, plankton, suspended particles or clouds of bubbles). The distinction between target echo and reverberation is, of course, purely conventional since it is not linked to different physical phenomena and depends only on the type of system considered.

In order to model the backscattered echoes, two categories of objectives have to be defined. First of all, the objectives are sufficiently reduced in size to be completely insonified "simultaneously" by the radius of the acoustic signal. They behave like punctual sources: their backscatter strength is an intrinsic characteristic, independent on the distance from the sonar or on its characteristics (beamwidth, duration of the signal), provided that the assumption of the punctual form is respected.

In contrast, the other targets are too large to be completely insonated at the same time from the same radius (eg. Large branches of fish, seabed or sea surface). The strengths of these objectives will depend on their geometric interception by the sound beam. The target force is no longer a point value, but depends on space (surface or volume), associated with a surface or unit backscatter coefficient. The latter is, therefore, an expression of the

amount of energy dispersed by a dispersion element of the spatial unit, therefore considered in dB per m^2 or dB per m^3, respectively. The back-scattering force depends on the angle of incidence and frequency (Lurton, 2010).

A strong point of the seafloor mapping sonar is that they are intrinsically able to record the two type of information (target geometry and reflectivity) altogether in a ideally compatible way, since one same echo can be used for both purpose. However, it took years for the two functionalities to be usable at the same level of quality – and it is still an ongoing progress. Nevertheless, and without being overoptimistic, there is a widely accepted agreement today that the sonar system used for seafloor mapping can usefull provide two level of information from the same recorded signal:

- water depth and/or morphology;
- seafloor acoustic reflectivity.

Conceptually, water depth is relatively straightforward information to derive from the record of timedelays of echoes: it is all a matter of time measurements and geometry. The processing is far less obvious when the aim is to obtain information on the nature of the seafloor from echo intensities. Indeed, the backscatter phenomena is a peculiar concept: it is both intuitive (a sound that is sent back towards its source, more or less intense according to the target and its range) while still very complex structurally – the received echo is a combination of acoustic and geophysical processes, accounting for both transmitting and recording electronics of the sonar and intricate physical phenomena happening both in the water and at the interface. Hence, in order to access the backscatter information intrinsic to the seafloor, the recorded echo first need to be cleaned of that part of the signal that is not directly related to the target itself. This means first that the characteristics of the sonar sensor should not be affect the estimation of the target reflectivity, while they certainly impact on the received echo observable intensity. It is also intuitive that the measured echo levels depends on the range between the sonar and the target – a distance target obviously raise a fainter echo than a close one; hence the propagation loss inside the water column needs to be corrected, according to the local environmental condition and to the particular acquisition geometry. After this appropriate compensation have been applied, the measured echo intensity can be reasonably considered as representing the seafloor effect alone, and can be translated into the backscatter strength of the target, which is its inherent capability for sending back acoustic energy to the sonar system. This “reflectivity” characteristic is linked fundamentally to the target’s material mechanical characteristics (a hard material send back higher echoes than a soft ones) and its fine scale geometry (a rough interface scatters more acoustical energy than a smooth one). Hence measured backscatter can, up to some point, be considered as a first-order indicator or proxy for the seafloor interface nature, composition and small-scale structure, and hence provide a direct link with geology, biology and ecology – which is indeed the goal to keep in mind.

The angular dependence of the backscatter response is a paramount feature, implying both constraints in the data processing and in the potentialities of their interpretation (Hughes Clarke et al., 1997, 2007). A rough and hard seafloor interface (coarse material or rocks)

tends to scatter the sound waves homogeneously in all directions, and the echo level depends little on incidence angle; the intensity recorded over the swath width is then rather stable whatever the angle (Figure 8). On the other hand, a soft and flat fluid-like sediment has a mirror-like response, sending back a maximum of intensity at the vertical and very little at oblique angles; the sonar image shows then a strong maximum in its center, and a fast decrease on the sides. All intermediate cases are indeed possible, depending on the interface roughness and the presence of scatterers either lying on the interface or buried in the surficial layers.

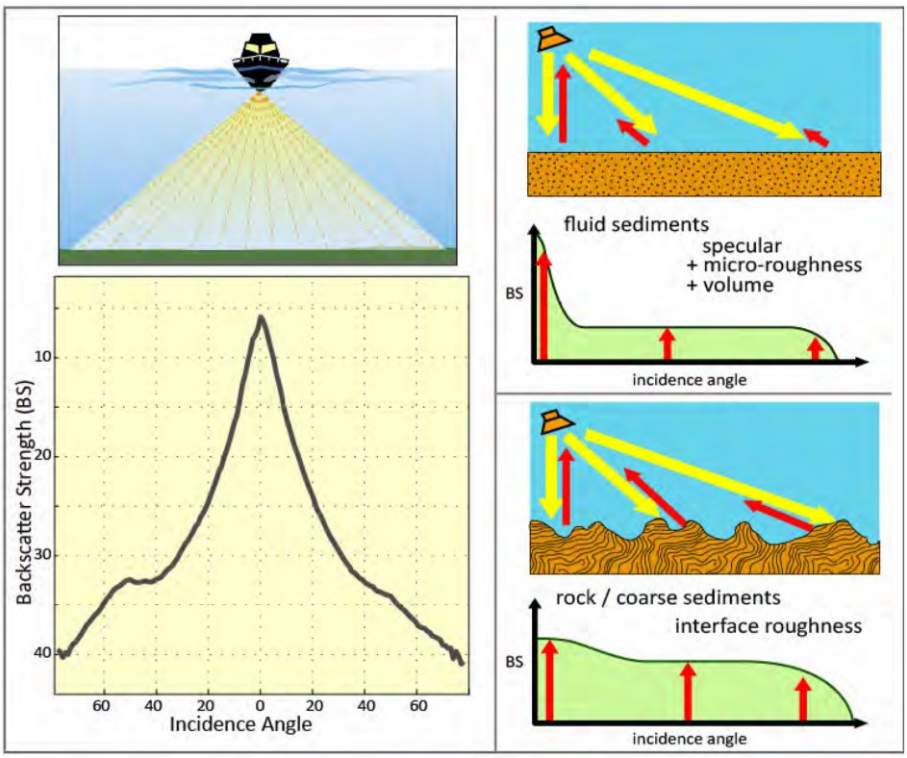

Figure 8 The angular dependence of Backscatter Strength (BS). The rapid decrease in the BS intensity with incidence angles shows well in the BS angular profile (bottom left): high BS values at the nadir (0° incidence) decrease rapidly with gazing angle. The shape of the angular profile is directly influenced by the interface roughness (right); it is not necessarily symmetrical in practice (example shown here), depending on local features (from Lurton, and Lamaque, 2015).

The variation of the incident angle cause a variation of intensity of signal on the seafloor image. This require an harmonization dedicated work in order to make the seafloor surface easily interpretable.

The post-processing activity is finalized to flattering the angle response in order to have, for an homogenous flat seafloor, a constant signal on the processed image, but on the opposite point of view, the preservation of the angular dependence is a mandatory tool for facilitating the seabed classification activity. all this implies, in both cases, to define accurately the shape of the seabed features. That means that we have to know very well

the bathymetry and is for this reason that the MBES is the better solution. Having, in the meantime, a good determination of bathymetry and a good estimation of angular reflectivity, with the comparable resolution. The resolution of a MBES is identified as the extent of the beam section intersecting the seafloor interface and its function of angle of emission, water depth, and the physical lobe dimension (typically 1° hence about 2% of range) (Lurton, 2010; Lurton and Lamarque, 2015).

We consider, simplifying the environmental, that the seafloor will be flat and horizontal, but with the surface roughness if observed at a small scale. This condition neglects the seabed morphology, the inner structure of sediments and the presence of heterogeneities, but is sufficient for the understanding of fundamental notions and phenomena. The incident acoustic wave and its specular reflection, are strictly connected with the medium of the seafloor, with the characteristic impedance of the sediment and with the smooth of the interface. The intensity of this reflected signal is then only controlled by the "hardness" of the seafloor and the direction of the acoustic wave.

The contrast between the water and sediment acoustic impedance is defined as Hardness, where the acoustic impedance is the product of density and sound speed.

The transmission source (Tx) and the receiver plate (Rx), in case of the reflection angle is higher, can be installed separately. In this case, we talk about the bistatic configuration, used often by low-frequency seismic reflections (Lurton, 2010). One exception is the single beam echosounder, in this case the beam direction is perpendicular to the seafloor and the Tx and Rx could be installed in one transducer only. This is partially the solution applied for the MBES even if the discrimination of each sound lobe raises a number of specific issues, especially in low frequency. So, from the studies done, it is possible to determine, having the knowledge of the boundary condition at the seafloor, the quantity of the acoustic wave reflected (Kinsler et al., 2000). In case of transmission with a normal incidence angle, the reflection coefficient or better the ratio between the reflected and the incident pressure is regulated by the characteristic impedances of the seawater and the seabed, where $(Z = \rho c)$. Table 1 presents the values of the acoustic quantities corresponding to the different types of seabed sediment.

Table 1 Geoacoustical characteristics of typical sediments. Adapted from APL 1994, using the classical Wentworth scale for sediment nomenclature and nominal values for c1 and ρ1 (1500 m/s and 1000 kg/m3, respectively) (from Lurton and Lamaque, 2015).

	Clay	V. Fine Silt	Fine Silt	Medium Silt	Coarse Silt	V. Fine Sand	Fine Sand	Medium Sand	Coarse Sand
Grain Size Mz(ϕ)	> 8	7-8	6-7	5-6	4-5	3-4	2-3	1-2	0-1
Density (kg/m^3)	1145	1147	1148	1149	1195	1268	1451	1845	2231
Velocity (m/s)	1470	1476	1479	1482	1523	1585	1661	1767	1875
Absorption (dB/λ)	0.08	0.11	0.17	0.37	1.18	1.02	0.87	0.89	0.89
V (0°) (dB)	0.058 (-24.8)	0.060 (-24.4)	0.062 (-24.2)	0.063 (-24.0)	0.096 (-20.3)	0.145 (-16.8)	0.233 (-12.7)	0.370 (-8.6)	0.472 (-6.52)
Critical angle (°) *(intromission angle)*	*(68.6°)*	*(71.2°)*	*(72.5°)*	*(74.0°)*	80.0°	71.2°	64.6°	58.1°	53.1°

In other terms, more is Z and more will be the reflected echo from the seafloor.
So, in case of denser sediment, the reflection coefficient will higher than soft sediment. in the Table 1 it's possible to see that more is the density of the sediment, more will be the velocity. Of course, with the oblique angle, we have to take in mind that the reflected wave is directed along the specular direction and the reflection coefficient (V), as we will see later, is angle-dependent.
In the case of oblique transmission, the incident reflection coefficient is function of the relationship between the impedances of the two materials (water & sediment) but is also dependent on the angle of transmission and incidence. In
Figure 9 it's presented an example of the reflection coefficient for different materials related to the incident angle.

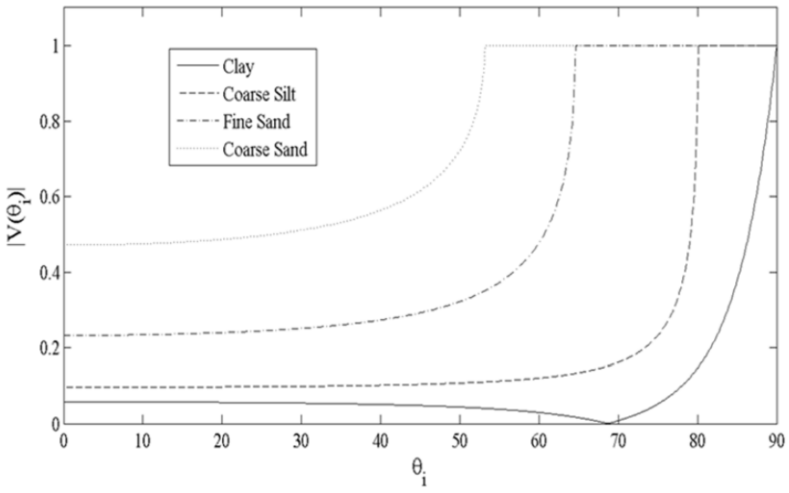

Figure 9 Angle-dependent smooth-surface reflection coefficient for clay, coarse silt, fine sand, and coarse sand using the properties from Table 1 (from Lurton and Lamaque, 2015).

As we can see, the reflection coefficient remains constant until a critical angle value, at which point all of the transmitted signal is reflected and only an evanescent wave is transmitted into the seabed.
As we said, this condition is possible due to often the seabed has a sound speed faster than seawater (Table 1). This is not true for clay, where its velocity is slightly slower than seawater. For a particular incidence angle, no sound will be reflected and all sound waves will be directed into the seafloor (angle of intromission). Even for clay, increasing more the angle, we will have all the transmitted signal reflected.
The specular reflection is only theoretical, in reality, the seafloor is never perfectly flat and smooth and the ideal specular reflection does not actually occur. The acoustic wave, with its own wavelength, intercept the seafloor and is scattered around the specular direction. The angular spread of this scattered wave is a function of the roughness. In case of low-moderate roughness seafloor, the specular direction maintains the majority of the scattered wave. On the opposite, with high roughness seafloor conditions, the incident wave is spread in all directions, and the specular component will be lost (Figure 10). This signal, scattered in all direction, gives rise to the echo received by the receiving unit and, even at grazing angles, this is the working principle for all multi swath system.

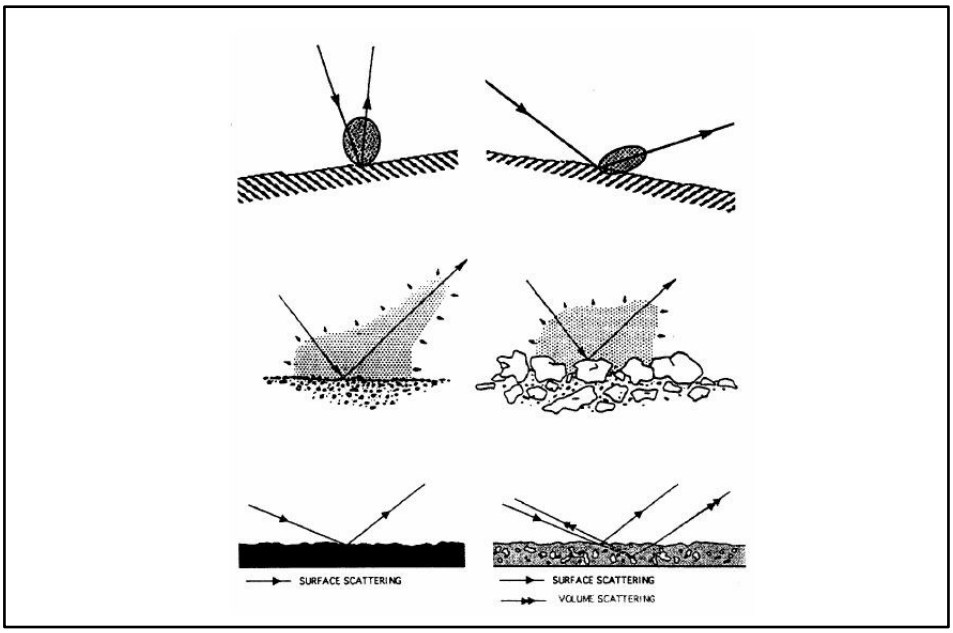

Figure 10 Backscattering from the seafloor is influenced by three factors (from top to bottom): local geometry of insonification, roughness of the seafloor at scales comparable to the sonar's wavelenght, intrinsic properties of the seafloor (e.g. rocks vs sediments) (from Blonder and Murton, 1997).

As easy to understand, the interface roughness of the seafloor, has to be considered in relation to the wavelength of the acoustic signal. In the modern MBES the wavelengths move around a less than one centimeter to one decimeter. So, the acoustic backscatter is strictly connected with the roughness, which is defined as the ratio of the geometrical roughness to the acoustic wavelength.

If we express the geometric roughness as the standard deviation h of the seabed interface elevation, we could define the roughness interface in function of the wavelength and so of the frequency:

- a smooth interface: the wavelength is bigger than the seabed irregularities, the seafloor could be associate to a perfectly smooth interface. In this condition, we will have a very high specular reflection and, as a consequence, a very low backscatter;
- a rough interface: the wavelength is lower than the seabed irregularities, and the scatter will be a significant proportion of the incident power. For this condition, more acoustic energy is scattered to all directions.

As discusses until now, it's impossible to define a priori, from the acoustic point of view, if seafloor is rough or smooth. As we saw it's related to the frequency that we are going to use. For example, for the seismic investigation, where the very low frequency is used and the wavelength is measured in meters, between 1 to 100, it is correct to hypothesize that the specular reflection from the seabed interface(s) is a valid approach for interpretation. On the other hand, during the investigation with high-frequency sonars, it is possible to arrive at 450kHz (approximately 0.5 cm wavelength) and roughness is significant at the millimeter-scale of sand grains. Here, the specular echo, backscatter, is likely diminished, most of the acoustic field is scattered over a wide range of angles, and interpretation of the echo from the seafloor has to take into account the roughness of the seabed features. (Lurton and Lamarque, 2015).

At the frequencies used by seafloor mapping sonar, the backscatter from the seabed can generally be separated into two contributions (Lurton, 2010):

- energy scattered by the interface (specular backscattering);
- energy penetrating the sediments and reflected back by volume heterogeneities (volume backscattering). This process can become predominant at oblique incidents.

As described above, the acoustic effect of the seafloor are driven by many different processes and their relative importance depends on the signal frequency (Lurton, 2010):

- the seafloor basically acts as a rough interface scattering the incident sound wave. The backscattered signal is the one used by seafloor mapping sonar.
- A noticeable part of the incident energy may penetrate the seabed because of the small impedance contrast between water and sediment. Even if absorption inside sediments is much higher than in water, low acoustic frequencies can propagate with reasonable levels.
- Process similar to those in water propagation may occur inside the sediment.
- Various scatters lie at the interface or are buried inside the sediment (shells, living organism, minerals, etc..). They may generate additional scattering.

The various ideas above regarding reflection and scattering from the seafloor are incorporated into models that describe the seafloor backscatter strength at all angles (Lurton and Lamarque, 2015). Moreover, the physical processes, their interpretation and modelling differ greatly with frequency considered.

An important aspect of these models is the strong angle-dependence of the seafloor backscatter. Closer we get to vertical, more the reflection takes over, and this is the direction of the most intense echo level from the seafloor (Figure 11). The grain size sediments is strictly connected with the influence of the specular reflection. Seafloor composed of smaller grain-size sediments will be characterized by low roughness, and in these cases, the influence of the specular reflection decreases very quickly with increasing incidence angle. The regime of the specular reflection is more evident in a smoother interface (the specular region will have the narrowest angular sector and highest level relative to oblique incidence angles). The scattering effect will dominate with the oblique incidence angles, due to few, if any, facets of the seafloor point back towards the direction of origin of the signal.

The hardness interface (impedance contrast) and the roughness are the primaries cause for the intensity of backscatter; in soft sediment, the oblique incident angles is the range where the volume backscatter is at its highest. This situation has more advantages for the seabed mapping, thanks to its stability and to the good separation that is observable between various seabed types.

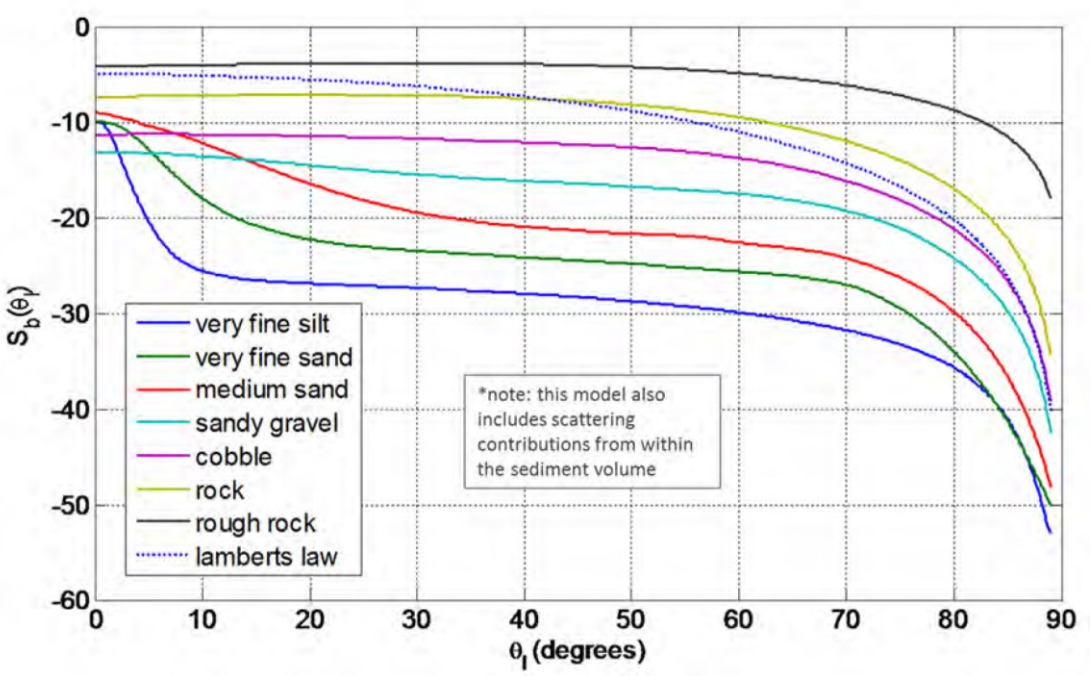

Figure 11 Example of angle-dependent backscatter for different substrate types at 100 kHz, based on model results using the APL-UW High-frequency Ocean Environmental Acoustic Models Handbook, APL-UW TR9407 (1994). (from Lurton and Lamarque, 2015).

With the decreasing of the grazing angles, the backscatter response of the seafloor collapses as:

- the intercept between the seafloor and the acoustic wave are limited
- the roughness response decreases;
- the shadow effect has become more important and this leads to a decrease in the effective backscatter cross-section.

The most favorable angle sector for backscatter measurement appears to be the “plateau” regime.
The backscatter mosaics are often “normalize” angle-dependent backscatter to a reference value taken in the range of the plateau regime. This to replace the slow and limited angle variation of the plateau by no variation at all. We need just an appropriate compensation – moving to one value measured as the reference angle.
In a homogeneous seabed condition, area will appear with an average of constant backscatter – the way it should have been recorded if the whole swath width would have been insonified at a constant angle.
As known, a smooth surface at low frequencies may look rough at high frequencies. In the Figure 11 , it has showed a model result assuming a frequency of 100 kHz.

In Figure 12, it’s showed the evidence that for different frequency, in the same conditions - medium-sand seafloor - we have a different backscatter strength. At 30 kHz, the surface look like a smooth, with a high specular reflection and a low oblique incidence scattering (dominated, in this case, by volume scattering), on the contrary, at 400 kHz, with an order of magnitude higher, it's provide a much more uniform (with angle) backscattering strength.
The range of frequency showed in Figure 12, put in evidence that the seabed response may be variable between 14 dB close to the normal incidence and 7 dB at oblique incidence, even if the exact frequency dependence should depend on characteristics of the roughness spectrum of seabed.

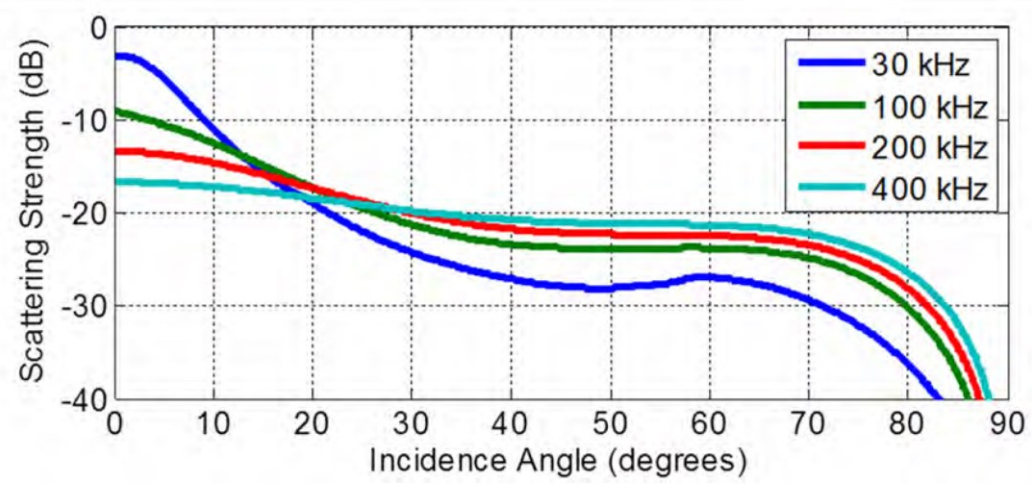

Figure 12 Example of angle-dependent backscatter for medium sand at different frequencies, based on model results using the APL-UW (from Ocean Environmental Acoustic Models Handbook, APL-UW TR9407 (1994).

What we have seen until now, Figure 11 and Figure 12, suggest some caution must be taken when interpreting seafloor backscatter measurements. Modern MBES have a great capacity to acquire data on highly variable angles of incidence (0°- 65° or more) and, at the

same time, they have a frequency agility capability, up to 1/8 of the nominal frequency. All these possibilities, which are certainly useful for the acquisition of the bathymetric data, if not taken into account correctly, can strongly modify the backscatter signal received and provide a considerable errors of interpretation.

2.4. Use of backscatter for seafloor mapping

The foundation of each REA activity at sea, especially in shallow water and littoral area, need the necessity to integrate the acoustic backscatter data, as an ancillary data of a high-resolution Multibeam survey, together with the water column data and the nature of the seabed, allowing to have the base for a complete, detailed and mostly rapid picture of the morphology and dynamics of the area.

The characterization of the seabed is, nowadays, an essential element for the study of the sea and in the same way, the determination of the "Good Environmental Status".

Acoustic seabed classification is a technology for mapping superficial seabed properties and sediment distribution with echosounder (Anderson et al., 2008). The idea is that a change in sediment composition often implies a change in acoustic properties. This results in a systematic difference in the recorded echoes, provided the data have been corrected for extraneous influences, such as variable water depth or instrumental settings.

Information about seabed composition is useful in a range of problems, including sonar performance prediction, benthic habitat mapping and marine resources management (Brown and Blondel, 2009; Ellingsen et al., 2002; Freitas et al., 2003; Harries, 2012), environmental monitoring (Medialdea et al., 2018) and geotechnical engineering (Bartoloma, 2006). A scientific understanding of the physical processes that form the seabed is also a goal in itself, and new acoustic technique for seabed mapping are instrumental to achieve this (Eiden and Lanmark, 2013).

While once the acoustic instrument was the single beam and therefore it was limited to the single point data, today the MBES is the main instrument in all Geophysics, Oceanographic and, of course, Hydrographic survey; in particular the great variety of instruments, different frequencies and different techniques of structuring the data and analysis, allow a wide used for various purposes. The MBES information is used by national hydrographic services for the acquisition of bathymetric data aimed at safety for navigation, are used by research bodies for the base of each research related to the sea. In particular, the most important prerogative of the MBES is to acquire not only the depth but also the backscatter signal reflected from the bottom and along the water column.

The capacity of the new MBES systems associated with the increased computing potential has allowed, for multiple end-users, to increase the use of backscatter for scientific purposes and more. Even in modern hydrography we no longer speak exclusively of depth data, in terms of surface, but of characteristics of the seabed, classification, spatial disposition and features.

Thus, a study of the innovative systems for REA-type activities cannot fail to start from the use of MBES systems and acoustic backscatter.

Acoustic seabed classification

Despite the increasing interest of using MBES backscatter, standards of seabed backscatter acquisition and processing are still under development. A set of guidelines and recommendations was developed by the Backscatter Working Group (or BSWG; http://geohab.org/bswg) mandated by the Geological and Biological Marine Habitat Mapping scientific committee (GEOHAB).

On top of the primary bathymetric function, MBES are able to record seabed reflectivity (also referable to as the backscattering strength). The intensity of the acoustic backscatter received from the sonar is the result of numerous physical parameters, including the angle of incidence, the frequency of the signal (the wavelength) and the type of sediment with its physical characteristics (like seafloor roughness and sediment grain-size). After applying the most important corrections (grazing angle, water depth, swath area, sound velocity, morphology of the seafloor, local absorption, etc…), it is theoretically possible to characterize the seafloor with acoustic facies, which put in relationship the seafloor patches with the different acoustic backscatter acquired (Lurton and Lamarche , 2015)

Some modern techniques use multispectral analysis at different frequencies to take advantage of the different backscatter behavior as a function of frequency (Brown et al., 2017).

Historically, the routine till now followed for the seafloor characterization was a monoparametric, semi-automatic approach, with mandatory sampling. The main aim of my study is to define a new routine with the use of a multiparametric and automatic approach, to decrease uncertainties of the characterization and with quick analysis results.

Two analytical techniques were applied, with the aim of identifying the classes able to best represent the organization of the seafloor acoustic facies:

- current classification technique - Monoparametric analysis.
  One of the classic backscatter mosaic classification techniques consists in an analysis of the surface of acoustic intensities: the surface was divided into areas of greater similarity, in terms of backscatter values. A K-Mean clustering algorithm was used, with the aim of minimizing the intra-cluster (classes) distance: this analysis required the subjective selection of the number of clusters (classes) in which the set of data is divided. At the end of the operations, a raster surface was created, with classes with different colors, which represent a decibel range;
- multiparametric analysis (New classification technique: aim of the study)
  The other kind of analysis took into account more variables to divide the seafloor into classes. In addition to the acoustic intensity, it also considered depth and roughness representing the heterogeneity of the seafloor (Montereale-Gavazzi et al., 2017;

Zakariya et al., 2018). Each point of the surface was associated with a set of three values. These three variables were saved both as georeferenced Geotiff raster and as xyz data matrices:

- the Geotiff rasters were merged into multi-channel surfaces, displayed as false-colour images: each of the channels (R, G, and B) was associated with one of the 3 variables;
- the xyz data matrices could be visualized into a Cartesian space (3D Scatterplot), a three-dimensional space in which each of the three variables is represented by one of the x, y and z axes. A standard coastal survey (5-10 km^2) with a standard resolution (0.5 m^2) usually ranges from 30 millions up to 100 millions pixels. Plotting this amount of data in a 3D Cartesian space can be very time consuming. It is possible to work in very small sub-areas and plot them in a 3D space, but several hours are needed just to plot an entire surface and it is nearly impossible to make further analysis or computations. In order to have faster algorithms, it was decided not to use all the values of roughness as a parameter, but to hierarchically divide the data into two groups: a surface defined as "smooth" and a "rough" one. This decision was supported by the constraint and limitation imposed by the wavelength (fixed in some echosounder) in discriminating a seafloor smooth or rough. For this reason, the 3D scatterplot was split in a couple of 2D scatterplots, while the 3-channel multilayer surface was split into a couple of 2-channel surfaces (without the blue channel). Working in two dimension instead of three speeded up the analysis process by nearly 85%;
- areas with known seafloor have been selected manually on the multilayer surface, with the associated variables of the points that composed it, to determine the acoustic features. Repeating this manual selection on different areas, the Cartesian surface of the scatterplots has been divided into polygons, each of them containing all values of a class. The selection of the multiparametric classes is an iterative and empirical selection supported by additional data, such as sediment samples, aerial photos, divers video, historical studies, etc. Using a point-in-polygon algorithm (winding number algorithm), all data were assigned to one class: to compare the results, a raster surface was generated with the same colours of the classes as in the monoparametric classification (Demarte et al., 2018).

Study area – Otranto coast

In September 2017, the Hydrographic Vessel ITS Galatea (Figure 13) acquired MBES data in the Otranto coastal area.

Figure 13 Hydrographic survey vessel and workboat

Otranto coast develop in the southernmost zone of the Adriatic Sea, in the homonymous Otranto Strait, that connects with the Ionian Sea. The morphology of the coast is variable, with cliffs (Figure 14), sometimes over 20 m, and low and sandy coasts.

Figure 14 Cliff zone of Otranto coast

Regarding the local hydrology, there is a lack of fresh water sources, with no defined structures in the study area and its surroundings, with the exception of small coastal lake, 9 km to the north of Otranto.

Figure 15 Otranto survey area

The survey area was comprised in a rectangle with the following vertices (WG84) (Figure 15):
South-West: 40° 08' 08"N 018° 28' 56"E
North-East: 40° 10' 05"N 018° 31' 05"E

Data acquisition

The vessel was equipped with the following system (Figure 16):

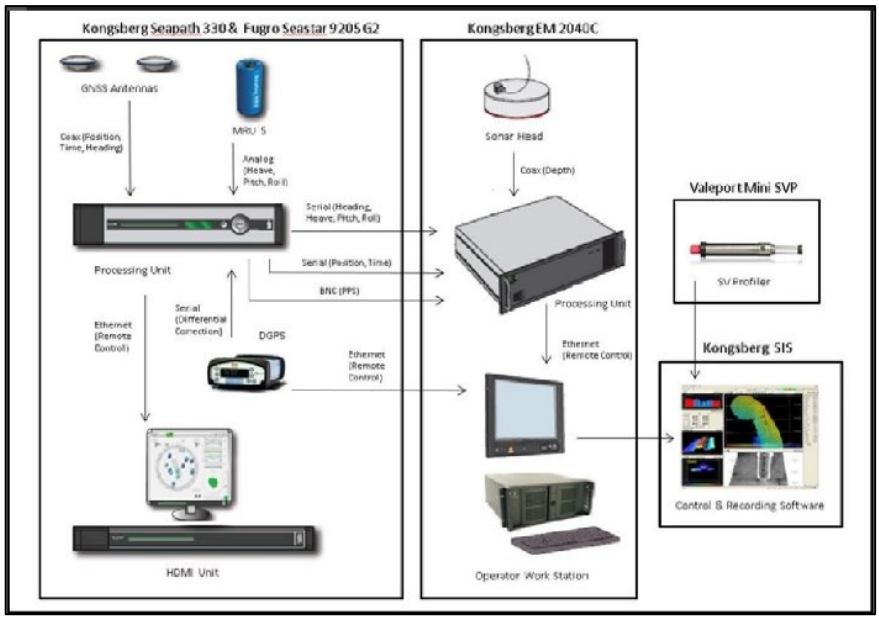

Figure 16 Acquisition System

a) Multibeam Echosounder: Kongsberg EM 2040C (Single head):

It's a true wide band high resolution shallow water multibeam echosounder.

Nominal Technical Specifications:

- Frequency range from 200 kHz to 400 kHz with steps of 10 kHz.
- Pulse lengths from 14 microseconds up to 12 milliseconds.
- Raw range resolution (cT/2) at the shortest pulse is 10.5 mm.
- Combination of continuous waves (CW) and frequency modulated (FM) pulses.
- Maximum depth range is 520m at 200 kHz.

b) Inertial Measurement Unit: Kongsberg Seatex MRU5 with Seapath 330:

It's a heading, attitude and positioning sensor, with linear accelerometers, MEMS type angular rate gyros and two GNSS receivers for position and velocity determination.

Nominal Technical Specifications:

- Roll and pitch accuracy: ±0.01° RMS for ±5° amplitude.
- Heading accuracy: ±0.05°/0.075° DMS depending on baseline length.
- Heave accuracy: the highest between ±2/5cm or ±2/5%, depending from real-time or delayed signal.
- Time measurement accuracy: ±0.001 s.

c) GNSS Receiver: Fugro Seastar 9205G2:

It's a multi frequency receiver with GPS, GLONASS and Galileo reception capability.

Nominal Technical Specifications:

- Horizontal Accuracy: ±10 cm (95%).
- Vertical Accuracy: ±15 cm (95%).

d) Sound velocity profiler: Valeport Mini SVP:

It's a sound velocity sensor, with a temperature sensor and a strain gauge pressure transducer.

Nominal Technical Specifications:

- Resolution: 0.001 m/s.
- Accuracy: ±0.02 m/s.

The survey was carried on with a nominal frequency of 300 kHz in the main lobe, with FM pulses; the software used for the data acquisition was SIS (Seafloor Information System).
The offsets of the vessel system have been measured with a Trimble S6 topographic total station (accuracy: ± 2mm + 2ppm).
Tide and pressure data have been collected from the ISPRA station installed inside the Otranto port (www.mareografico.com).

Data analysis and processing

Depth and backscatter strength values have been gridded in a geographic space and projected in UTM zone 34N with WGS84 ellipsoid, with a resolution of 0.5 m^2. Bathymetric data were de-spiked and elaborated with the CUBE algorithm (CarisHips&Sips®) to create the surface. Backscatter intensity was processed with the "SIPS Backscatter" engine. Most of the parameters (frequency, sound speed, pulse duration, across and along-track beamwidths, transmit power, nominal spreading, received gain and local absorption,) was read directly from the raw sonar files, along with the necessary raw data (intensity, range and beam angles). The local absorption was computed with the simplified model for absorption in sea water (Ainslie and McColm, 1998), which requires the user to enter local values for salinity and temperature. The instantaneous ensonified area is computed assuming an elliptical cone for the beam footprint and a spherical shell for the pulse (de Moustier and Alexandrou, 1991) and considering the surface from the neighbouring soundings or bathymetric surface. Geometric corrections, despeckle, Beam Pattern, AVG (Angle-Varying Gain) and TVG (Time-Varying Gain) algorithms are applied to the data. The analysis was limited to the angles from 15° to 65° (Leblanc and Foster, 2015).
The surfaces thus obtained were exported both as a geo-referenced raster in GeoTiff format and in ASCII text files as matrices (Figure 17)

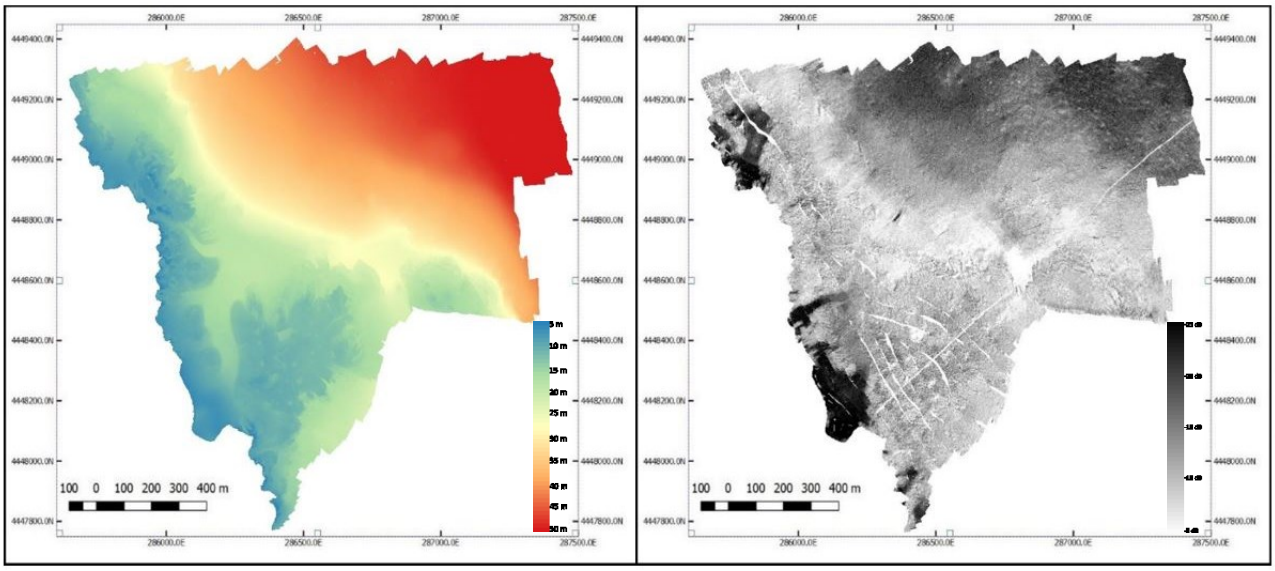

Figure 17 Bathymetry (left) and Acoustic Backscatter surface (right) of the northern part of the Otranto survey

Monoparametric Classification

Scheme of the procedure:

1) Backscatter distribution histogram

During the survey, the seafloor was analysed with the monoparametric classification technique. Backscatter values were visualized both as cumulative frequency distribution curve (Figure 18) and distribution histogram (Figure 19).

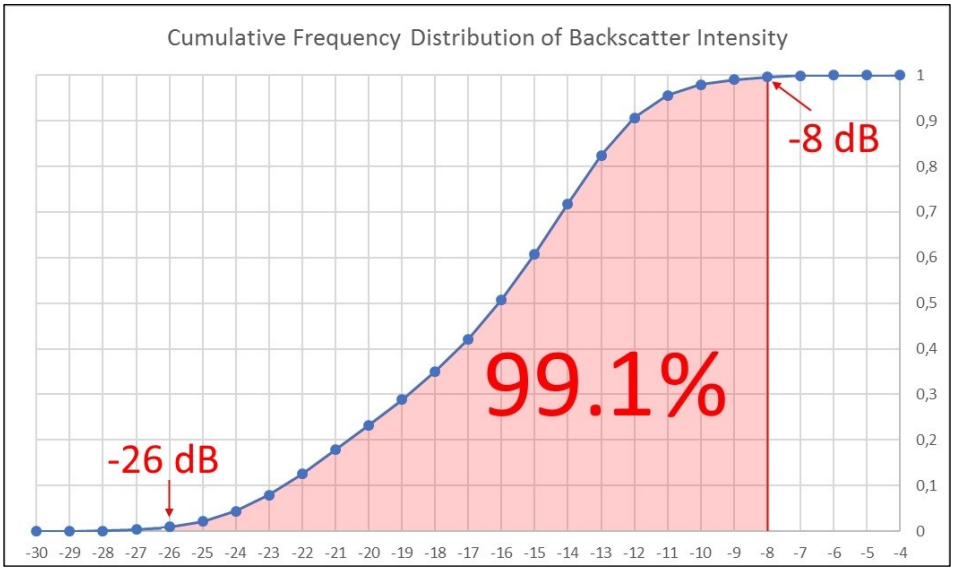

Figure 18 Cumulative frequency distribution of the backscatter intensity

The manual selection of the number of classes is mandatory to apply the K-means clustering algorithm, to divide the full dataset in that number of clusters. In the case study area, the range of acoustic backscatter values varies between -30 dB and -4 dB.

2) Selection of the number of classes

It was decided to use the assumption proposed by Weber and Lurton (2015) of a 3 dB spacing for each class. Since the cumulative frequency distribution plot (Figure 18) shows that 99.1% of dataset is comprised between -26 dB and -8 dB, in an acoustic backscatter range of 18 dB, we selected six classes.

3) K-means algorithm (semi-automatic)

K-means algorithm was apply to divide the dataset in this selected range (Figure 19).

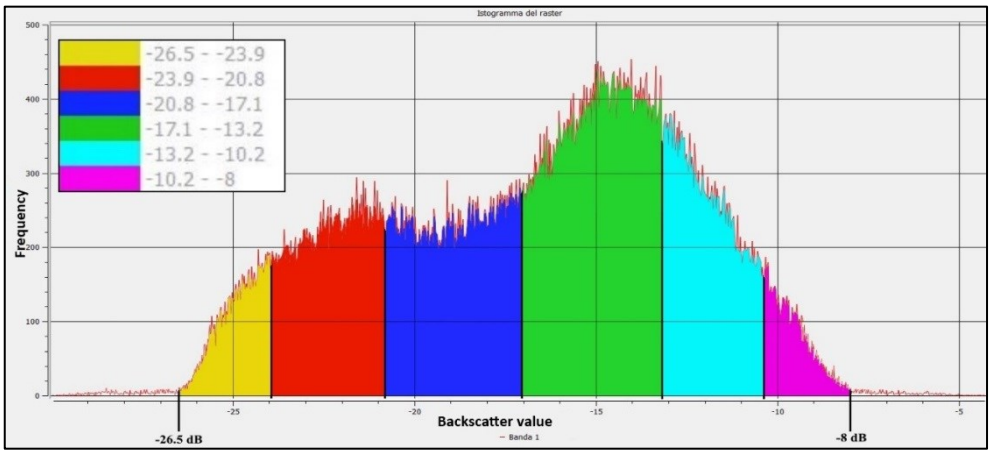

Figure 19 Histogram of the backscatter values, sliced by a k-means clustering algorithm into 6 classes. Ranges are shown in the legend

4) Backscatter classification

The result of this operation is a thematic map composed by areas of six different colours, corresponding to the clustering (Figure 20)

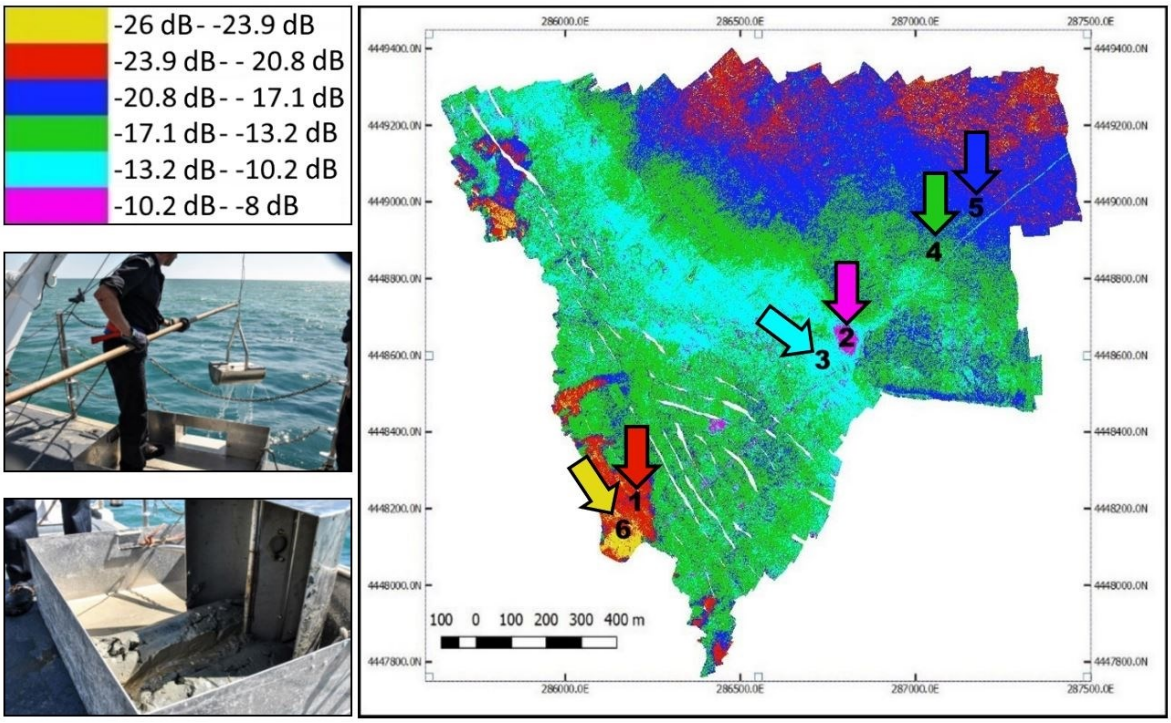

Figure 20 Monoparametric classification of the raster surface, with the 6 points selected for sampling sites (arrow from 1 to 6)

Ground truth

The sample effort for this study was planned using the classified surface and was realized with a Van Veen grab sampler. The characterization of the seabed classes was performed selecting six sites to collect samples (Figure 20).

The physical-chemical properties of the samples were analyzed by ENEA laboratories (Italian National Agency for New Technologies, Energy and Sustainable Economic Development). All samples, except one, that was *Posidonia oceanica* (sample n°3), were analyzed on sieves. Standard Test sieves was ASTM (American Standard Test Slieve Serie) as a series of sieves decreasing meshes with size intervals in Krumbein phi scale, using a mechanical stirrer of the sieve stack. The samples were not chemically treated, so all fractions containing bioclasts or shells fragments were not removed.

The analysis permitted the production of cumulative grain size curves of sediment samples (Figure 21).

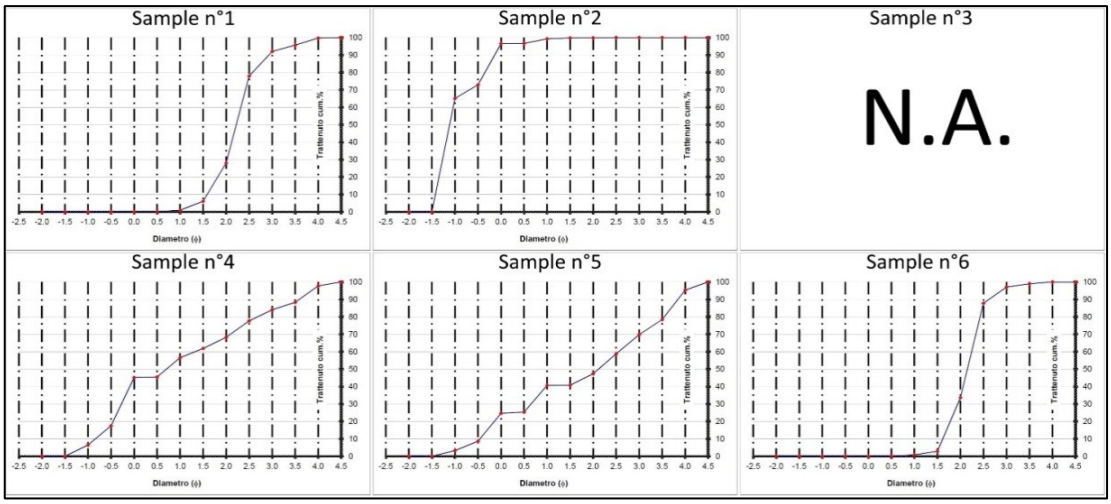

Figure 21 Cumulative grain size curves (φ) of the five sediment samples. The Sample n°3 was *Posidonia oceanica*

The mean backscatter (calculated in a circle with a 5 meters radius around the points) was plotted with the relative value of median grain size: the graph shows the expected linear trend between the two variables, with a determination coefficient value (R2) of 0.9909 (Figure 22).

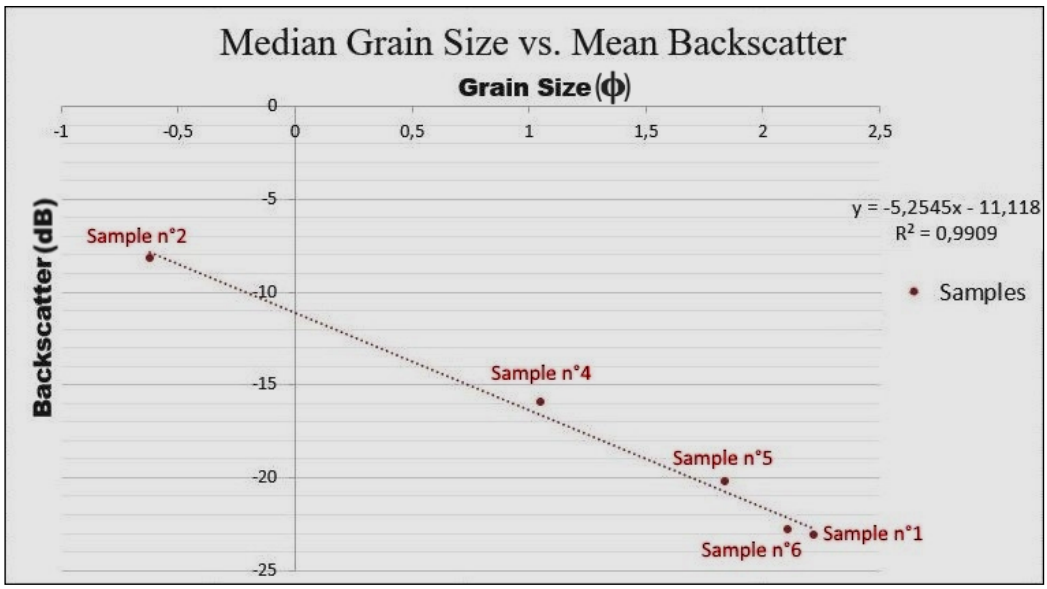

Figure 22 Mean backscatter intensity vs. Median grain size, highlighting the linear correlation. Sample n°3 is not displayed (Posidonia oceanica seagrass)

Multiparametric classification

Scheme of the procedure:

1) Roughness surface elaboration:

After the grain size analysis, the multiparametric classification was performed. The backscatter and bathymetric surfaces were processed in situ, during the survey and monoparametric classification. To elaborate the roughness surface of the seafloor, the

slope surface was calculated in each point as the angle between the vector perpendicular to the plane tangent to the depth surface and the vector normal to the horizontal plane. The roughness of the seafloor has been elaborated on the slope layer, as the largest inter-cell difference of a central pixel and its surrounding cell (Wilson et al., 2007)(Figure 23). It's important to notice that the roughness value does not represent the sediment roughness in terms of granulometry, but the roughness of the seafloor relative to the surface resolution. It can be represented as a standard deviation of the central pixel in a grid of pixel: for our classification, we used a grid of 5x5 pixel, with a resolution of 0.5 m^2 for each pixel.

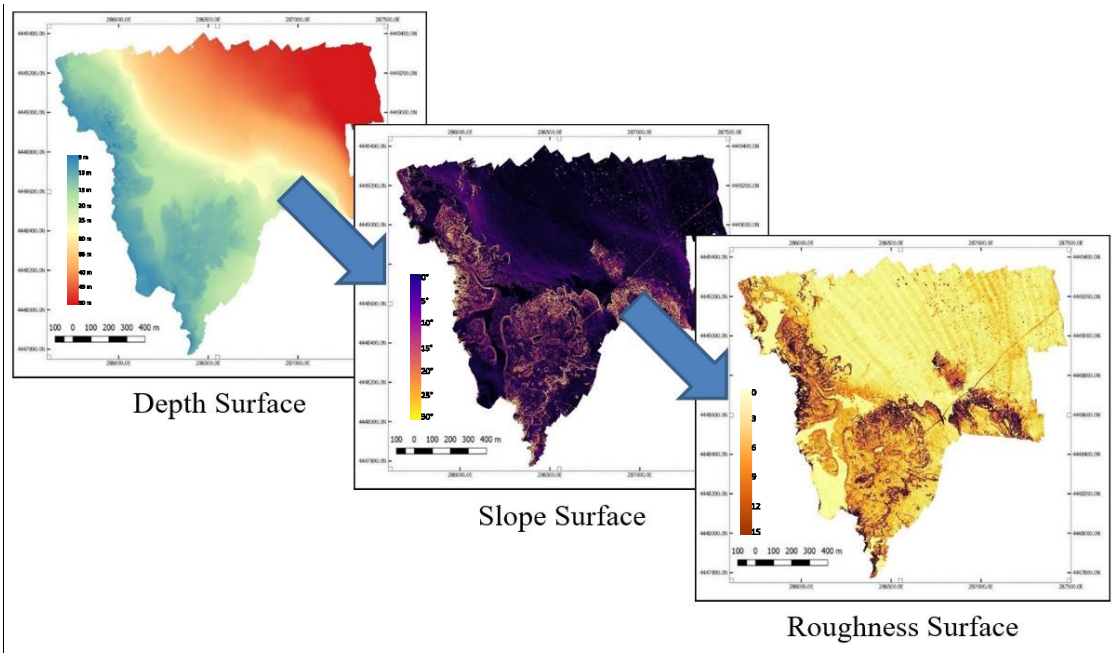

Figure 23 Elaboration of roughness surface from the depth and slope surface

2) False color image and scatterplot:

Usually, false color images utilize wavelenghts regions of electromagnetic radiation associated with different color of the visible light (red, green and blue): the process that we used in this approach consists in using different layers to highlights details that otherwise are not easily recognizable. For our study, the raster surfaces (GeoTiff) of backscatter, depth and roughness were then merged into a single 3-channel multilayer surface (Figure 24).

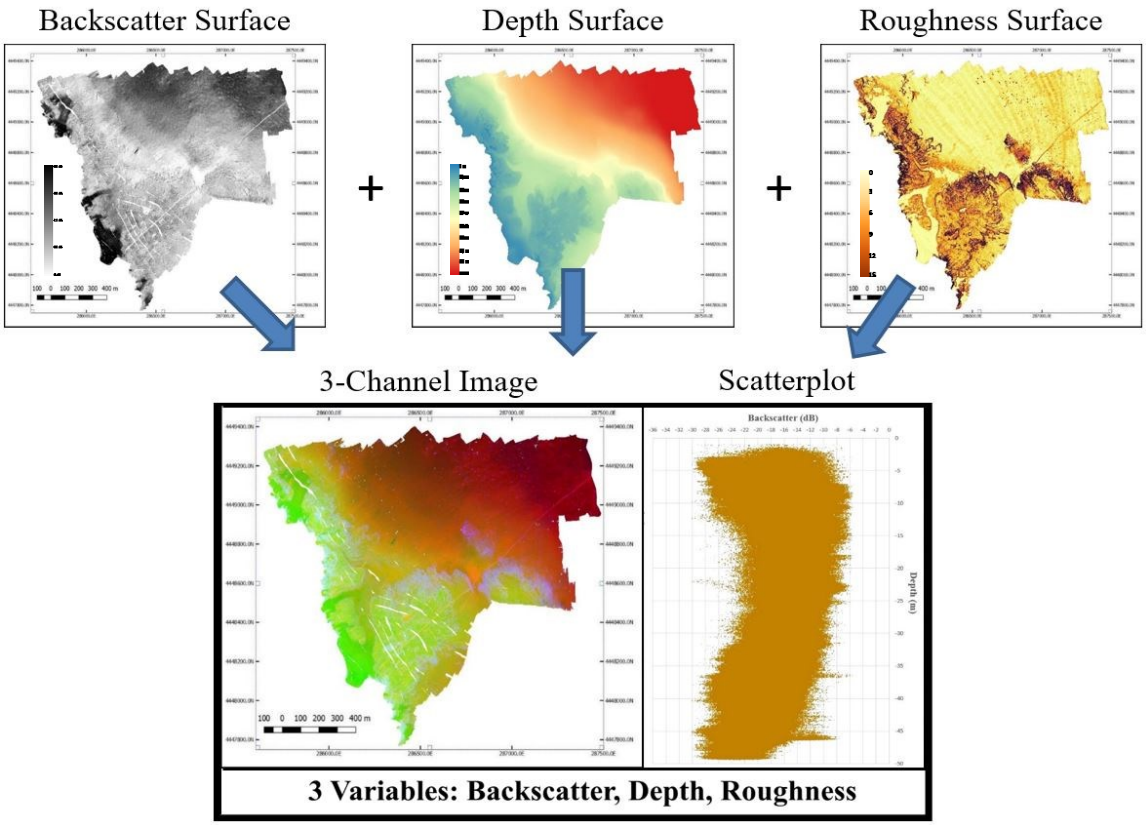

Figure 24 False color (3-channels) multilayer surface created from backscatter (R), bathymetry (G) and roughness (B). The 2D scatterplot shows the trend of backscatter (x-axis) along depth (y-axis)

3) Creation of "smooth" and "rough" surface (from roughness)

A roughness value was empirically selected to separate the sandy ("smooth") and the rocky ("rough") classes. Data were divided into two separate sets of data: the classification proceeded two times, one for each set of values (Figure 25).

In this way, we could exploit the influence of the third variable, the roughness of the seafloor, in a hierarchically way. In fact there was different materials with a similar backscatter range, but very different roughness values. With data divided in two couple of surfaces, we proceeded in the analysis creating couples of 2D scatterplots (Figure 25).

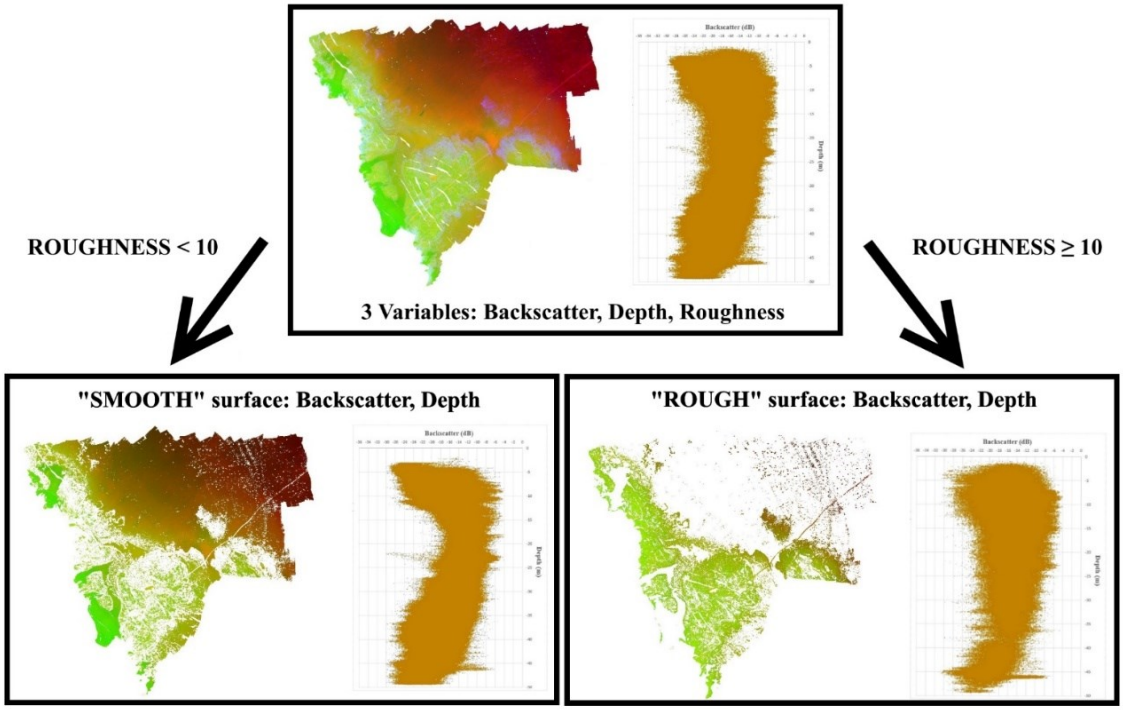

Figure 25 The original dataset has been divided in two: a "smooth" surface and a "rough" surface, with their respective scatterplot

4) Multiparametric class selection

To proceed with the classification, different kind of information has been collected: "in situ" samples, aerial photos and ortophoto, historical data from previous studies (CoNISMa, 2006) and video from local divers. Aerial photos allowed to easily discern targets like rocks and Posidonia oceanica up to the maximum visible depth (in this case study area was in average 20 m); the limit in their use is that it's difficult to distinguish between different sandy class, if they have the same color (Figure 26).

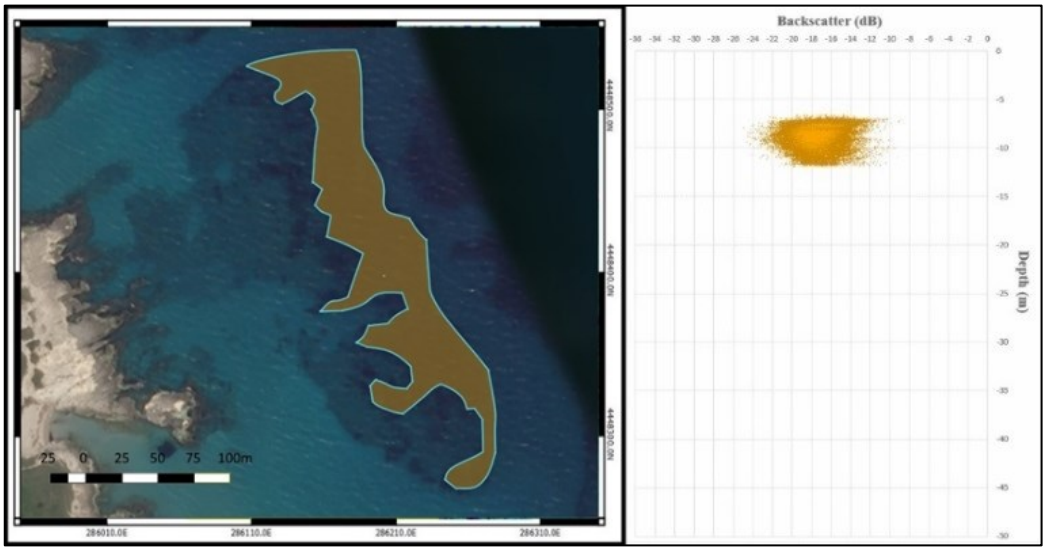

Figure 26 Manual selection of a patch of Posidonia using an aerial photo. The scatterplot of the selected area shows the trend of backscatter for that specific class at that depth

Aerial photos do not give enough information to distinguish between granulometry of sandy or muddy areas. The first selected target (class) was the Posidonia oceanica (Nardini, 2017), because of the importance of this target in the Mediterranean Sea, for at least two reasons:

- ecological and environmental: seagrasses are keystone biota providing structural complexity which supports and maintains bentho-pelagic coupling and biodiversity. It serves as a valuable naturally occurring protection against coastal erosion, as well as producing oxygen in the marine environment and storing carbon (Boudouresque and Meinesz, 1982);
- safety purpose: mine hunting and shallow water surveys are strongly affected by the presence of seagrasses meadows (McCarthy and Sabol, 2000).

The same procedure was performed to the selected macro-classes (Wentworth classification): Fine sand (Class 1), Fine/Medium sand (Class 2), Medium Sand (Class 3), Posidonia oceanica (Class 4), Rocks (Class 5), Coarse/Very Coarse Sand/ Concrete (Class 6). (Figure 27A). Colored polygons on scatterplots (Figure 27B) are the results of these heuristic and iterative operations.

5) Multiparametric classification

The entire dataset was divided in order to respect the computed classes and a thematic coloured map was produced (Figure 27C)

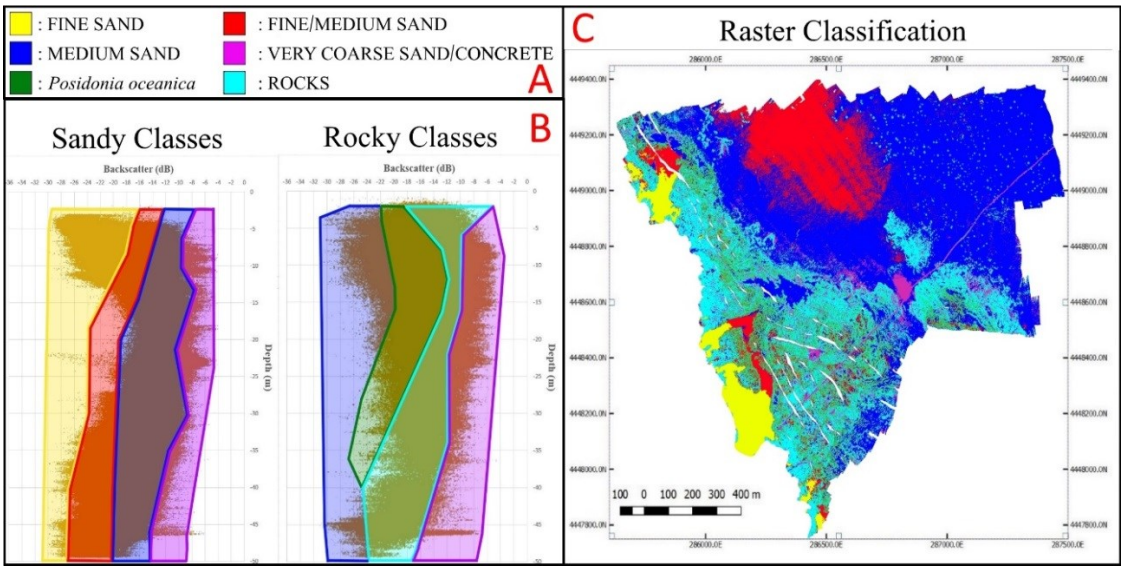

Figure 27 Otranto case study: seafloor classes colors (A); polygons that contains the classes over the respective scatterplot (B); Multiparametric classification of the raster surface (C). *(Colors in B have a transparent effect from the software that originates this image)*

Results

The two resulting surfaces, obtained with the two different analytical techniques, were compared (Figure 28).

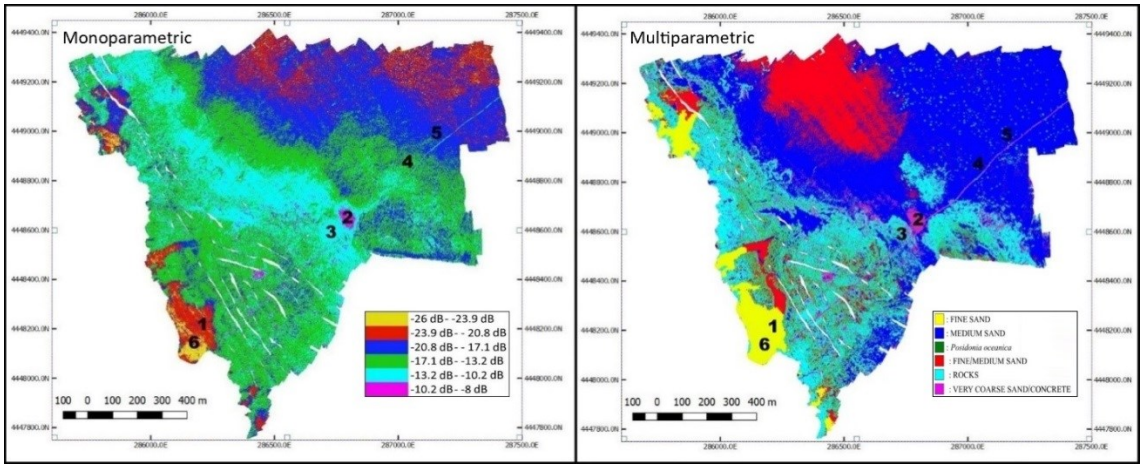

Figure 28 Comparison of the two classification surfaces: monoparametric (left) and multiparametric (right), with the positions of the ground-truths

The six ground truth was taken in order to cover each of the 6 classes found with the monoparametric classification. However, the laboratory analysis showed that samples 4 and 5 both belong to the same class (medium sand in the Wentworth classification) (Table 2). The multiparametric classification has therefore taken this fact into account by assigning the backscatter values of these samples in the respective classes.

Table 2 Median grain size and Wentworth classification of sediment samples for each ground-truth sample

Sample	Median Grain Size	Wentworth Class
N° 1	2.22 φ	Fine Sand
N° 2	-0.62 φ	Very Coarse Sand
N° 3	N. A.	Posidonia oceanica
N° 4	1.05 φ	Medium Sand
N° 5	1.84 φ	Medium Sand
N° 6	2.11 φ	Fine Sand

To correctly evaluate the accuracy of the result, many more direct samples would be required. Nevertheless, the cross-check of the classes was possible using aerial photos (visibility up to a depth of 20 m). A clear example of the differences of the results using the two methodologies is proposed in Figure 29: in the monoparametric classification (Figure 29B) the most abundant class is the green class; the direct sampling on the green class revealed it to be medium sand: sample n°4 was taken in green class area (Figure 28 left), but at a different depth than Figure 29.

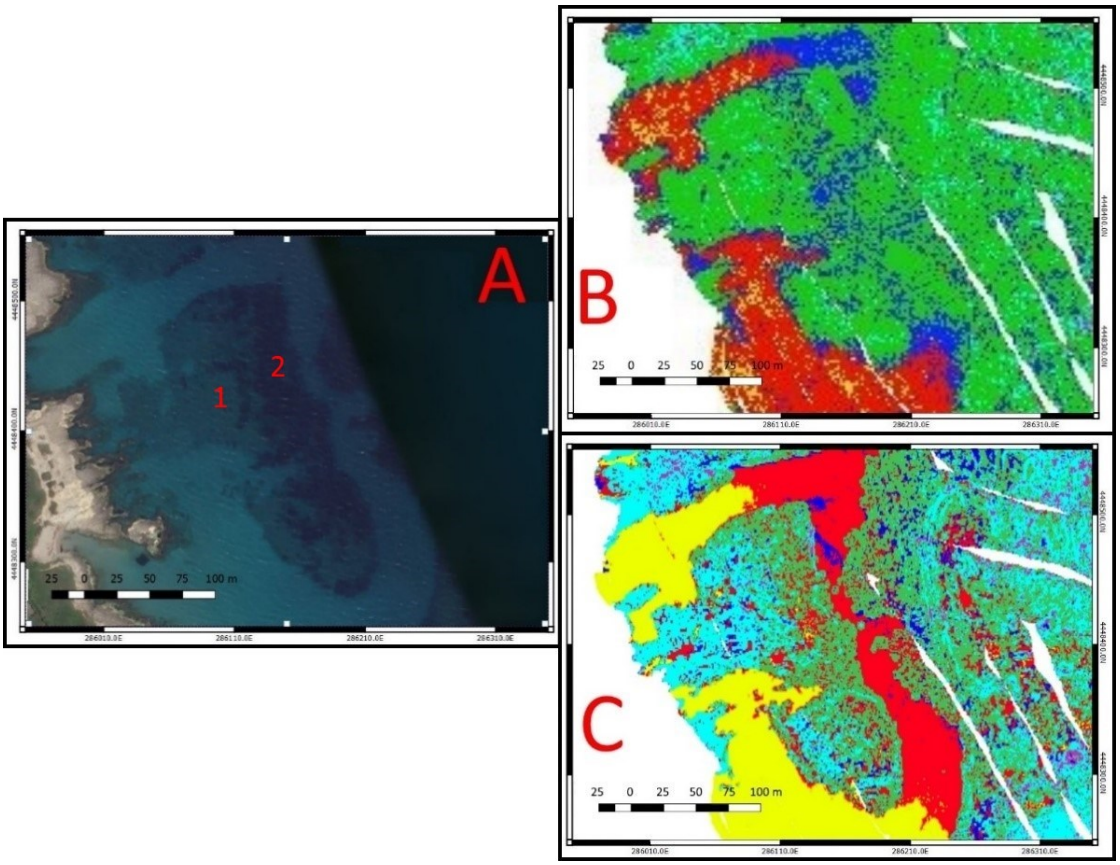

Figure 29 Comparison between an aerial image of a rocky *(1)* seafloor with a *Posidonia oceanica (2)* patch (A), the monoparametric classification (B) and the monoparametric classification (C).

The aerial photo (Figure 29A) together with in situ exploration, shows that the area in the figure is composed mainly by rocks (Figure 29A-1) and Posidonia oceanica (Figure 29A-2); this information has been used for multiparametric classification (Figure 29C).

Validation

To test the results obtained, the classes characterized in both methods were applied on a different case study. The choice for the area fell on Olbia (Sardinia) coastal sector for the following reasons:

- the hydrographic vessel used during the survey was equipped with a similar equipment used in Otranto case study (same multibeam echosounder system, but with different offsets), with the same frequency and setup;
- the hydrographic survey was geographically far away, with geological and oceanographic differences, to avoid that these aspects affected the possible results.

The survey was carried on, in April 2016, one year before the Otranto case study, by the Italian Navy Hydrographic Vessel ITS Aretusa with a Kongsberg EM 2040C multibeam set at nominal frequency of 300 kHz. No sampling has been performed during this survey.
The area was comprised in a rectangle with the following vertices (WG84) (Figure 30):

South-West: 41°00'6"N 9°35'58"E
North-East: 41°01'23"N 9°39'18"E

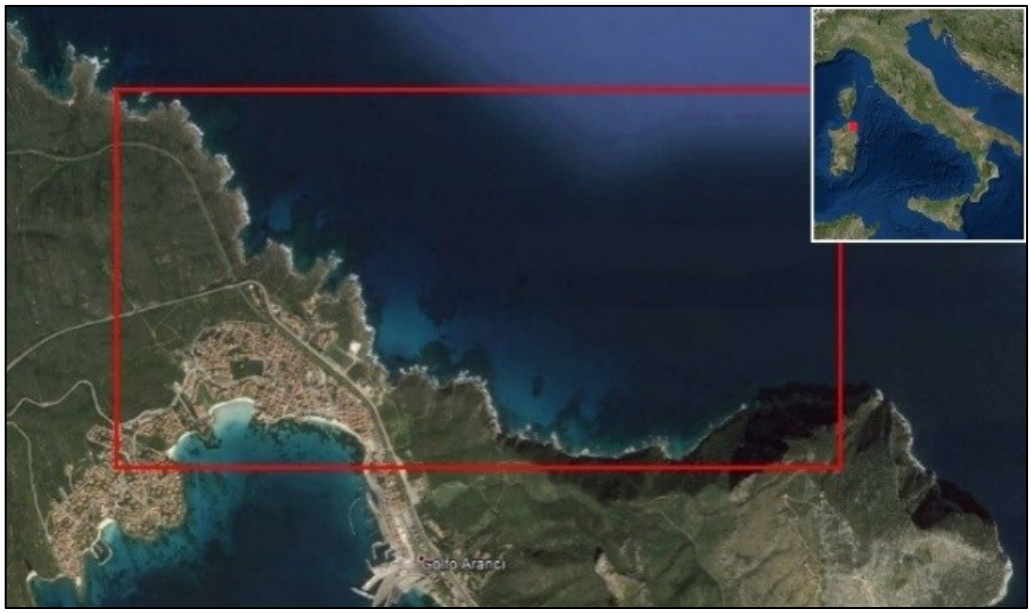

Figure 30 Northern coast of Olbia survey area

Analysis and processing

Depth and backscatter surfaces were elaborated using the same parameters of Otranto case study: the only difference was the value of the water temperature and salinity (for local absorption). Then we applied both monoparametric and multiparametric classification.

- Monoparametric classification followed the same steps than in Otranto case study. Backscatter data was visualized as a distribution histogram comprised between -32.3 and -3.8 dB. We chose to classify the values of backscatter comprised between -26 dB and -8 dB with 6 classes, to have comparable ranges with the Otranto case study (more than 99% of the dataset was comprised in this range of values).
- Multiparametric classification followed the same steps than in Otranto case study, with some differences. Roughness surfaces was elaborated in the same way, then we created the false color image. The dataset was then divided into a “smooth” and a “rough” surface (using the same value empirically selected in Otranto case study) and the two corresponding 2D scatterplots were elaborated (Figure 31)

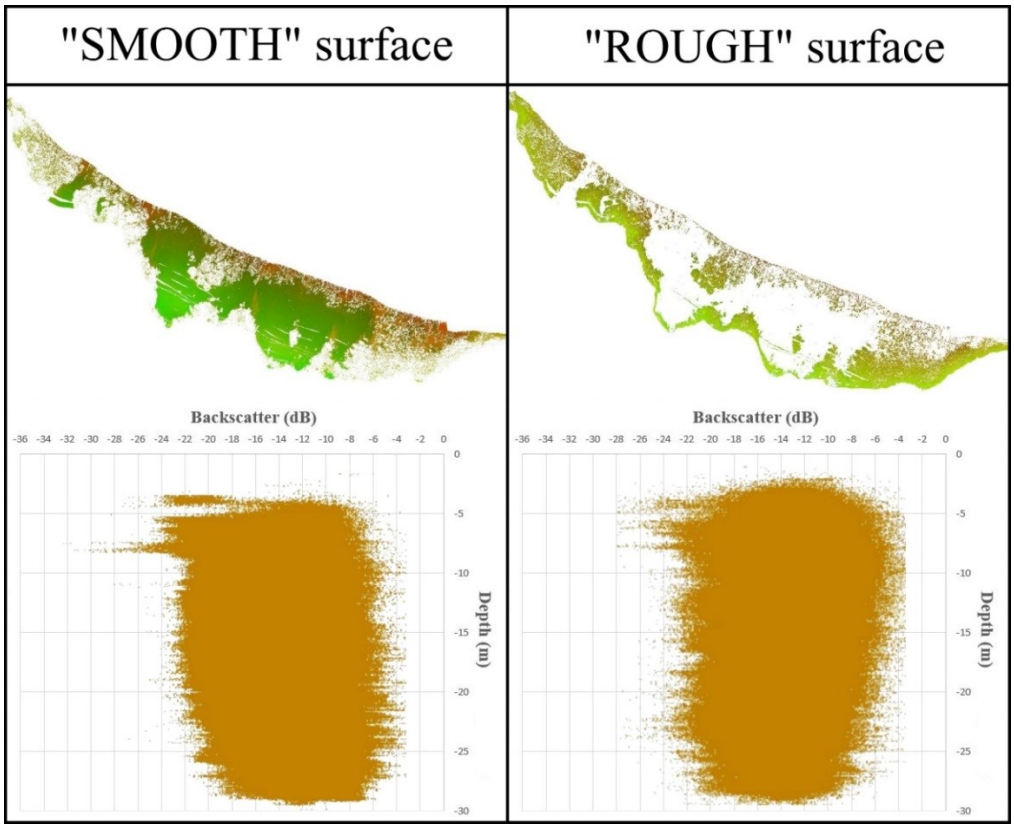

Figure 31 The Olbia dataset has been divided in a "smooth" surface and a "rough" surface, with their respective scatterplot

The class selection was not performed, the same classes defined during the Otranto case study (Figure 32A) were applied to the Olbia survey. The dataset was divided by an automatic extraction algorithm (winding number algorithm), characterized with the same polygons as before (Figure 32B), producing a raster classified surface (Figure 32C). The polygons in Figure 32B are the same of Figure 27B, but since this survey depth ranged from the surface up to 30 m of depth, they have that depth limit.

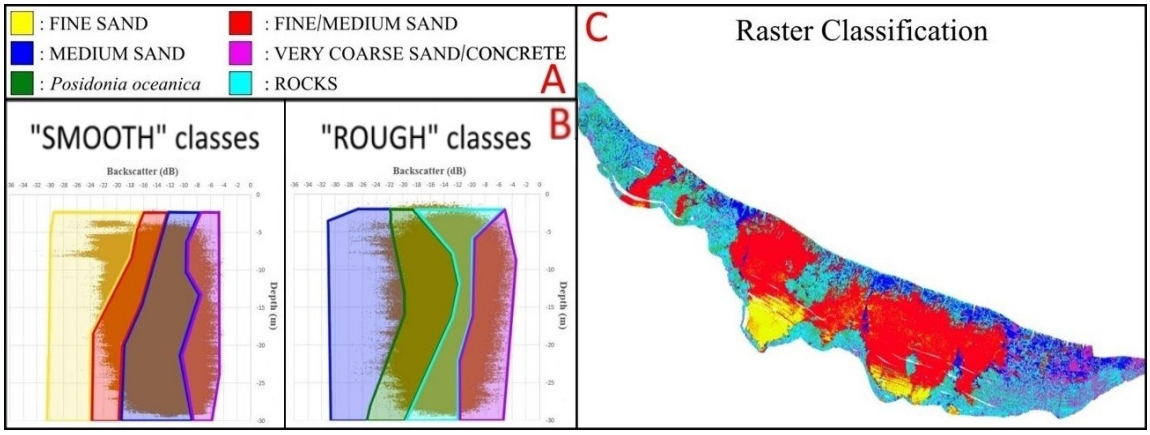

Figure 32 Olbia case study: seafloor classes colors (A); polygons that contains the classes over the respective scatterplot (B); Multiparametric classification of the raster surface (C)

Monoparametric and multiparametric classification rasters were compared (Figure 33)

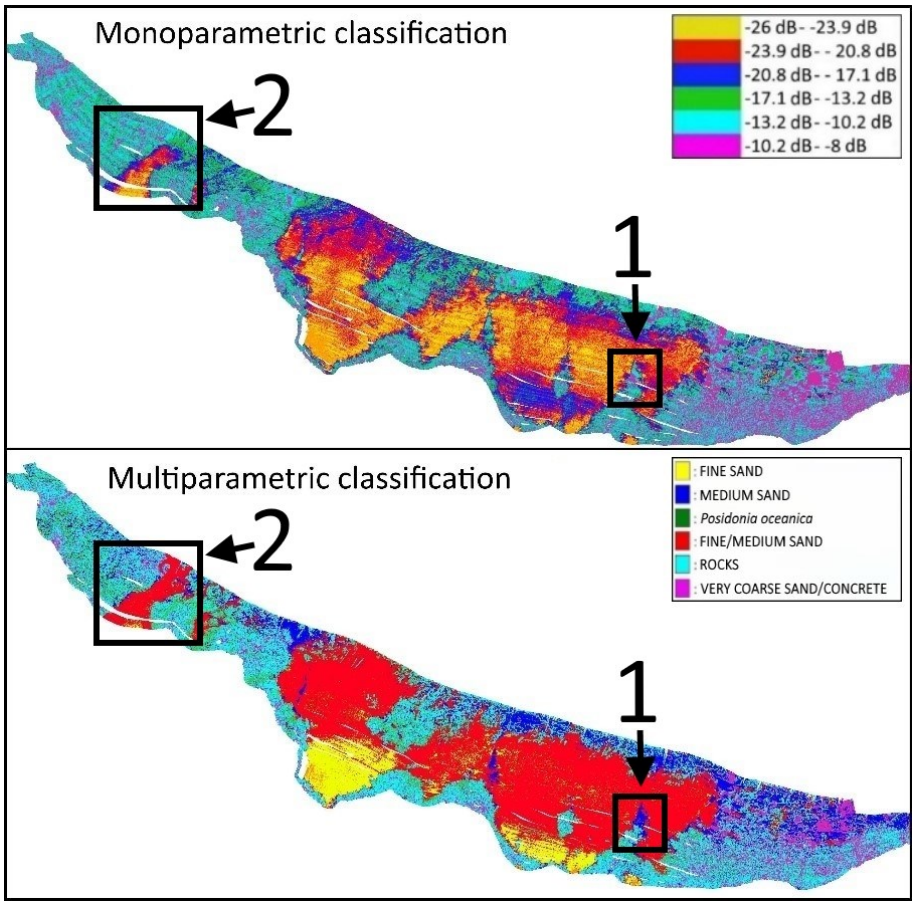

Figure 33 Olbia case study: comparison of the two classification surfaces: monoparametric (up) and multiparametric (down). Numbers 1 and 2 areas represent the areas selected for the examples

Comparison of results

To make a correct evaluation of the representativeness of the two thematic maps, we need to compare the results of the two classification methods with ground truths. In this case study, due to the lack of seafloor samples acquired during the survey, we took advantage of available aerial photos checking additional data (videos from divers and morphology) to define patches of different seafloor classes. Then, we selected areas with clear visible seafloor and we checked the percentage of coverage (number of pixel of the class over the total number of pixels) for each class found with both methods to evaluate which one had better results.

- Example n°1 (Figure 33 and Figure 34):

The selected area showed the presence of a darker coloured area, different from the surrounding; according to previous information and additional data, we can associate this patch to dark sand mixed with dead *Posidonia oceanica*. This difference in colour was

highlighted and confirmed by a LIDAR (Light Detection and Ranging) survey, carried on at the same time.

Monoparametric classification showed that classes 2, 3, 4, 5 and 6 had more than 50% of coverage; in multiparametric classification, classes 2, 3 and 5 had more than this percentage of coverage (Table 3).

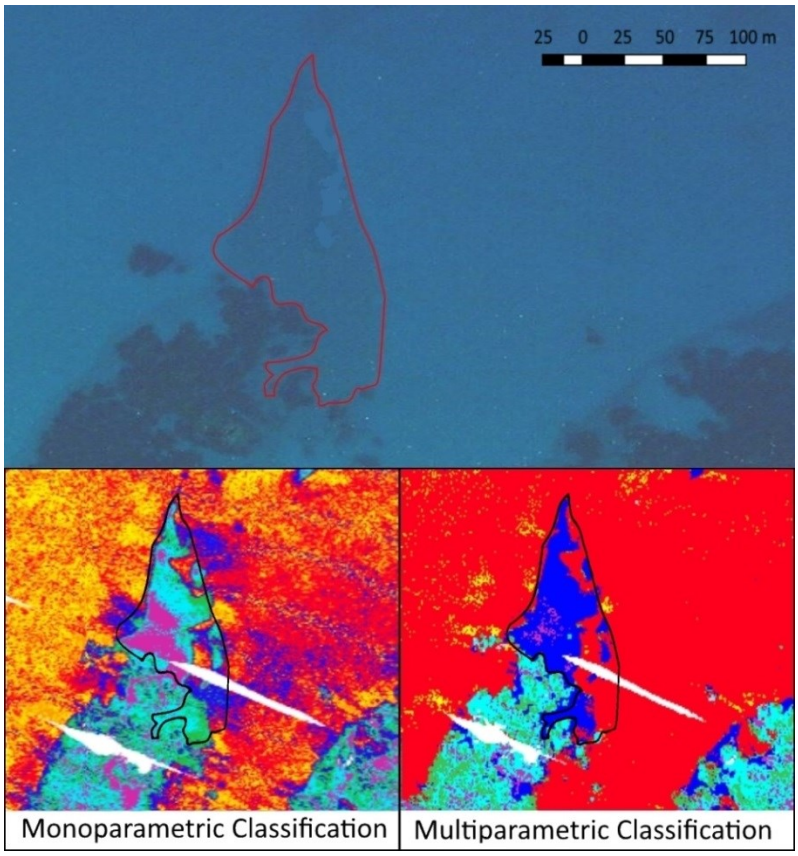

Figure 34 Example n°1 - UP (WGS84): Manual selection over a dark sandy area (130m x 144m). Down (UTM 32N/WGS84): (left) Monoparametric classification results. (right) Multiparametric classification results

Table 3 Example n°1 - Monoparametric classification using a statistical approach. Multiparametric classification using 6 different classes identified at the beginning of process

Monoparametric Classification		Multiparametric Classification	
CLASS	COVERAGE	CLASS	COVERAGE
Class 1	11.97%	Class 1	25.12%
Class 2	41.72%	Class 2	71.38%
Class 3	29.03%	Class 3	0.31%
Class 4	16.06%	Class 4	0.17%
Class 5	0.95%	Class 5	2.60%
Class 6	0.10%	Class 6	0.42%
TOTAL SURFACE:		24066.5 m²	

- Example n°2 (Figure 33 and Figure 35):

The selected area showed the presence of light coloured area; according to previous information and additional data, we can associate this patch to a sandy channel surrounded by rocks and Posidonia oceanica patches. Monoparametric classification showed that classes 2, 3 and 4 had more than 50% of coverage; in multiparametric classification, classes 1 and 2 had more than this percentage of coverage (Table 4).

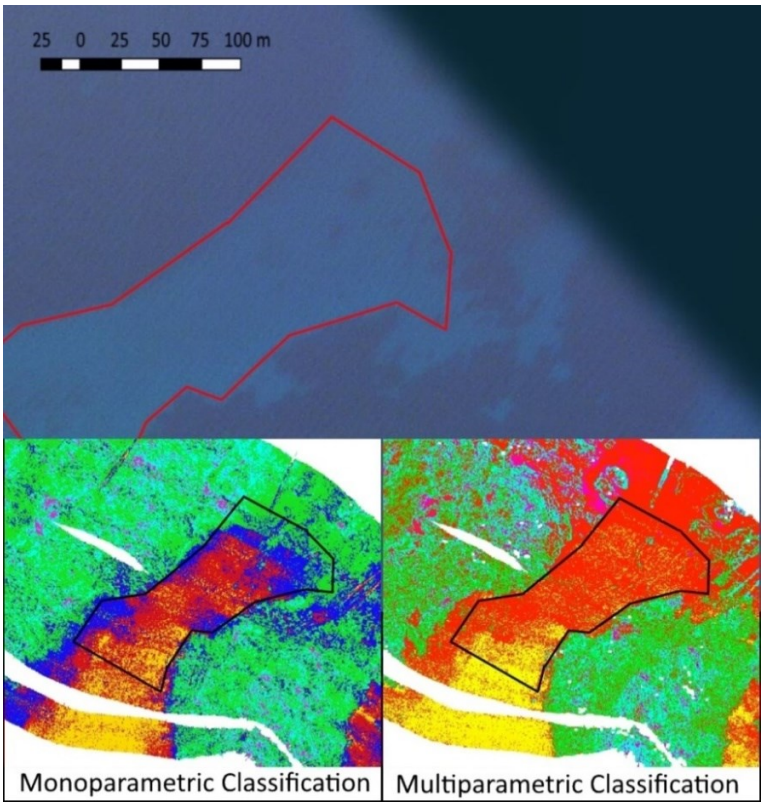

Figure 35 Example n°2 - **UP**: (WGS84): Manual selection over a sandy channel (100m x 115m). DOWN (UTM 32N/WGS84): (left) Monoparametric classification results. (right) Multiparametric classification results

Table 4 Example n°2 - Monoparametric classification using a statistical approach. Multiparametric classification using 6 different classes identified at the beginning of process

Monoparametric Classification		Multiparametric Classification	
CLASS	COVERAGE	CLASS	COVERAGE
Class 1	2.40%	Class 1	3.21%
Class 2	13.29%	Class 2	31.06%
Class 3	17.66%	Class 3	57.04%
Class 4	33.27%	Class 4	1.29%
Class 5	25.33%	Class 5	5.73%
Class 6	8.05%	Class 6	1.67%
TOTAL SURFACE:		4919 m²	

While the monoparametric classification make use only of the backscatter variable to classify the seafloor, the multiparametric classification, using the classes identified in the calibration, compensate the variation of backscatter values of the same class with the different depth and roughness values. In both examples, results from monoparametric classification showed the presence of at least 4 main classes, with an heterogeneous seafloor. Differently, multiparametric classification showed the major presence of 2 classes, with the sporadic presence of the others.
With our knowledge of the selected areas, we can assert that the results of multiparametric classification are more representative of the reality than those obtained with monoparametric analysis.

Remarks

Two analytical techniques were applied with the aim of identifying the classes able to better represent the organization of the seafloor acoustic facies (monoparametric and multiparametric classifications).
In particular, the monoparametric classification has been carried out during the survey operations (after the elaboration of the backscatter and depth surfaces) applying the K-means clustering algorithm. The multiparametric classification (the parameters used are backscatter, depth and roughness) was performed after the laboratory analysis of the samples (acoustic data, sediment samples, videos and aerial images) following the monoparametric classification. In order to have faster algorithm, it was decided to use a discrete hierarchically classes of data. In this case the roughness it is divided into two main classes: smooth and rough.
Then this heuristic technique was calibrated empirically and iteratively: each time that we applied it, the results were checked with supervised data and the values of the classes were modified, then we applied them again to the whole set of data available, until the percentage of correspondence with ground-truth was 100% accurate. At the end of the calibration process, all the coordinates associated with seafloor samples (with known granulometry) fell within the corresponding seabed class.
The results obtained from the data acquired in the case study of Otranto, which took place with the aim of classifying the seabed, were applied to a job carried out a year before purely for hydrographic purposes.
The automatic extraction of the classes, using the values characterized in Otranto, provided more accurate results in comparison to the monoparametric classification, at least as percentage of coverage (Table 3 and Table 4) .
The results confirmed that the near real-time approach set in this work for planning the characterization of the seabed with an automatic approach was successful, since it was found to be more accurate than the monoparametric one.
The follow-up for this work will be the implementation of new variables for the classification of the seafloor: one possibility is the addition of a fourth variable, the slope

of the seafloor linked with the grain size of the sediment, to create a fourth layer of the hierarchic classification.

It will also be necessary the acquisition of more samples of the seafloor to identify the classes more accurately: this could help to increase the number of classes detected, aside from more studies in anthropized areas to improve the detection of non-natural targets.

2.5. Seabed classification and Water Column Images in Kveithola Trough

The NW Barents Sea continental margin has been the target of several surveys in the last decade: SVAIS (R/V Hesperides) in 2007, EGLACOM (R/V OGS Explora) in 2008, GLACIBAR (R/V Jan Mayen) in 2009, CORIBAR (R/V Maria S. Merian) in 2013, PREPARED (R/V G.O. Sars) in 2014 and EDIPO-DEGLABAR (R/V OGS Explora) in 2015.

The Italian Navy Arctic marine geophysics campaign, HIGH NORTH, allowed the acquisition of a wealth of morphobathymetric data that are processed with other surveys acquired.

The HIGH NORTH program gave the opportunity to collect new Multibeam data, in order to complete some areas along the continental margin that haven't been completely covered previously, to achieve the environmental characterization of the seabed and water column and improve the morphobathymetric charts in some key areas.

The Kveithola Trough is an area North West of the Barents Sea, that extends along the E-W direction, for about 90 km with a maximum width of 15 km and an average depth of 300-350 m.

The Kveithola trough (Figure 36) was surveyed to map some structures linked to the presence of authigenic carbonates and/or chemosynthetic communities on the seafloor sampled during previous cruise in 2016.

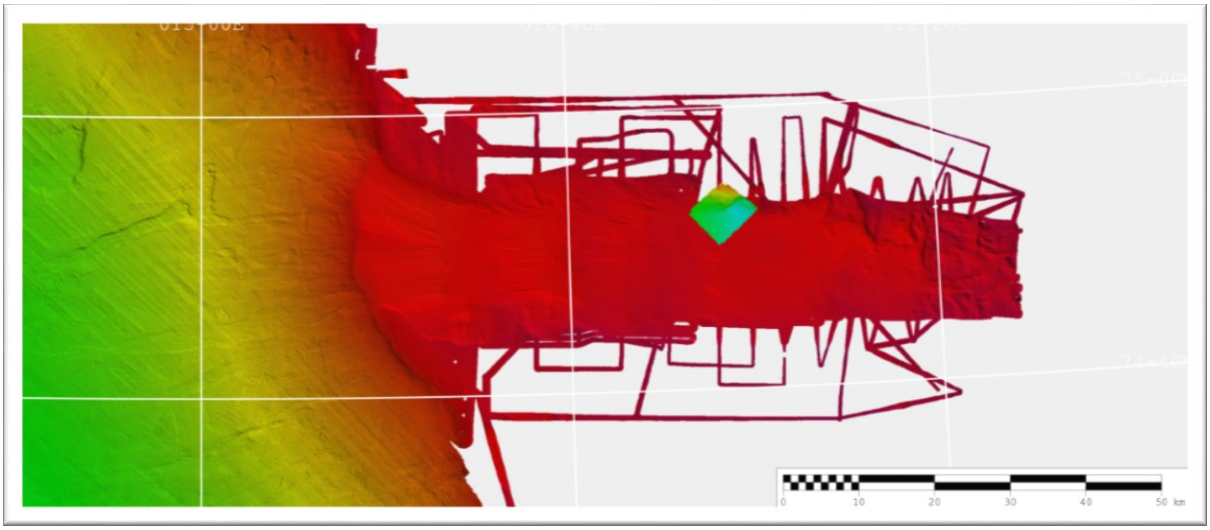

Figure 36 Kveithola Trough Mouth Fan

The acoustic survey was used to locate the sediment sampling and to investigate these communities, testing the multiparametric method displayed in the chapter before.

Data acquisition

The investigation was conducted in late summer 2017 on board Italian Navy Ship R/V Alliance through high resolution Multibeam, 680 square kilometres of bathymetry, Backscatter and Water Column data were collected in order to describe the seabed morphology and to add useful information for safety of navigation.
The main instrument used to investigate the area was the MBES Kongsberg EM 302 keel mounted. Positioning was delivered by the integrated system Kongsberg Seapath 330 receiving STARFIX L1 differential corrections decoded by the FUGRO SEASTAR 3610 decoder.
Sound Velocity profiles applied to data during the survey were collected by means of the SEABIRD SE 911 CTD probe. Pressure, Temperature and Salinity data was converted by the "SBE Dataprocessing" software using the Chen-Millero algorithm and loaded within the acquisition software (SIS (Seafloor Information System) versione 4.3.0,) each time they were available.
Data validation was achieved by means of the software CARIS "Hips & Sips" version 10.1.
The first product that we obtained from multibeam echo sounders was a bathy surface. To determine depths, we use the TWTT (Two Ways Travel Time) principle. Calculating the time every single acoustic pulse takes to reach the sea bottom and return to the receiver we can determine distance, knowing the sound velocity in water. In Figure 37 is represented a particular type of bathy surface, a CUBE surface. CUBE stands for Combined Uncertainty and Bathymetry Estimator.

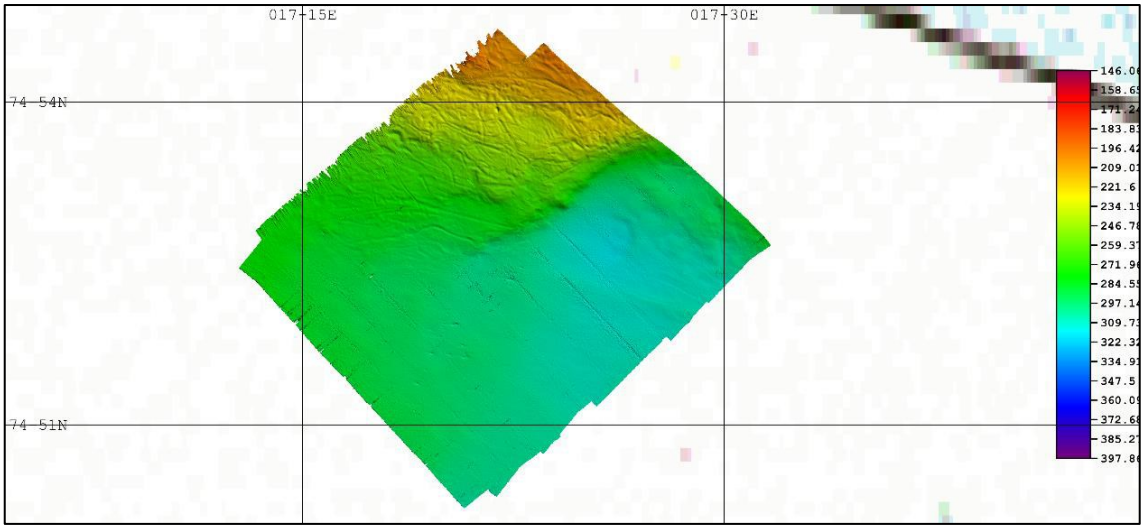

Figure 37 CUBE Surface (Combined Uncertainty and Bathymetry Estimator)

That means that we use the depth and uncertainty information of high density data to compute the best estimate for depth and uncertainty at specified nodal positions.
After that, we pass to the use of backscatter intensity layer, as showed in the previous chapter, to create a backscatter mosaic. We produce the backscatter intensity layer; in

black we has strongest intensity values and in white lowest intensity (Figure 38). The intensity backscatter values relative to the bottom was included in an interval between -56.595 dB and -5.472 dB, with mean of -19.115 dB.

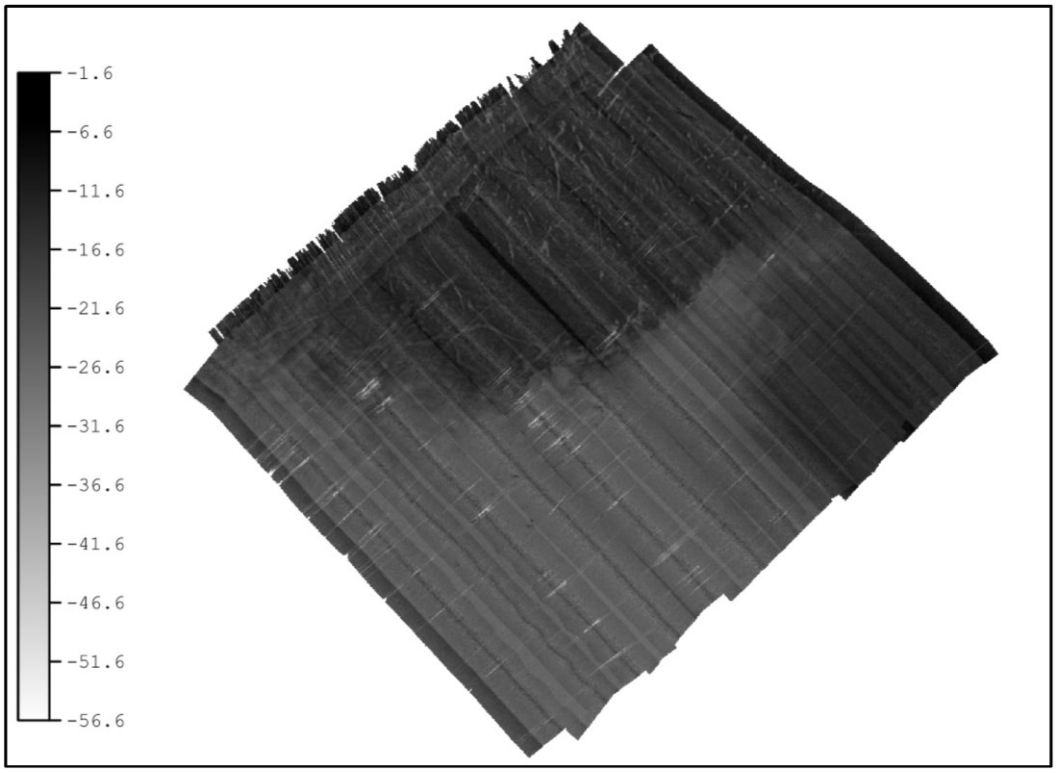

Figure 38 intensity backscatter mosaic

The backscatter intensity data, relative to the seabed, are useful to identify the upper sediment composition – sand, mud, gravel, and also if they are fine, medium or coarse. We need to relate a specific backscatter intensity range to a specific type of target.
Having a look at the diagram in Figure 39, it is possible to understand how the backscatter intensity signal is distributed around two peaks. Plus a diffuse part present on the border area.

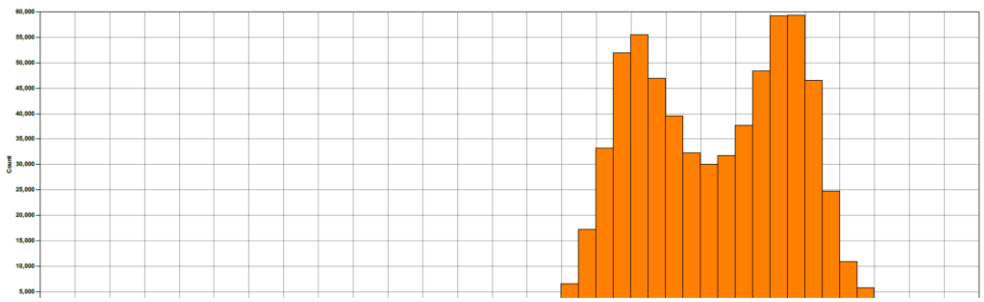

Figure 39 Statistic Intensity Backscatter distribution

As explained in the chapter 2.3, and well summarized in the table 1, the backscatter is influenced mainly by the roughness (in function of the wavelength) and by the property of

the seafloor. This allowed us to identify the areas of possible subsequent investigation through direct sampling of seabed sediment

Bottom sediment sampling

Bottom sediment sampling were obtained with a box-corer (Figure 40) characterized by a stainless box sized 30x20x50 cm working with 125 kg weighted head, and the gravity core SW104 for the recovery of undisturbed sediment-water interface.

Figure 40 box-corer sampling in the Kveithola Trough

Sediment surface description and photographs have been performed on the fresh sediment surface prior to box core sub-sampling. Two comparison charts for textural and colour characterization were placed next to the sampled sediments for photographs.
Immediately we compare with the Munsell color chart, in such a way as to memorize those volatile characteristics such as the color of the sediment due to the oxygenation of the material when in contact with the air (consequently determining a variation in the color). In a second step a measurement was made with the penetrometer on the surface layer (Figure 41).

Figure 41 Penetrometer and description sheet

Down core sediment description were performed on a pre-cut plastic liner (Figure 42). After the description, one half section was analysed for shear strength and subsequently sub-sampled at every 1-cm and stored at -20°C for further shore-based analyses. The second, untouched, half section was instead photographed and stored at +4°C.

Figure 42 two half section of sub-sampling corer

BOX-CORE SUB-SAMPLING

Each box core was sub-sampled as follows:

- n. 1 core of 9 cm ø, stored at +4°C (ENEA);
- n. 1 core of 9 cm ø, stored at +4°C (IIM);
- n. 1 pre-cut core of 9 cm ø, for core description and sub-sampling at 1-cm (OGS);
- n. 2 cores of 4 cm ø, for micropaleontology, living foraminifera and meiofauna, stored at -20°C (UniPI);
- n. 1 stainless cylinder of 7.5 cm3, for the determination of the sediment's density;
- n. 3 surface samples (upper 2 cm), for living foraminiferal study, stored at -20°C (UniPI);
- n. 3 samples at 0-1 cm; 1-5 cm; 5-10 cm, for water content and preliminary textural analyses performed on board ship (IIM);
- n. 3 samples for macrofauna at 0-2 cm; 2-5 cm, 5-10 cm below sea floor in plastic bag stored at -20°C (UnivPM).

On board sediment analyses included the measurement of the shear strength by means of a pocket penetrometer (Table 5), and the determination of sediment bulk density, water content, and mud/sand ratio.

Table 5 example of pocket penetrometer measurements

KVEITHOLA Trough						
	HN17-19BCO-04		HN17-20BCO-05		HN17-21BCO-06	
Depth (cm)	kg	kg/cm²	kg	kg/cm²	kg	kg/cm²
0-2	0.000	0.000	0.100	0.003	0.250	0.007
2-4	0.000	0.000	0.300	0.008	1.200	0.033
4-6	0.400	0.011	0.300	0.008	2.250	0.062
6-8	0.600	0.017	0.400	0.011	3.350	0.092
8-10	1.350	0.037	1.500	0.041	4.000	0.110
10-12	1.900	0.052	1.550	0.043	4.500	0.124
12-14	2.400	0.066	2.500	0.069		
14-16	2.650	0.073	2.750	0.076		
16-18	1.500	0.041	2.900	0.080		
18-20	1.500	0.041	2.800	0.077		
20-22	1.400	0.039	2.900	0.080		
22-24	2.400	0.066	2.950	0.081		
24-26			2.900	0.080		
26-28			2.100	0.058		

The sediment density at the sea bottom surface was determined using a stainless cylinder having a fixed weight and volume (about 7.5 cm^3), here referred as density-cylinder. The density-cylinder was pushed into the sediment surface, weighted and left to dry in the oven for 24 hours at 105°C. The dry sediment was then weighted again and the density was obtained as difference between wet and dry sediments with respect to the sediment (cylinder) volume applying the following equations:

- Bulk density=Ww (weight wet sediment)/Vc (weight density-cylinder);
- Dry bulk density=Wd (weight dry sediment)/ Vc (weight density-cylinder).

Sediment water content and sand/mud ratios were determined for the sediments located at 0-1, 1-5, and 5-10 cm depth. The wet water content was determined as: Ww (weight wet sediment)-Wd (weight dry sediment)]/Ww (weight wet sediment); whereas the sand/mud ratio was obtained by wet sieving at 63 microns.

Sediment core description and the results from the preliminary sediment analyses are reported in a dedicated Sediment sheets (Figure 43).

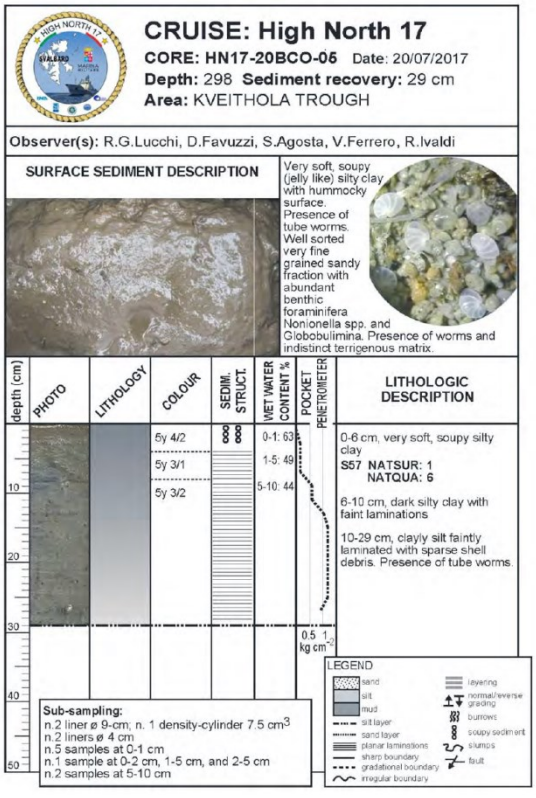

Figure 43 Example of sediment sheet

Water column features mapping

The use of the Water Column (WC) data is possible since few years thanks to the computational capabilities of recent computers. The information stored is relative to the entire column and not only relative to the bottom, which implies a large amount of data.

To this, as a direct consequence, it must be added that the Water Column Imaging (WCI) data processing software is not yet fully mature, given the size of the data files and the limited market demand of the WC data.
Its principle of operation and data extraction are relatively simple; for the bathymetric data, only the information relative to the echo of greater intensity (the bottom) is recorded - while with the WC all the information received while the acoustic signal crosses the water is recorded. The semicircle area thus identified (Figure 44) is called minimum slant range - the shorter radial distance between the sonar transducer and the seabed. The interference due to the side lobes becomes unsustainable once the minimum slant range distance is exceeded. For distances greater than this, the quality of the WC is considerably compromised and makes the measured data unusable.

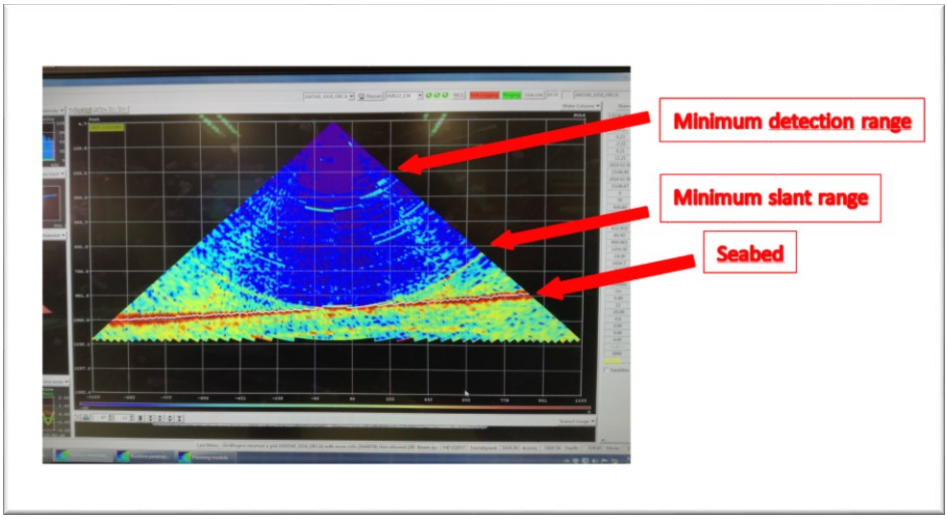

Figure 44 Example of Water Column Image (WCI)

These considerations help us to understand a very important concept: not all the WC signal can be utilized for target detection. There will inevitably be a loss of information along each swath due to the influence of the side lobes and to the physical limits of the minimum slant range curve, with a yield, with respect to the soundproofed area, of about 30%.
As we saw when we extract the bathymetry from acoustic data, we use a time filter in order to select only those signals that comes from the sea bottom. With the water column analysis we leave the multibeam arrays of receiver always in listening. Acting like these, it is possible to collect the acoustic backscattering for all the water column, and reveal the presence of anomalies, like anthropogenic features, fish or other obstacles for acoustic waves. For analyse these types of data we follow essentially three steps on software CARIS: swath editor, subset editor and additional bathymetry visualization.

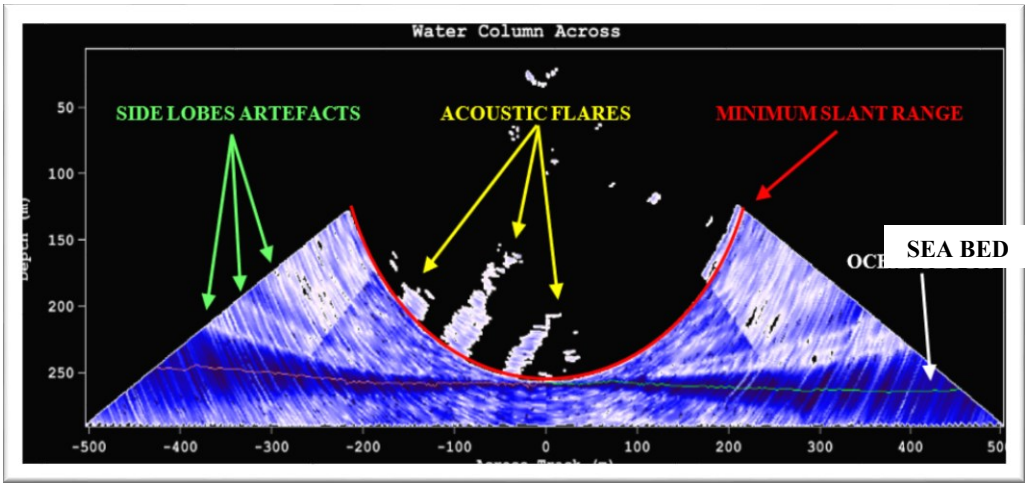

Figure 45 Swath Editor image

Now let's focus on a typical Swath Editor image (Figure 45). This image was obtained selecting a backscatter intensity range between -32 dB and 0 dB. As we can see there are several disturbance coming from the directions far from the nadir of the multibeam. This is due to the mutual interference between the side lobes and the main lobe that create the so called side lobes artefacts. The curve that separate the area affected from the noises and the area not affected is the minimum slant range curve (in red).

This image, permit to understand that all the information acquired by the system at distance greater than the minimum slant are to be considered "not usable" and we have to concentrate our attention in the direction close to the nadir. .

After some experimentations we are confident to say that the useful portion for detection of WC information will be around the 28,5% of the insonified area.

Swath Editor is a tool that help to investigate the water column in a 2D dimension. After we select a track line and activate this tool we can investigate each acoustic swath performed at a certain time. Let's focus on the anomaly showed in Figure 46. Here we can better appreciate the noise due to the mutual interference. On the left we have a 3D image with no filter and on the right an image with a filter for distance greater than the minimum slant range. In the image on the left, we cannot reconstruct the lower part of the acoustic flare, conversely, we clearly notice the missing data in the image on the right. With Subset Editor tool we can visualize the anomalies, previous found with the Swath Editor, in 3 dimensions. The final step of the analysis consists in importing the acoustic data like additional bathymetry and make the computation regarding the dimension of the anomalies and the backscattering intensity. In the Kveithola trough, substantially we found 2 types of target: fish schools and gas plumes.

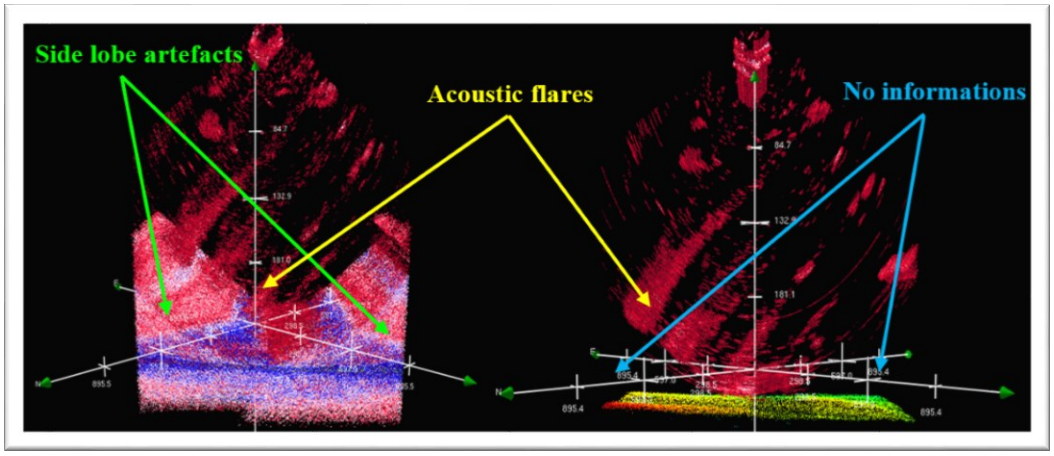

Figure 46 mutual interference and minimum slant range curve

These two types of target could be detected because they have an high response in terms of backscatter intensity. The intensity was considered in a range between -32 dB and 0 dB. When we talk about feature identification we need to speak always in probabilistic terms, we use to say: a probable target. You can have the certain only if you made additional measures in situ.

However, there are characteristics that could give us more confidence in attributing a specific target to our point clouds. In case of fishes, the greatest intensities in terms of backscatter are related to their bladder. Therefore, we could expect a point cloud not very compact but with spaces (Figure 47).

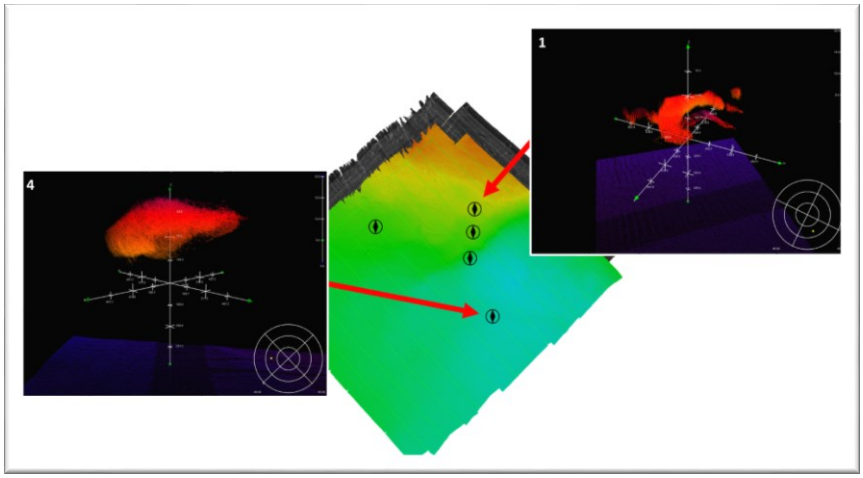

Figure 47 Anomaly 1 and 4 – Fish schools

Also the extension and the depth of the cloud suggest clear that only this type of target, fishes, is possible in water (Figure 48; Figure 49; Figure 50).

Characteristics Anomaly 1

- Vertical length: from 37.272 m to 89.890 m (52.618 m);
- Horizontal length: 148.70 m x 111.37 m;
- Backscatter Intensity: from -31.994 dB to -13.387 dB.

Characteristics Anomaly 4

- Vertical length: from 101.960 m to 157.468 m (55.508 m);
- Horizontal length: 336.32 m x 330.08 m;
- Backscatter Intensity: from -31.994 dB to -10.497 dB.

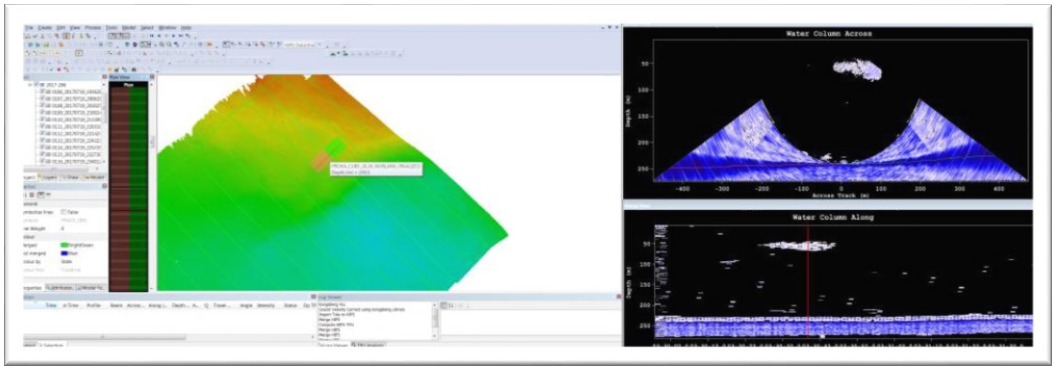

Figure 48 Anomaly 1 - Swath Editor view

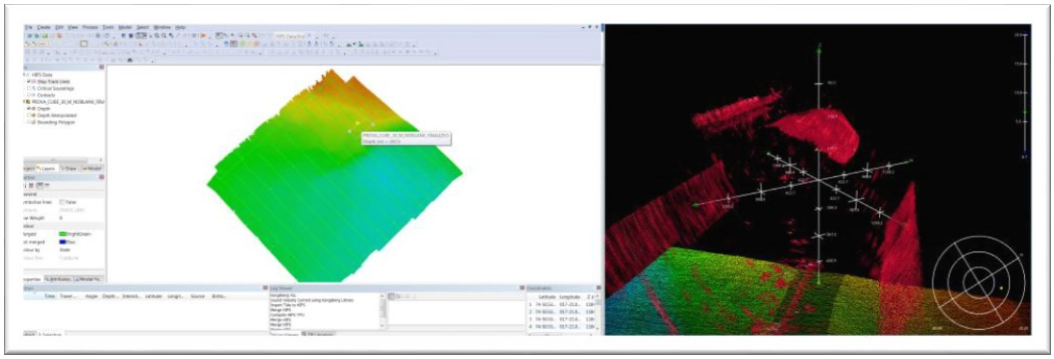

Figure 49 Anomaly 1 - Subset Editor - Water Column

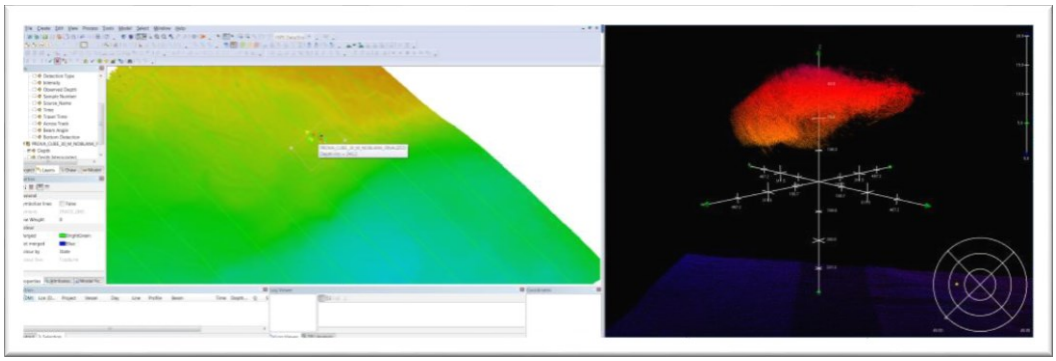

Figure 50 Anomaly 1 - Additional bathymetry view

The other type of target found was gas plumes. In this case the shape of the point cloud help us a lot. The towering form suggest that something was flowing from the seabed. If the water column were not affected by under water currents the plums would have been perfectly vertical (Figure 51). But we know, also from some measure in the area, that an underwater current was affecting the slope of the plumes.

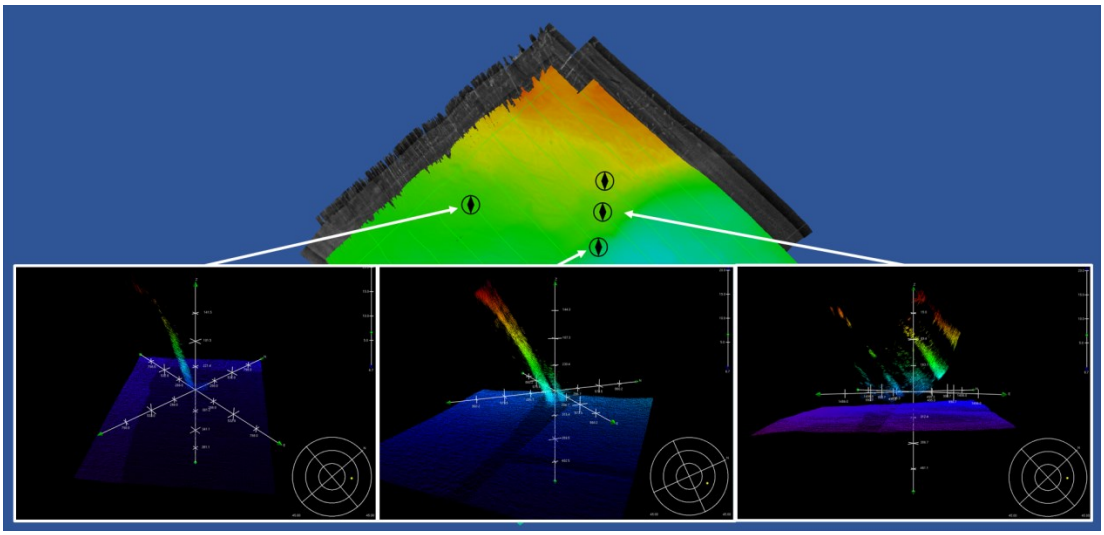

Figure 51 Anomaly 2,3 and 5 – methane gas seeps

Below the characteristics of the three investigated anomalies

Characteristics Anomaly 2

- Vertical length: from 43.732 m to 245.403 m (201.671 m);
- Horizontal length: 325.61 m x 115.22 m;
- Backscatter Intensity: from -31.994 dB to -13.027 dB;
- Depth: 257.6 m.

Characteristics Anomaly 3 (Figure 52 and Figure 53)

- Vertical length: from 102.156 m to 278.772 m (176.616 m);
- Horizontal length: 246.83 m x 57.94 m;
- Backscatter Intensity: from -31.994 dB to -3.947 dB;
- Depth: 290.8 m.

Characteristics Anomaly 5

- Vertical length: from 97.425 m to 255.310 m (157.885 m);
- Horizontal length: 131.94 m x 36.16 m;
- Backscatter Intensity: from -31.994 dB to -8.529 dB;
- Depth: 268.6 m.

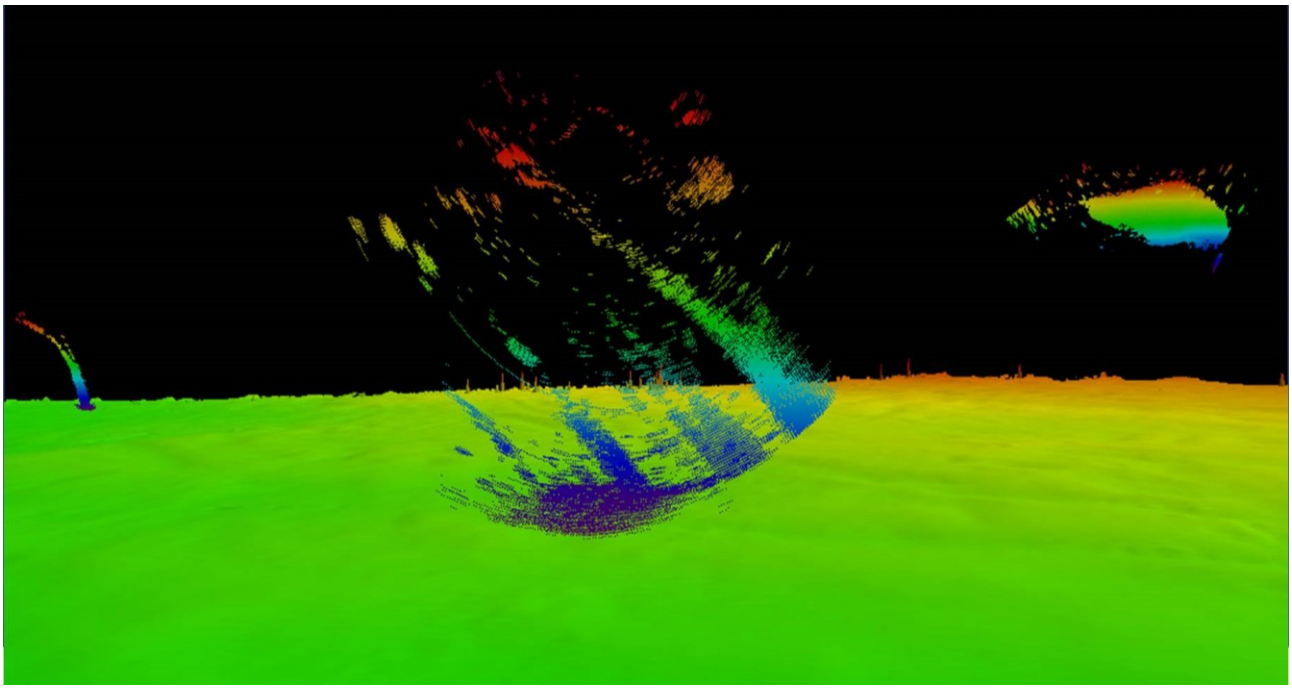

Figure 52 From left to right - Anomaly 3, 5 & 1 – Water column image

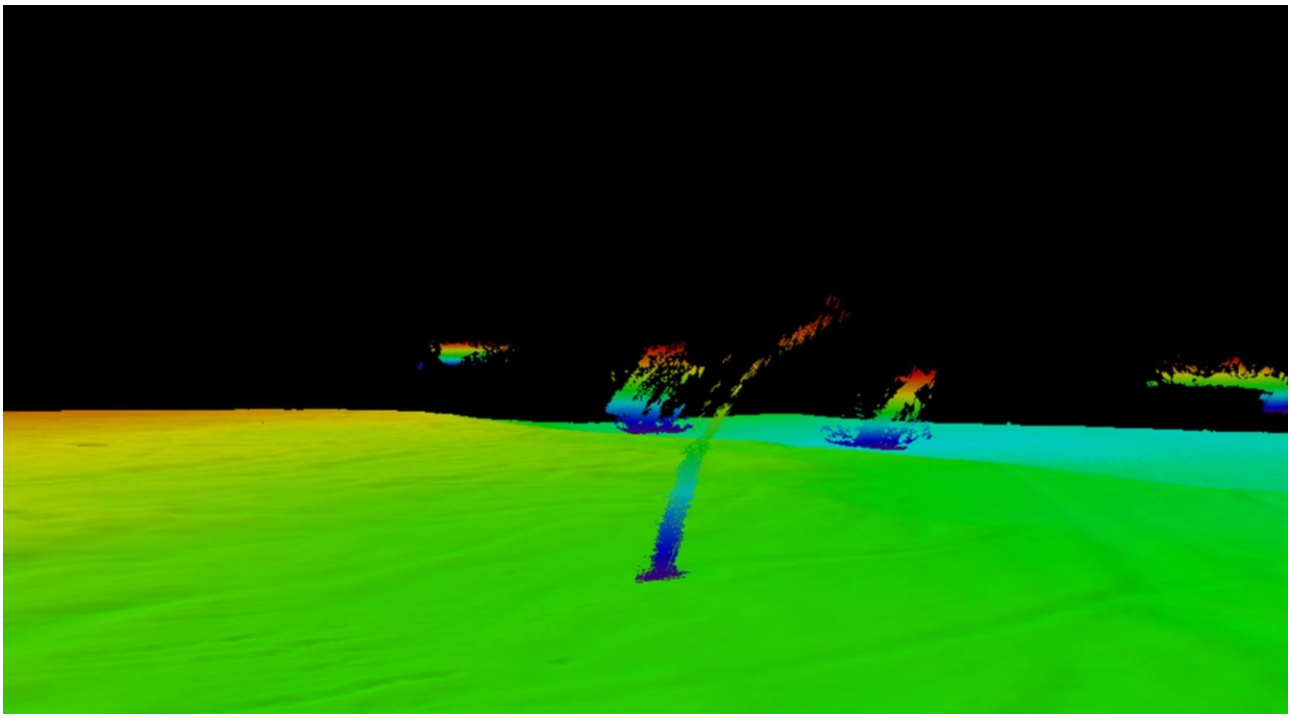

Figure 53 Water column image

3. Remote sensing in support to the REA activity

Observation from the sky has always been very attractive to the scientists. The latter considers remote sensing as a resource with enoumous potentility. For various years, researches and observation methods were based on scientific campaigns conducted in the area of study. The data collection and analysis for the marine environment was led through the usage of conventional equipment, always in the area of interest.
Remote observation, which is generally carried out through sensors transported by satellite or aerial vectors (in the last decade autonomous remotely controlled vehicles – drones – have been used too), opened up new frontiers for research, due to the increased capability concerning spatial resolution and, for the aerial drones, concerning the enhancing of endurance. In some case the "all weather" capability of the embarked sensor, for example, radar satellite sensor, open new chance for the end-user.
The versatility proper of such system and the capability of monitoring ample areas of the earth's surface in minimal timeframes, alongside a reduced logistic effort when compared to the traditional methods, catalyzed a large interest of the scientific community. Science nowadays is increasingly attentive to remote sensing and at the same time, more and more attracted to the observational skills and the great potentiality of the new generation satellites and remote sensing capability.

3.1. Bathymetry from satellite

Generalities

Nowadays, the earth satellite observation and remote sensing, result to be the most powerful instruments for investigation activity and rapid environmental recognition.
Within the REA covert activities, carried out with satellite assets, the multispectral images still represent the most challenging. In particular, satellite multispectral images are used for the determination of the bathymetry in shallow and very shallow water, for monitoring coastal dynamics, to investigate the health status of the coastal vegetation and to study oceanographic and geophysics properties.
The following part of the dissertation let us to describe the various methodologies for the reconstruction of seabed morphology and its characteristics shapes useful for the REA activities.
The light that penetrates the seasurface, in the presence of particular conditions, can propagate itself until it is reflected by the seabottom, then spread again reaching the water-air interface and contributing significantly to the budget of the water-leaving radiance (L_w). This is possible where the depth of the water column is much smaller than the extension of the photic zone or in a coastal context. Starting from this assumption, it is

therefore possible to exploit the images obtained from optical sensors to extrapolate information about the benthic environment.
Over time, the execution of bathymetric surveys with traditional acoustic techniques has been carried out in areas subject to high maritime traffic and in densely populated and usually easily accessible regions. In this way, many coastal areas of remote regions, and difficult to access, still remain unexplored today due to the difficulties inherent in traditional methodologies, but also because of the high costs that such activities would require.
In this context, the idea of being able to determine the bathymetry from images taken by remote passive sensors (satellites, planes, drones), without having to deploy logistical resources that would entail considerable costs, turns out to be one of the solutions that can be pursued to map these remote areas.
At the same time, remote detection techniques are strongly characterized by rapid activities, such as REA operations, where the acquisition of environmental data must be carried out quickly and sometimes with minimal involvement on the ground.
With the development of state-of-the-art multispectral optical sensors, which made it possible to obtain images in an ever-increasing number of bands and significantly higher geometric and radiometric resolutions, it was however possible to obtain high-quality bathymetric data and, therefore, usable for various applications.

Depth estimate methods

When Satellite Derived Bathymetry (SDB) is mentioned, a distinction between the methods that involve a direct or an indirect estimate of the depth must be made. The first ones derive the bathymetric data from the radiance measured by satellite images; the second ones put hydrodynamic processes' study on the spotlight, as they are influenced by the bathymetry, whose variations can reflect a variation of the seafloor itself.
An example of this last type, especially in the REA activity when the estimation of the bathymetry with these empirical methods are sometimes mandatory, is radar bathymetry, which is determined by the height change and the roughness of the sea surface. It is easy to imagine how a sea current, interacting with a variation of the seabed, tends to accelerate or decelerate, hence it will entail a variation for the wave and roughness parameters. We are obliged to point out that this is an "estimation" of the data, even if in some cases it will be sufficient to proceed. The uncertainties of this method and the necessity to precisely know the currents' and the wind's behaviour in the area of interest, make this methodology hardly applicable to the prefixed aims.

Algorithms to calculate bathymetry

Over time, due to the considerable difficulty of defining bathymetry by means of indirect methods and the concurrent improvement of the multispectral embarked sensors, the development of calculation algorithms aimed at estimating bathymetry from radiance data

collected by optical sensors has been favored. These methods are based on different starting hypotheses and assume variable levels of complexity of calculation (Demarte et al., 2007; Ohlendfor et al., 2011; Camacho, 2006).
The fundamental principle of Satellite derived bathymetry is that different wavelengths or frequency of light will penetrate water differently. During the passage of light through the water, the light becomes attenuated by interaction with the water column. The intensity of light after passage length d through water, is given by:

$$I_d = (I_0)e^{(-kd)} \qquad [8]$$

where I_0 is the intensity of the incident light and k is the attenuation coefficient, which varies with wavelength. Equation [8] can be made linear by taking natural logarithms:

$$\log_e(I_d) = \log_e(I_d) - Kd \qquad [9]$$

The Red light will attenuate rapidly in water and does not penetrate further than few decimeters. The blue light penetrates much further and in clear water the seabed can reflect enough light to be detected by a satellite sensor even when the depth of water approaches 30 m.
The depth of penetration is dependent on water turbidity. Suspended sediment particles, phytoplankton and dissolved organic compounds will all effect the depth of penetration and so limit the range over which optical data may be used to estimate depth.

Lyzenga's method

Lyzenga in 1978, on the basis of what has already been stated in the Lambert-Beer law, namely that the light is attenuated exponentially with the increase in the depth and with the wavelength, assuming that the attenuation coefficient of the water is constant throughout the area, he hypothesized a relationship between the observed reflectance R_w, the depth value z and the reflectance of the bottom A_b. This relationship can be expressed as $[10]$:

$$R_w = (A_b - R_\infty)e^{(-gz)} + R_\infty \qquad [10]$$

Where $\mathrm{A_b}$ is the seabed's albedo, $\mathrm{R_\infty}$ is the reflectance of the water column in the deep water and g is the function of the diffusion attenuation's coefficient for the ascending and descending light radiation. From such equation it will be possible to derive the depth [11]:

$$Z = \frac{1}{g}[ln(A_b - R_\infty) - ln(R_w - R_\infty)] \qquad [11]$$

The estimate of the depth starting from a single band using the equation described above will however depend on the bottom albedo. In fact, a decrease in the albedo due to the type of the bottom involves an increase in the estimated depth.

The validity of this relationship is therefore limited only to the case in which its dependence on the bottom albedo is canceled: this is obtainable only in the areas with a homogeneous bottom.
In 1985 Lyzenga showed that the use of two bands, could provide a correction for the variation in the type of the seabed. Starting from the equation he had previously developed, he stated the following relationship [12] where $X_i \, and \, X_j$ represent the different *i* and *j* bands :

$$Z = a_0 + a_i X_i + a_j X_j \qquad [12]$$

Where [13]:

$$X_i = ln[R_w(\lambda_i) - R_\infty(\lambda_i)] \qquad [13]$$

The constants $a_0, a_i \, and \, a_j$ are usually determined thanks to multiple linear regressions.

Jupp method

This method is composed by two sequential phases: calculation of the DOP zone (Depth of penetration zone) for each of wavelength available, interpolation of the depth within the DOP zone. This method is essentially based on the principle that radiations of different wavelength are attenuated in a different way, hence they will extinguish at a different depth
The method of Jupp (1988) has three critical assumptions::

a) the light is exponentially attenuated as the depth increases;
b) the water attenuation coefficient (k) is considered constant on the whole image;
c) the seabed's albedo (or reflective property of seabed) remains constant on the whole image.

Such depths (where the attenuation doesn't permit the seabed reflection) will constitute the limit depth for the determination of the DOP. The depth calculation Z, is made through the usage of the following equation [14]:

$$z(depth) = \sum_{i=1}^{N} \frac{ln(L_e)_i}{-2k_i N} - \sum_{i=1}^{N} \frac{ln(L_b)_i}{-2k_i N} \qquad [14]$$

Where L_e is the radiance measured by the sensor, N is the number of spectral bands taken into account and L_b is the seabed's radiance.

Ratio method

An important limitation of the linear algorithm (equation [11]) is that it does not account for changes in seabed albedo or, in other words, changes in bottom type (e.g. a benthic environment covered in dark grass versus one covered in white sand). The major part of the

errors introduced by the previous algorithms is generated by the incapacity of distinguishing the various kinds of the seabed. Such incapacity of distinguishing the different seabed albedo prompted the researcher Richard P. Stumpf to develop a new technique that could overcome the problem. This new algorithm is based on the different absorption ratios of the different visible wavelengths.As stated in the previous paragraph (expression [8] and [9]), as the depth increases, the intensity of the blue and green bands will diminish with different values of observed reflectance $\ln(R_W)$, which has the higher absorption (green), will diminish quicker than $\ln(R_W)$ of the band with the lower absorption (blue). Consequently, the ratio between the two factors will increase with increasing sefloor depht.

Analyzing the algorithm of the ratio, it can also be shown how it implicitly compensates for the problems related to the variability of the type of seabed analyzed. In fact, while a variation in the type of seabed affects both bands taken into consideration in a similar way (W.D. Philpot 1989), a variation in depth has a greater influence on the high absorption band. Consequently, the variation in the ratio due to the depth is much greater than that caused by the variation in the type of seabed albedo, suggesting that different types of seabed placed at the same depth will have the same ratio. The estimated depth will be independent of the variation of the bottom type and will only require a ground truthed calibration with the true data.
Thus, the depth will be:

$$Z = m_1 \frac{ln(nR_w(\lambda_i))}{ln(nR_w(\lambda_i))} - m_0 \qquad [15]$$

Where m_1 is a calibration constant to scale the ratio to the depth, n is a fixed constant for every area (which is chosen so that the logarithm argument is always positive and the ratio will be linear with respect to the depth) and m_0 is an offset for the 0 m depth (Z=0).
Under these conditions, the calibration of the ratio method, and therefore the determination of the three values just mentioned, can be carried out by comparing the estimated data with the ground truth value (Lidar depth, singlebeam or even derived from nautical charts).

3.2. Photogrammetric analysis from aerial drone

Generalities

What has been observed so far about light propagation in the atmosphere and in the water, through different means of transmission and instances of propagations, has been important to understand and proceed with the study of the bathymetry through multispectral satellite images. However, technological developments and the reduction of camera's size, will shortly allow to get multispectral sensors on unmanned vehicles too. Hence, the theory developed for satellites will be usable also for light vehicles flying a few

dozens of meters away from the sea surface. The technological developments of the last years in the field of the RPAS (Remotely Piloted Aircraft Systems) has brought to the market reliable and stable air vehicles, which makes them suitable for photogrammetric evaluations. The reduction of size of the sensors has made possible to install them on RPAS, overcoming their limit of having a low transportable payload. As of now, the industry is strongly investing in the usage of such means in the agricultural and terrestrial field, leaving behind the segment dedicated to the marine sector, which penalised the development of RPAS for the use in the coastal/littoral environment.

Principles of photogrammetry

Photogrammetry is the survey technique that allows to obtain metric and geographic information, alongside shape and position of three-dimensional objects, such as lands and buildings. This is possible thanks to the elaboration of geo-referred digital photo. It can be used with excellent results in the instance of very extended surveys, obtaining a metrically complete model, which corresponds to the reality. In digital photogrammetry, which is now more popular than the traditional one, there are two different geometric ways of taking a photogrammetry picture. The first one is “central geometry” (the most used, as it is easy to elaborate the captured images) and the “complex geometry” (which makes a linear scansion or a swinging mirror). Once the image acquisition is done, it is necessary to undertake a process of reconstruction of the geometries, analytically made taking advantage of the application of a rigorous mathematic model.
The final aim of the photogrammetric surveys is to generate one or more products between the ones listed below:

- Orthophoto: pictures in which, through the rigorous reconstruction of the three-dimensional geometric model, the positioning errors due to the capture mode or to the irregularity of the terrain’s morphology (when it is not ascribable to a flat surface) are corrected;
- Mosaics: union of single adjacent images. If such product is obtained by putting together multiple orthophoto, it will then be defined orthophoto mosaic;
- Topographic charts: planimetric charts accompanied with altimetric information, which is possible to report with point or line with precise level or altitude;
- thematic charts: they are the graphic representation of how certain territorial themes vary.
- Three-dimensional models of the terrain: DTM (Digital Terrain Model), DSM (Digital Surface Model).

Photograms and systems of reference

In the photograms there is a rigorous central perspective of the represented objects, where the centre of projection coincides with the centre of the photo. Aerial photogrammetry uses photogrammetric cameras mounted on aerial vehicles, which can frame the territory,

this allowing to reconstruct the geometry of the objects represented on it. The traditional photogrammetric process can be summed up in three fundamental phases:

- Acquisition and storage of the images;
- Orienting the images and reconstruction of the three-dimensional model through stereoscopic techniques
- Returning, which is the measurement of the object and the formalization of its dimensional characteristics.

The central perspective geometry, represents the operative fundamental of photogrammetry. Such approach allows to acquire photograms of very big dimensions, which are instantaneously generated through a unique geometrical scheme for the represented space object. This means that any object point (any point belonging to the photographed object) has a corresponding image point (point of the image acquired through photogrammetric image), univocally determined by transformation laws, whose parameters are the same for any point, and whose point bind the two spaces, object and image. The determination of such parameters constitutes the operation of photograms' orientation.

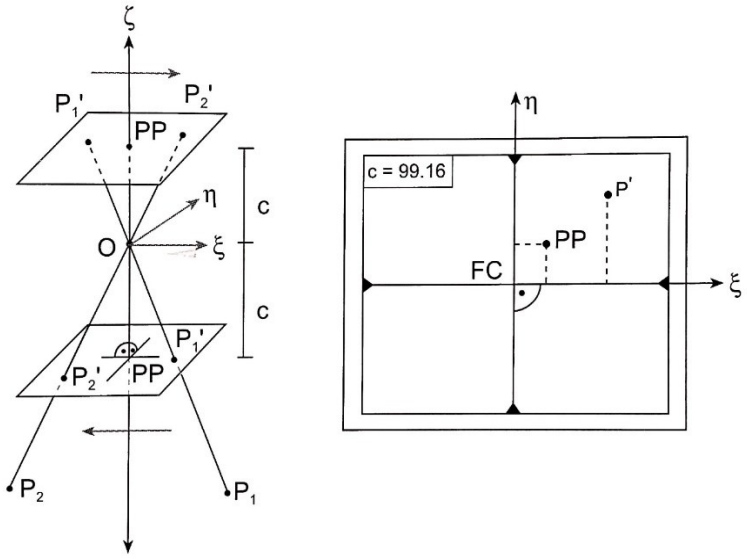

Figure 54 Internal system reference (from Kraus, Pfeifer ,1998)

The image space (Figure 54), is individuated by its own system of reference with ξ and η axes and origin in the principal point PP, individuated as intersection on the image plane of the straight lines linking the fiducial mark.

The coordinates ξ_0, η_0 of the principal point PP and the main distance c (also called focal distance), locate the position of the projection centre on the image plane and define the internal orientation of the photogram

The coordinates X_0, Y_0, Z_0 of the center of the image, in relation to the system of reference and the three angles of rotation ω, ϕ, κ that individuate the camera's asset in the moment of the capture, define the external orientation of the photogram (Figure 55). Where ξ, η, ζ

are the image coordinates, x, y, z are the coordinates in a local system and, finally, X, Y, Z are the coordinates in the object system (or terrain coordinates).

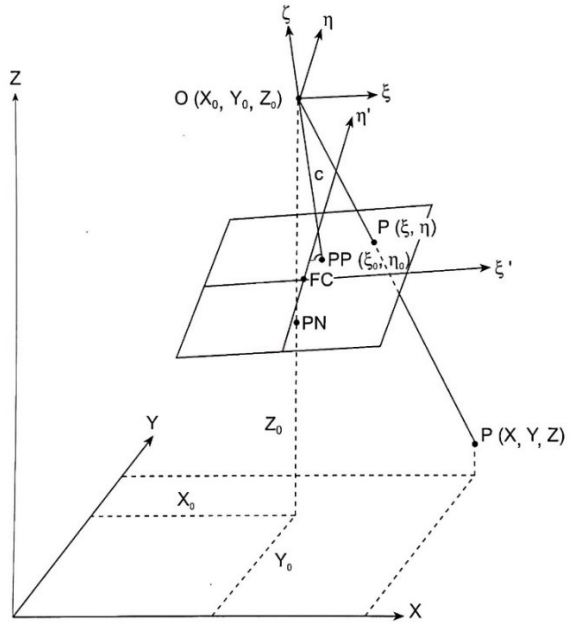

Figure 55 Relation between coordinates of image points and object points (from Kraus, Pfeifer ,1998)

In this way, for the reconstruction of the geometry of the capture of a photogram nine parameters are needed, whose determination can take place in different ways. The internal orientation of the parameter, being constant and relative to the photogrammetric camera in use, are supplied by the manufacturer in the calibration certificate.
The external orientation parameters can instead be determined in two main ways:

- directly, undertaking measurements of asset and positioning, coinciding in the moment in which the photogrammetric capture is done;
- indirectly, with the auxilium of know points on the ground, also called ground control point, that allow to orient the photogram in the elaboration phase.

In any given case, the photogrammetric process, is based on the possibility of putting in relation the image coordinates ξ, η, ζ and the object coordinates X, Y, Z. These relations [16], [17], [18], [19], that take advantage of the nine points of internal and external orientation, are the so called collinearity equations:

$$\xi = \xi_0 - c\frac{r_{11}(X-X_0)+r_{21}(Y-Y_0)+r_{31}(Z-Z_0)}{r_{13}(X-X_0)+r_{23}(Y-Y_0)+r_{33}(Z-Z_0)} \qquad [16]$$

$$\eta = \eta_0 - c\frac{r_{12}(X-X_0)+r_{22}(Y-Y_0)+r_{32}(Z-Z_0)}{r_{13}(X-X_0)+r_{23}(Y-Y_0)+r_{33}(Z-Z_0)} \qquad [17]$$

$$X = X_0 + (Z - Z_0)\frac{r_{11}(\xi-\xi_0)+r_{12}(\eta-\eta_0)-r_{13}c}{r_{31}(\xi-\xi_0)+r_{32}(\eta-\eta_0)-r_{33}c} \quad [18]$$

$$Y = Y_0 + (Z - Z_0)\frac{r_{21}(\xi-\xi_0)+r_{22}(\eta-\eta_0)-r_{23}c}{r_{31}(\xi-\xi_0)+r_{32}(\eta-\eta_0)-r_{33}c} \quad [19]$$

The angular asset parameters of the capture (ω, ϕ, κ) are intrinsic in the coefficients r_{ik}, that constitute the elements of spatial rotation matrix R, defined as it follows [20]:

$$R_{\omega,\phi,\kappa} = \begin{pmatrix} cos\,\phi\,sin\,\kappa & -cos\,\phi\,sin\,\kappa & sin\,\phi \\ cos\,\omega\,sin\,\kappa + sin\,\omega\,sin\,\phi\,cos\,\kappa & cos\,\omega\,cos\,\kappa - sin\,\omega\,sin\,\phi\,sin\,\kappa & -sin\,\omega\,cos\,\phi \\ sin\,\omega\,sin\,\kappa - cos\,\omega\,sin\,\phi\,cos\,\kappa & sin\,\omega\,cos\,\kappa + cos\,\omega\,sin\,\phi\,sin\,\kappa & cos\,\omega\,cos\,\phi \end{pmatrix} [20]$$

Where the rotations ω, ϕ, κ have to be meant as around the axes X, Y, Z and will be defined as:

ω: primary rotation, or transversal rotation

ϕ: secondary rotation, or longitudinal rotation

κ: tertiary rotation, or careening

The direct equations highlight that for each object point there is a unique image point, while through the inverse equations it is possible to deduct that for each image point there are infinite object points dependant on Z. Thus, starting from a single photogram, it is not possible to reconstruct the three-dimensional geometry of the object contained within.

The application of such mathematic model to the real case, still has to face the approximations that force the adoption of measures appropriate to reduce the divergences of the theoretical model. In particular, it is of paramount importance to take into account the errors introduced by the photogrammetric complex, formed by:

- camera
- objective
- photogram

For this reason, curves of average calibration for the radial and tangential distortion are normally calculated, in order to correct the projection error due to a misalignment of the spherical lenses of the objective, bringing back the real geometrical model within the allowed error margins.

Plan of flight

A photogrammetric survey is based on a plan of flight that is previously established, and it is composed by :

- navigation plan
- a document with all the specifics of the acquisition

The navigation plan contains all the routes (Figure 56) and the flight's heights. For the determination of the routes to follow, it has to be taken into account that a flight proceeds

by adjacent lines, which to say a sequence of photograms along the flight trajectory.

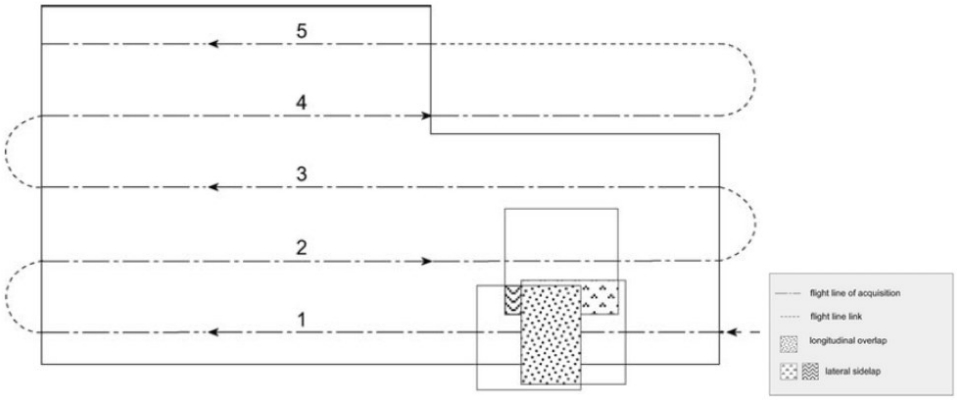

Figure 56 example of flight plan with a representation of flight line of acquisition with lateral sidelap and longitudinal overlap

The routes must be defined in a way that respects the overlapping requirements which are essential to obtain a good stereoscopic reconstruction. Generally, longitudinally adjacent photograms must have an overlapping of 60-70%, while transversally adjacent photograms must have an overlapping of 20-30%. In such a way, beside guaranteeing the stereoscopy, the continuity of data and the possibility of aerial triangulation is secured too. The complete flight plan, beside the flight specifics, it also has useful information for the survey and the specifics of acquisition sequences. In Table 6, some geometrical parameters useful for redacting the flight plan.

Table 6 Geometrical parameters that address the flight plan redaction

Photogram's scale	$m_b = h/c$
Photogram's side on the ground	$S = s * m_b$
Base on the photogram	$b = B/m_b$
Relative flight height	$h = c * m_b$
Absolute flight height	$Z_0 = h + Z$
Logitudinal covering (%)	$l = 100 * \frac{S-B}{S} = 100 * (1 - \frac{B}{S})$
Transversal covering (%)	$q = 100 * \frac{S-A}{S} = 100 * (1 - \frac{A}{S})$
Coverage area of the photogram	$F_b = S^2 = s^2 * m_b^2$
Base for a covering (%)	$B = S * (1 - \frac{1}{100})$
Interaxle between adjacent sequences of photograms for transversal covering	$A = S * (1 - \frac{1}{100})$
Number of models for each adjacent sequence of photograms	$n_m = \left[1 + \frac{L}{B}\right]$
Number of photograms for each adjacent sequence of photograms	$n_b = n_m + 1$
Number of adjacent sequence of photograms each block	$n_s = [1 + \frac{Q}{A}]$
Area covered by a model	$F_n = (S - B) * S$
Increase of usable area for each model	$F_n = A * B$
Shutter click interval (sec)	$\Delta t = \left(\frac{B[m]}{v\left[\frac{m}{s}\right]}\right) \geq 2.0$

where:

c: focal distance	Q: width of the block
s: side of the image at the edge	Z: average height of the terrain
L: length of the adjacent sequences of photograms and of the block	v: speed of the aircraft on the ground [m/s]

Restitution techniques

The third dimension, can be obtained starting from images in case there is a binocular view (just like human eyes), which is a necessary condition for the stereoscopic reconstruction. In photogrammetry, the capture of the same scene from two different point of views (or projection centres) allows then to obtain a three-dimensional vison of the observed object. The conditions that need to be met, in order to allow stereoscopy, are summed up below:

- the single images used for the stereoscopic vision must cover, at least partially, the same area; the stereoscopic effect will be possible only in the part shared by both the photograms;
- the flight height must be constant in order for the photograms to have the same scale
- the capture's axes must be as parallel as possible
- the ratio between the capture base b and the distance between observed object and capture centre (h) must generally be 1/2 - 1/3

For the purpose of stereoscopic reconstruction, it is important to define the homologous points: they are the representation of the observed object on different images and, thanks to the determination of the horizontal parallax of the homologous points, it is possible to extract the altimetric coordinate or the depth coordinate of the point itself. The geometry of the capture needs to be reconstructed to carry out the photogrammetric restitution. It is then fundamental to correctly orientate the photograms and to correctly structure the collinearity equations. The problem can be overcome in different ways.

In an ideal instance, the generation of the model should take place in a direct way, taking advantage of the data gained by satellite systems (GPS, GLONASS etc..) and of the asset data coming from inertial platforms (INS/IMU). Such information would not only allow to position the capture centre, but also to fully georeferencing the acquired images.

Traditional photogrammetry, instead, takes advantage of ground control points, points whose object coordinates are known. Through such points it is possible to reconstruct the geometric model and to georeferentiate the photograms.

In this case, the orientation of the photograms can take place in different ways, in function of the procedure chosen, by orientating a single photogram, a stereoscopic pair or a photogrammetric block.

Hence, this will result in:

- orientation of a single photogram, in the event in which the orientation of the two

photograms, forming a stereoscopic model, is determined in an independent way, relying on different anchor points. In this case it will necessary to determine six external orientation parameters of the single photogram, then there will be six collinearity equations. This method then requires the knowledge of at least three plano-altimetric points in which the object coordinates (X, Y, Z) are known, and the image coordinates will be measured;

- simultaneous orientation of the photograms in a phase. It requires the determination of twelve variables through the determination of a system of twelve collinearity equations;
- two steps orientation, which requires the formal separation of the equations, in order to preventively align a photogram in comparison to another (relative orientation). After that, the whole photogrammetric block will be orientated through the usage of a much smaller number of anchor points, compared to the number necessary for the other above-listed methods.

In the specific case in which a photogrammetric flight is made, when there is the need to orientate n models, corresponding to n stereoscopic pairs, in order to reduce the number of anchor points required, the method of aerial triangulation is used. Hence, the collinearity equations are not applied to the single model, but to the whole photogrammetric block.
The most used aerial triangulation in the photogrammetric sphere is the one of block compensation with independent blocks (Figure 57).
Such technique has the aim of determine the terrain coordinates of unknown points, starting from a sufficient number of junction point, and a low quantity of anchor points.

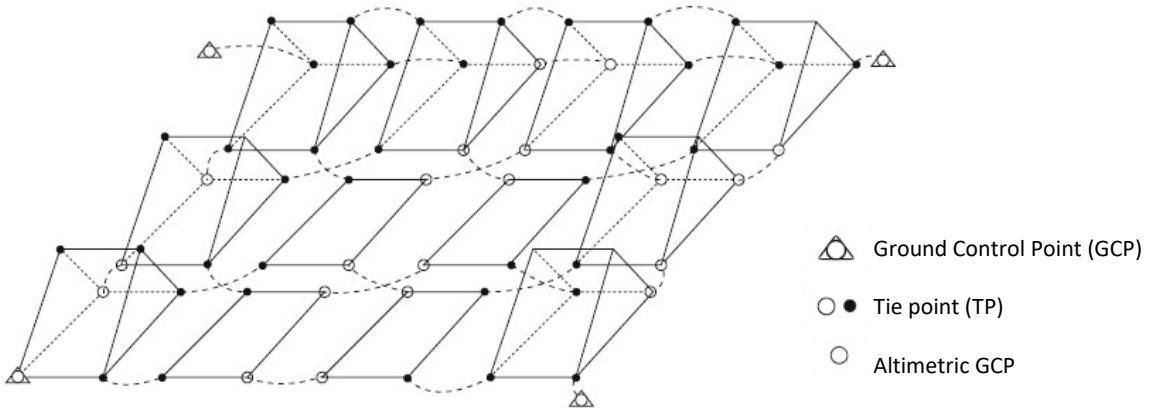

Figure 57 Conceptual scheme of compensation for independent model

The junction point, will allow to concatenate the single models, hence they will have to be chosen in a way that they will result to belong to more subsequent models.
The anchor points, are instead needed to correctly orientate the block itself, in relation to the terrain system, through compensations procedures of least squares, with the aim of determining the object coordinates of each represented point.

Specifics of the utilized instrumentation

The Remotely Piloted Aircraft System COLIBRI' has been used In order to conduct the photogrammetric survey, and it is constituted by the following main components:

- Ground Control Station (GCS), which is the user interface in charge of the system management;
- Flight Termination System, that allows to interrupt the flight in case there is a fault with the system
- Multi-rotor aircraft with four propulsors, with autopilot and data-link
- Payload subsystem, composed by a series of sensors installed on the aircraft, with the function of conducting the survey.

Specifically, the photogrammetric payload installed on the aircraft consists in:

- Optic sensor: digital camera NIKON COOLPIX A
- Tir sensor: FLIR VuePro640
- GNSS sensor TOPCON B110

The digital camera NIKON COOLPIX A is equipped with:

- CMOS APS-C 23.6 x 15.7mm sensor; 4928x3264 pixel
- fixed optic lens 18.5 mm

For the photogrammetric applications the camera is used in manual focus mode , as an automatic focus could produce a variation of the main distance between the various photograms acquired during the capture process.

The thermic camera FLIRVuePro is equipped with a 10.880 mm x 8.704 mm sensor, with a resolution of 640x512 pixels and able to detect the range of TIR frequencies between 7.5 µm and 13.5 µm. Furthermore, it has a focal opening of 9 mm with an opening of 69° x 56°. The camera allows the direct recording of the positions in the exif data of the taken images, and it manages the main settings through the dedicated application FLIR UAS.

The GNSS TOPCON B110 sensor, is a ultracompact satellite receiver able to provide the user with highly precise positioning data. Such precision varies in function of the chosen settings, from sub-metrics to sub-centimetric magnitudes, gainable, respectively, with a DGPS or a RTK setting.

The TOPCON B110 receiver supports the reception of GPS and GLONASS signal in the frequencies L1, L2, L2C, and the reception of the SBAS-QZSS corrections in the frequencies L1 and L2C form the WAAS, MSAS and EGNOS systems. In the below Table 7, the accuracies relative to the various possible configurations are reported.

Table 7 Satellite Posistion System Accuracy

Configuration	Accuracy
Standalone	H: 1.2 m; V: 1.8 m
DGPS	H: 0.3 m; V: 0.5 m
SBAS	H: 0.8 m; V: 1.2 m
Static	H: 3 mm + 0.5 ppm x baseline; V: 4 mm + 1.0 ppm x baseline
RTK	H: 10 mm + 1.0 ppm x baseline; V: 15 mm + 1.0 ppm x baseline

For the detection of the GCPs (Ground Control Points), which are necessary for the indirect georeferencing of the photogrammetric block, a receiver GNSS TRIMBLE TSC3 has been used, a receiver that is able to provide positioning data with a precision in the region of the centimeters.

Photogrammetric elaboration

The software DRONE2MAP was used for the photogrammetric elaboration, which allowed the reconstruction of the model of the area taken into consideration. Moreover, it enabled the extraction of the products subsequently elaborated in QGIS. After the upload of 266 RGB pictures, deriving from the A and B flights, the positioning file created with the PDM software has been uploaded, with the aim of geolocating the pictures taken (Figure 58).

Figure 58 Drone track and sequences of picture acquired

Afterwards, the GCPs' file was uploaded (used for the anchor points in the georeferencing of the model), containing the id numbers of the GCPs and their relative coordinates, reported in the system EPSG 32632. The utilized checkpoints' data has been detected through the GPS TRIMBLE TSC3 receiver and then converted in UTM 32 coordinates through the CONVERGO software (Table 8).

Table 8 UTM32 converted position

N. GCP	Latitudine	Longitudie	Altitudine
2	4916007,465	474928,935	7,62
3	4916010,851	474930,37	7,556
4	4916007,921	474924,232	7,648
5	4915994,179	474915,603	7,821
6	4915981,639	474914,662	7,673
7	4915964,069	474900,686	7,754
8	4915947,89	474887,482	7,899
9	4915945,511	474880,255	7,969
10	4915936,291	474876,465	8,03
11	4915920,526	474859,863	8,122
12	4915919,959	474853,562	8,166
13	4915906,558	474844,551	8,31
14	4915894,041	474830,61	8,429
15	4915880,404	474815,364	8,545
16	4915866,029	474800,64	8,682
17	4915837,883	474775,116	8,741
18	4915834,83	474775,437	8,617
19	4915839,228	474771,407	8,885
20	4915833,546	474766,463	9,029
21	4915832,452	474761,85	9,177
22	4915873,401	474817,392	6,559
23	4915869,028	474814,28	1,866
24	4915862,838	474813,459	1,151
26	4915928,912	474864,759	8,118

As it is impossible to uniformly detect GCPs within the whole investigated area, the GCPs have only been detected along the cycling path and the part of beach in loco, as in the image below (Figure 59)

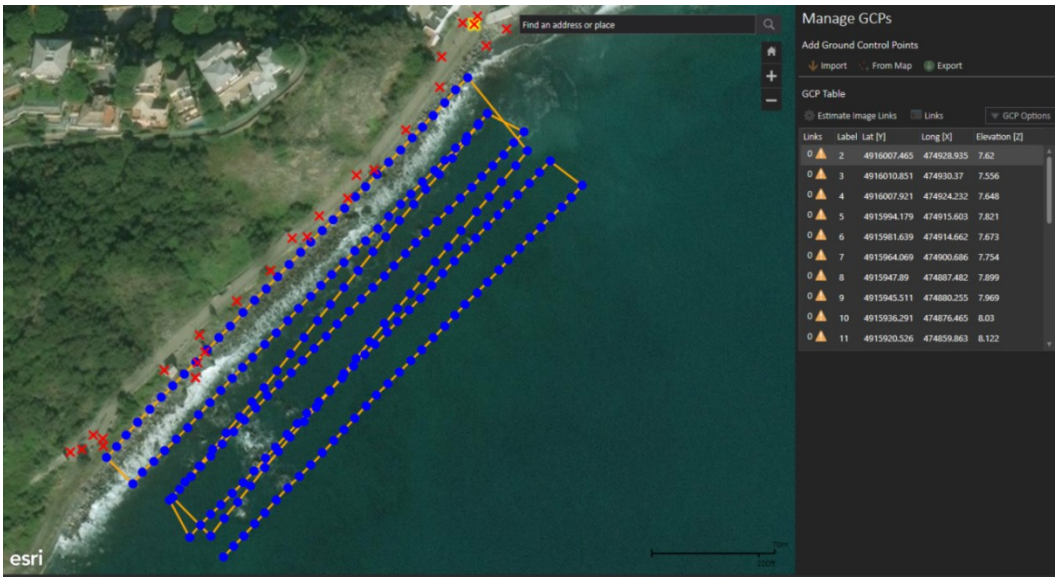

Figure 59 GCP marked by red crosses

Once the GCPs file has been uploaded, the individuation of those within the photograms was then undertaken, followed by the photogrammetric reconstruction. At the end of the photogrammetric elaboration, the following products have been created

- Points' cloud (Figure 60) made of 9.524.705 points and with a density of 891.31 points each cube meter, was built using the parameters in the Table 9.

Figure 60 Points' cloud

Table 9 Summary parameter

Image Scale	multiscale, 1/2 (Half image size, Default)
Point Density	Optimal
Minimum Number of Matches	3
3D Textured Mesh Generation	yes
3D Textured Mesh Settings:	Resolution: High Resolution Color Balancing: yes
LOD	Generated: yes
Advanced: 3D Textured Mesh Settings	Sample Density Divider: 1
Advanced: Image Groups	group1
Advanced: Use Processing Area	yes

- 3D Model (Figure 61)

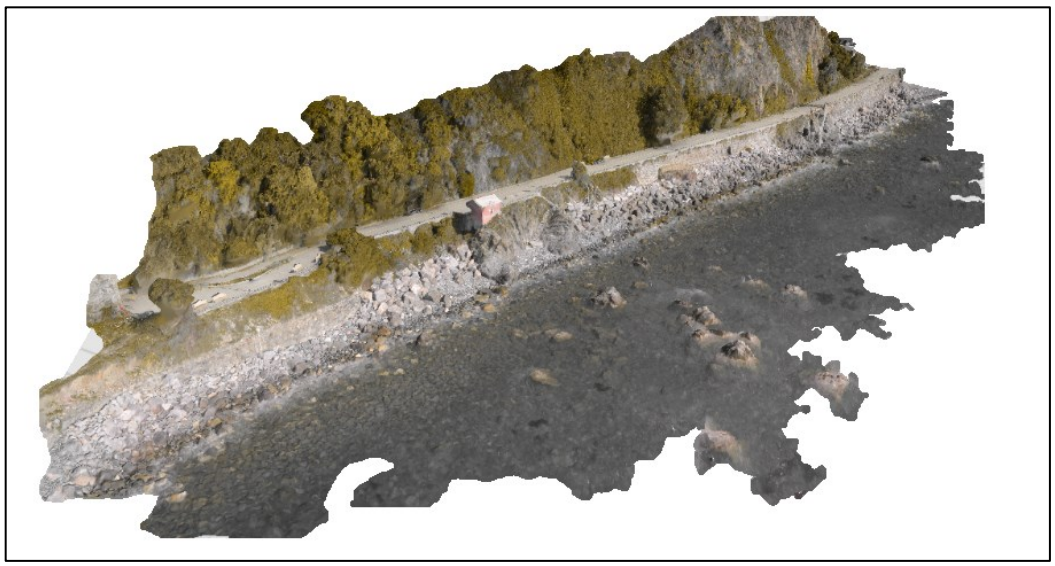

Figure 61 3D model

- Digital Surface Model and Orthomosaic (Figure 62)

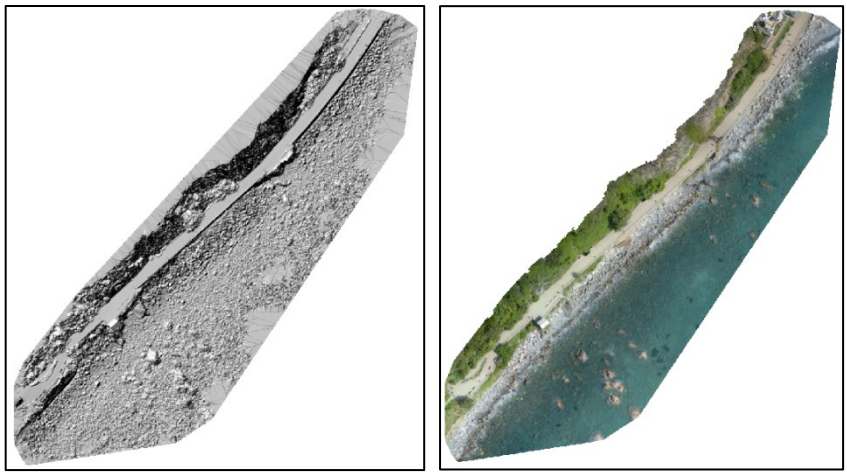

Figure 62 DSM and Orthomosaic

The elaboration of the infrared images was made following a similar process. Such images have been used to generate a IR orthomosaic (Figure 63) In this instance it has not been possible to run an indirect georeferencing through GCPs, as, the lower resolution of the IR pictures compared to the RGB ones, has made the identification of the detected GCPs impossible.

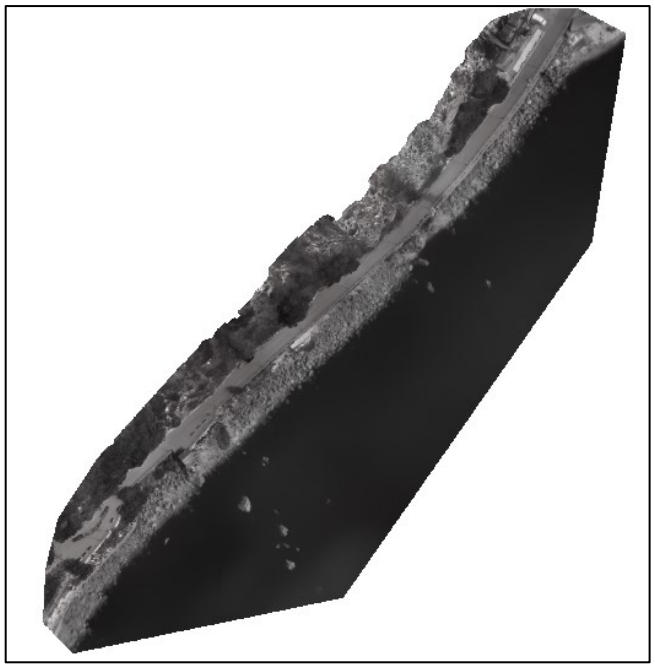

Figure 63 Infrared Orthomosaic

4. Concluding remarks and future perspectives

I would like to start this “concluding remarks chapter", remembering that in the "De bello Gallico", Gaius Julius Caesar exalted the studies conducted by his men on the tides and currents in the English Channel. This study was used to modify the construction of their ships and mainly adapting their strategies to the environmental conditions.

His passage represents perhaps one of the oldest citation of an environmental study aimed at reducing and mitigating, the impact of environmental conditions on human activities.

The study carried out on the innovative REA tools for the seabed mapping, during the three years of the doctorate, lead me to explore the double aspects of the investigation methodology and of the instrumentation. I then associated them with the production of the final documents and charts, an aspect that is often underestimated but which is of fundamental importance, especially in emergency situations, where the output is analyzed by decision-makers who are not necessarily technicians and experts.

In chapter one, I have introduced the concept of rapid environmental assessment, the so-called "REA", useful to frame the use that is made with the REA activity and to define the different types of products. As we saw in the first chapter, the concept of REA activity, are applied equally to all human rescue operations, search and rescue at sea, but also to the study of a particular geographical area after a natural disaster. There are many real cases or training activities in which I found myself applying the concepts of "REA support", for activities related to real calamitous events or simple exercises. Below, following a very simple path, some "finished" products are shown, ready to be used as a decision-making base or to be supplied to the competent body, in order to identify the different action strategies.

In the second chapter, I have moved on the description of the acoustic seabed mapping methodology, starting from the underwater acoustic principles, passing through the acoustic backscatter classification method, arriving at the frame of my doctorate, the study of an automatic process of seafloor classification based from the acoustic backscatter.

Finally, the third chapter is dedicated to the remote sensing applied to the REA activity in terms of satellite-derived bathymetry (SDB), reconstruction of Digital Elevation Model (DEM) through the use of satellite images and an aerial drone.

I have concentrated my analysis to the study of the backscatter and the possibility of characterizing the seafloor using the MBES tool, as I explained during the chapter on backscatter and seafloor mapping, the study allowed me to develop a multiparametric system tool and to arrive to set an automatic process for seabed classification. The multiparametric analysis process, at present, has the only limit of the "imagination" of the operator and the computing capacity of the computer systems available. In the

experimentation conducted over the years we started with 3 correlated parameters, we studied the behavior of the backscatter associating equal responses and correlating them with the parameters of depth and roughness (Figure 24 at page 48). But this is only the beginning of the study, it will soon be expanded, introducing other variables, for example, the tilt and the presence of particular typical features. All these parameters can contribute to the unique identification of the seabed classes and therefore can lead to a virtuous process of automation for the acoustic seabed classification. In Figure 64 it can be seen how the system clearly shows a concrete sewer pipeline laid on the seafloor. In addition, the tool is been able to associate the material in a unique way, even where it was covered by other transported sediments.

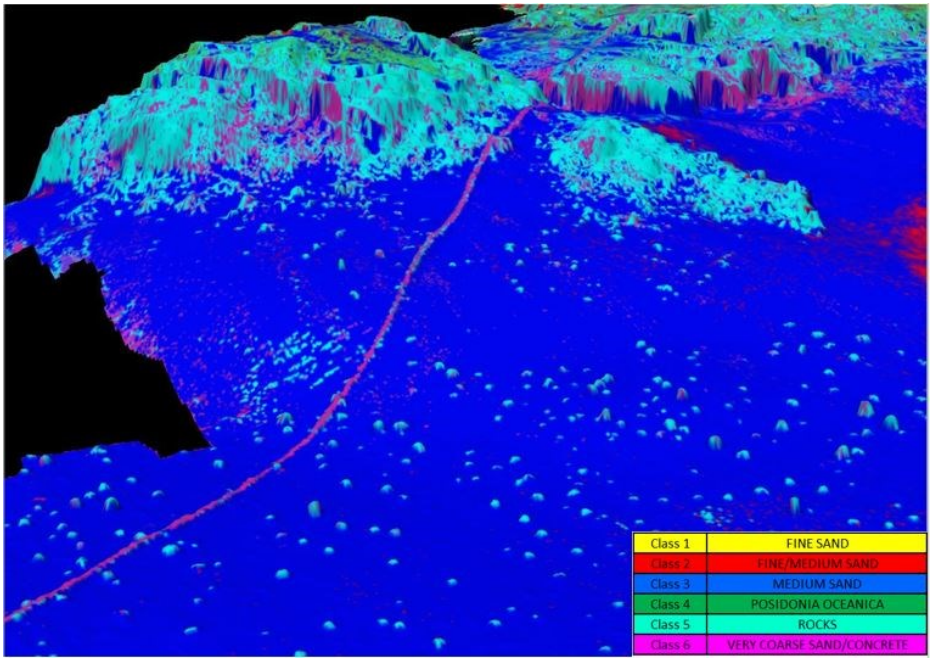

Figure 64 3D Seabed surface model with backscatter data - evidence of sewer concrete pipeline

In particular, the monoparametric classification has been carried out during the survey operations applying the K-means clustering algorithm, the multiparametric classification (backscatter, depth and roughness) was performed after the rapid analysis of the samples (acoustic data, sediment samples and ROV-videos) following the monoparametric classification. We are able to characterize, in an automatic process, until 6 classes with different MBES frequency and type. This capability to identify the type of sediment for which it was calibrated has raised the level of use of the MBES data exponentially, up to the use of this methodology even for the search of specific objects lied on the seafloor. The method requires an initial phase of setting up a "library", calibrated with the in-situ samples or visual identification. The library and the final characterization are unique to the system and are not affected by the general conditions of use or other "local" parameters.

Associated with the development of the Acoustic Seabed Classification, I have introduced the second use of backscatter in exploration and REA activities. The study aimed at optimizing the use of backscatter information in the water column exploration. As seen in the dedicated chapter, this tool is used in all those exploration and research analyzes along the water column, from the experiment conducted in Kveithola Trough (Figure 65), where we studied the leakage of methane gas from the sea bottom and the presence of schools fish and plankton up to use of the water column analysis technique for monitoring sensitive and strategic areas, such as offshore platforms, extraction wells or underwater pipelines.

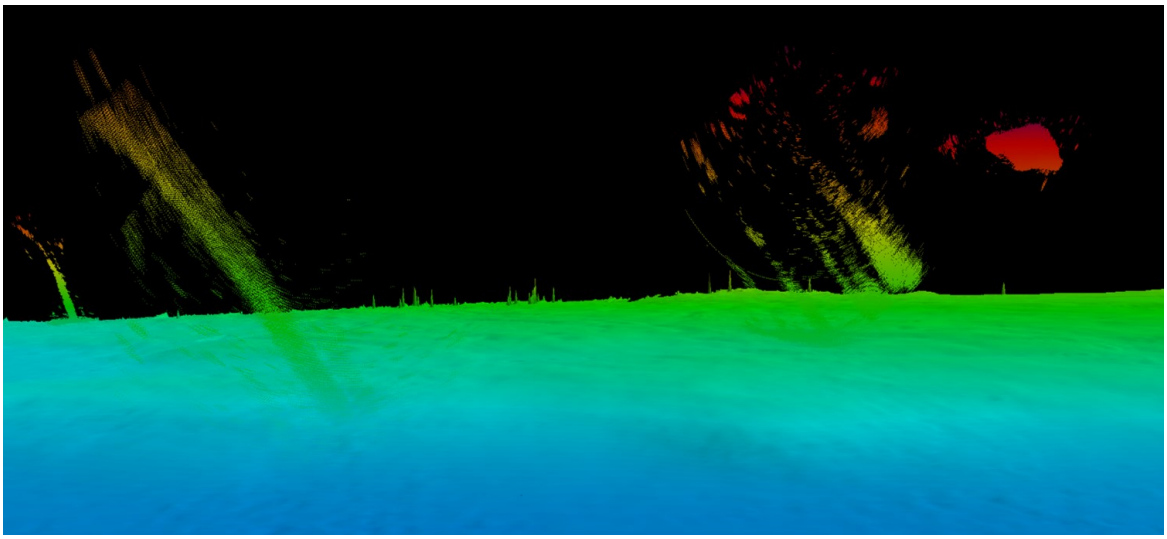

Figure 65 Kveithola – 3D seafloor and water column model using acoustic backscatter with methane flares and school fish from the seafloor in the water column.

In the Kveithola activity, thanks to the combination of using hardware and software with fully capacity, we were able to create many different products such as: bathymetric survey, backscatter mosaic and SBDAREAs for the seabottom classification and 3D maps for the water column image – using only one type of system, the MBES.

The Water Column with the high performance computer, represent the future of the Multibeam system and mapping along the all water masses. With a proper database of acoustic response for different types of targets we could, for example automatically identify the nature of acoustic anomalies and create thematic 3D maps. Another possible application of water column data is the implementation of Water Column 3D maps in the next generation of Electronic Nautical Charts (ENC) thanks to the new S100 international standards family. With this standards we could load on a single ENC multiple layer, not only the bathymetry and the nature of the seabed, but also 3D maps of acoustic anomalies in the water column, salinity, temperature, oxygen and many other types of parameter. Comparing the multiple layer, it will be easier to completely understand the processes that usually took place at sea. The use of MBES and the backscatter applications highlight the multidisciplinarity of the instrument and the polyhedral use of the acoustic data.

The REA activity at sea, eighter for emergency reaction plan, then military activity or pollution emergency and preparedness plan, can't be conducted, nowadays, without the use of MBES and its' acoustic backscatter products.

The principal product from which we start to use the MBES remains the morphobathymetric study of the area, with aims that can range from emergency intervention to establish changes occurring to the seabed but also to the realization of an operational product which helps to establish from boats an emergency escape route from an unsafe area. Figure 66 shows the example of a tactical chart simulating the abandonment of a seaside resort by the sea, following an emergency on the ground. The activity required an REA study of the area, the post-processing of bathymetric data, weather analysis and sea state forecast. In the REA activity, the ability to represent on the screen or paper chart all the information necessary to make the decision with the correct information without forgetting nothing and given the correct importance to all parameters is an added value.

The survey in Figure 66 requires about 6 hours of work with a nautical vessel equipped with interferometric MBES, in additional 6/10 hours were used for data analysis and post-processing. The production of charts was conducted strictly connected with the person in charge of emergency activities. One of the most important principles in the preparation of REA reports and documents is in order to define the standard to use and make it as simple and comprehensible as possible In the image above left, we see the representation of the coast affected by the evacuation, with a bathymetric model. On the right side, there are the binding conditions for emergency rescue boat based on the maximum draft, the estimated height, the wavelength present in the area and, knowing the characteristics of the vessel, the depth under the keel (underkeel clearance).

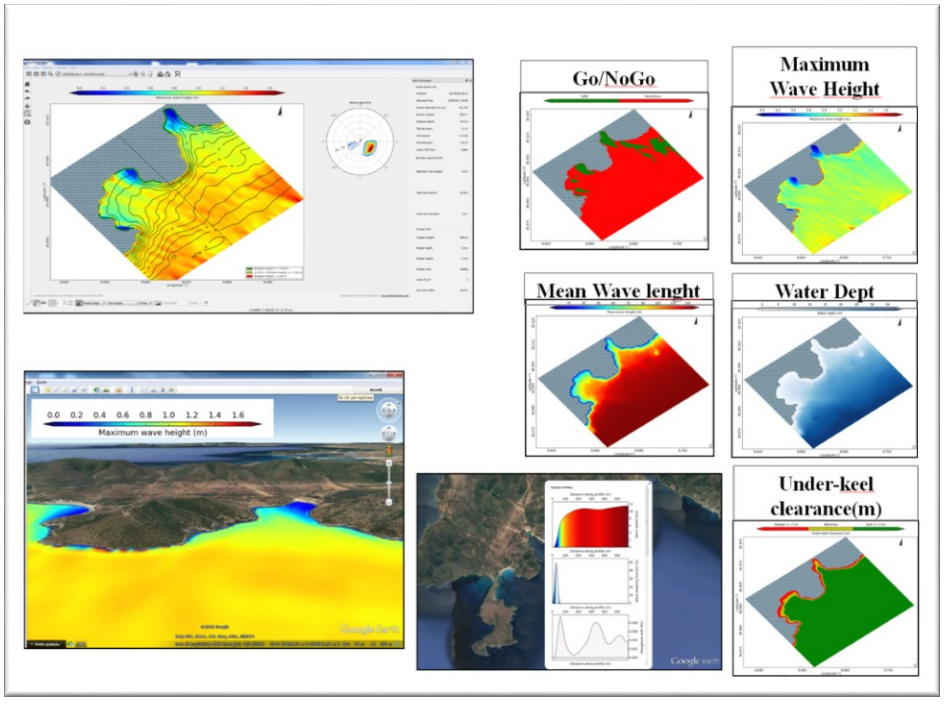

Figure 66 Teulada Gulf - Tactical chart for rescue operation

All made more intelligible with a wide use of GO/NOGO traffic light representations.
In conclusion I could say that using a single instrument – the multibeam echo sounder – it is possible to create different products like bathymetric maps, backscatter mosaic and detect anomalies in the water column. We could say that nowadays, the MBES is the most complete acoustic system for underwater investigations and in the meanwhile for the REA characterization activity.
Finally, for a complete littoral REA characterization, as can be seen from the description of a REA activity in the first chapter, it's necessary to complete the required information adding related Digital Elevation Model (DEM) and/or digital information like Infrared signature, digital visible (RGB) or Multispectral image and more else. In the third chapter of my research, I focused on the use of remote sensing, exploiting the major applications. In the three years, we have set-up an Office and trained personal as aerial drones pilot, equipped with the photogrammetric camera, in the visible spectrum and an IR video-camera. This activity allowed us to complete the overall picture of a REA survey, inserting images, in the visible spectrum (Figure 67), in the infrared (Figure 68) and managing the three-dimensional models of the terrain.

Figure 67 3D model molded on HD visible image

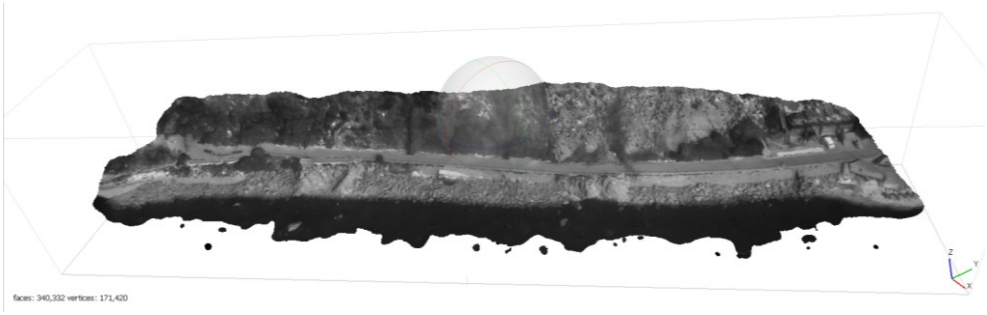

Figure 68 3D model molded on Infrared Image

This capability allowed us to reconstruct, with clouds of points, structures and buildings for a deep study. The following example concerned the study of a coastline, with the production of the topography to the adequate scale and a three-dimensional model for the analysis of possible criticalities on the emerged structures.

I conclude these remarks with the presentation of one tactical chart, in which all the elements discussed during the three-year doctorate are highlighted.
In Figure 69 a REA product is given to characterize a beach, used for landing rescue teams, carrying materials and personnel. The survey was conducted in about 6 hours, and other 6/10 hours was needed to analyzed the ground truth, including the seabed information and producing the aerial image drone reconstruction for a portion of the littoral area, to allow the operators to be easily oriented.

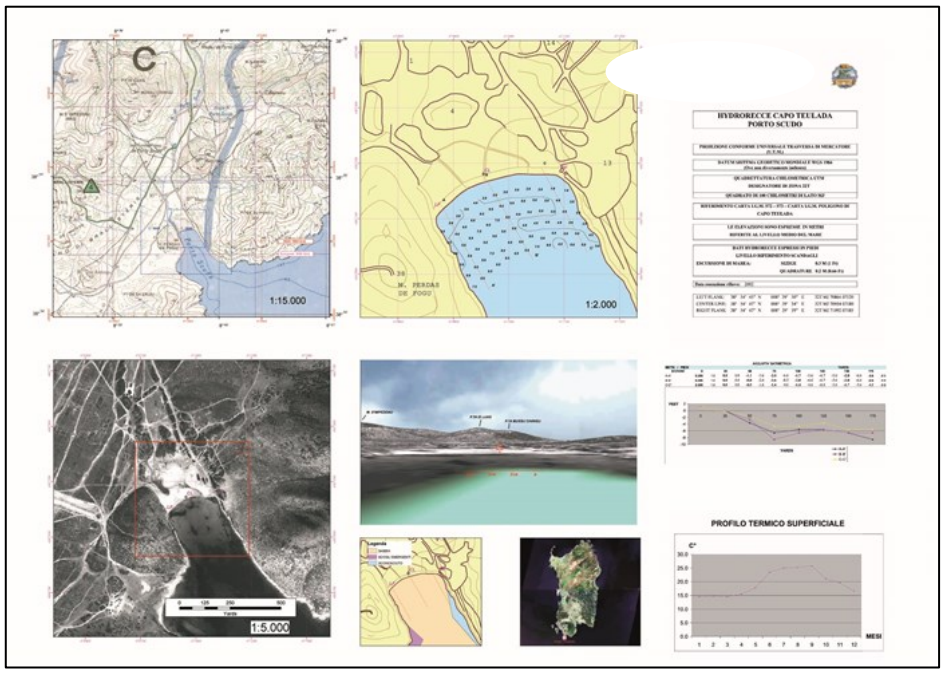

Figure 69 Capo Teulada – REA based map (from Italian Hydrographic Office)

The future perspective of the argument of my thesis could be divided by two, the near future, in which I will continue to develop the acoustic backscatter automatic detection and in the meantime the use of RGB image captured by aerial drone and, in just a bit longer time, in which I expect to have better performance by multispectral camera onboard aerial drone to perform better resolution at sea, in a very shallow water.

The steps forward, in the acoustic backscatter automatic detection, will soon lead to the implementation of other parameters to define better the classes, with more details, paying attention to the structural limit of the system. At the moment we use three parameters, backscatter, depth and roughness. Our study is directed towards the identification of a fourth variable, the slope of the seafloor linked with the grain size of the sediment, to create a fourth layer of the hierarchic classification.

Another fundamental activity that I will continue to develop will be the estimation of the seafloor from aerial drone images, with the developing of video cameras able to acquire multispectral images and new methodology to process the images. The study conducted is aimed at finding data acquisition methodologies, both geophysical and geospatial, exploring the new frontiers in terms of vectors/equipment and instrumentation to be used,

also in terms of planning the different phases of the project. Particular interest was the integration of different disciplines and instrumentation to achieve a complete 3D mapping, that combines the atmosphere, the surface, the water column and finally the characterization of the seabed and its first substrate, all integrated into the concept of Rapid Environmental Assessment.

References

Ainslie M.A., McColm J.G. (1998), A simplified formula for viscous and chemical absorption in sea water. The Journal of the Acoustical Society of America, 103, Issue 3, 1671-1672.

Alevizos E., Snellen M., Simons D., Siemes K., Greinert J. (2018), Multi-angle backscatter classification and sub-bottom profiling for improved seafloor characterization. Marine Geophysical Research, 39, Issue 1-2, 289-306.

Anderson J.T., Van Holliday D., Kloser R.,Reid D.G., Simard Y. (2008), Acoustic seabed classification: current practice and future directions. ICES Journal of Marine Science 65, 6, 1004-1011.

APL-UW High-Frequency Ocean Environmental Acoustic Models Handbook (1994), Defense Technical Information Center, 210 pp.

Asian Development Bank (2003), Environmental Assessment Guidelines, 165 pp.

Bartholoma A. (2006), Acostic bottom detection and seabed classification in the German bight, southern North sea. Geomarine letters 26, 177-184.

Blondel P., Murton B.J. (1997), Handbook of Seafloor Sonar Imagery. Wiley Praxis Series in Remote Sensing, 336 pp.

Boudouresque C.F., Meinesz A. (1982), Découverte de l'herbier de Posidonie. Parc National de PortCros. Parc Naturel Regional de la Corse, Cahiers 4, 79 pp.

Brown C.J., Blondel P. (2009), The Application of Underwater Acoustics for Seabed Habitat Mapping. Applied Acoustic - Craig, 70, 10, 1241-1370.

Brown C.J., Beaudoln J., Brissette M., Gazzola V. (2017), Setting the stage for Multi-Spectral Acoustic Backscatter Research. R2 Sonic White Paper, 1-13.

Bush D.M., Neal W.J., Young R.S., Pilkey O.H. (1999), Utilization of geoindicators for rapid assessment of coastal-hazard and mitigation. Ocean and Coastal Management, 42, 647-670.

Camacho M.A., (2006), Depth analysis of midway atoll using Quickbird multi-spectral imaging over variable substrates. Calhoun - Naval Postgraduate School, http://hdl.handle.net/10945/2674, 92 pp.

Clark J.R. (1996), Coastal Zone Management Handbook. Lewis Publisher, CRC Press LLC, 670 pp.

Collier J.S., Brown C.J. (2005), Correlation of sidescan backscatter with grain size distribution of surficial seabed sediments. Marine Geology, 214, 431-449.

CoNISMa, (2006), Inventario e cartografia delle praterie di Posidonia nei compartimenti marittimi di Manfredonia, Molfetta, Bari, Brindisi, Gallipoli e Taranto. Crisma edizioni, 23 pp.

De Falco G., Tonielli R., Di Martino G., Innangi S., Simeone S., Parnum I.M. (2010), Relationship between multibeam backscatter, sediment grain size and *Posidonia oceanica* seagrass distribution. Continental Shelf Research, 30, 1941-1950.

de Moustier C., Alexandrou D. (1991), Angular dependance of 12 kHz seafloor acoustic backscatter. The Journal of the Acoustical Society of America, 90, 522-531.

Deidda M., (2009), Impiego di immagini satellitari per il monitoraggio della dinamica costiera. ResearchGate, Paper, 10 pp.

Demarte M., Di Giorgio G., Di Vasta P., Ivaldi R., Surace L. (2009), Sviluppo di un modello REA nella caratterizzazione morfodinamica di un litorale. Atti 13a Conferenza Nazionale ASITA, 991-996.

Demarte M., Di Vasta P., Ivaldi R., Milli M., Surace L. (2008), Acquisizione di parametri morfodinamici di una spiaggia. Atti 12a Conferenza Nazionale ASITA, 1125-1130.

Demarte M., Nardini R., Marro M., Peluso C., Ivaldi R. (2018), A multiparametric method for the classification of the seabed from acoustic backscattered signal. IEEE International Workshop on Metrology for the Sea; Learning to Measure Sea Health Parameters (MetroSea), Bari, Italy, 150-155.

Demarte M., Vitti F., Flore F., Simeone E. (2007), Batimetria costiera con immagini satellitari multispettrali ad alta risoluzione. Atti 11° Conferenza Nazionale ASITA, 188, 6 pp.

Demirbas A. (2010), Methan as Hydrates. London: Springer Science & Business media, ISBN 1848828721, 186 pp.

Dolan M.F.J., Grehan A.J., Guinan J.C., Brown C. (2008), Modeling the local distribution of cold-water corals in relation to bathymetric variables: Adding spatial content to deep-sea video data. Deep Sea Resarch, Oceanographic Research Papers (part1), 55, Issue 11, 1564-1579.

Doxani G., Papadopoulou M., Lafazani P., Pikridas C., Tsakiri-Strati M. (2012), Shallow-water bathimetry over variable bottom types using multispectral worldview-2 image, XXII ISPRS Congress, 159-164.

Eiden E.J., Landmark K. (2013), acoustic seabed classification using QTC IMPACT on single beam echosounder data from the Norwegian channel, Northern Nord-sea. Continental Shelf Research 68, 1-14.

Elhegazy H. (2011), Gas Plumes analysis using Multibeam EM710 Water Column Image in Saint John River, Directed Research II, 1-34,

Ellingsen K.E., Gray J.S., Bjornbom E. (2002), Acoustic classification of seabed habitats using the QTC View system. ICES J. of Marine Science, 59:pp. 825-835.

Fish J.P., Carr H.A. (2001), Sound Reflections: Advanced Applications of Sdescan Sonar Data. Lower Cape Publishing, 272 pp.

Fonseca L., Mayer L. (2007), Remote estimation of superficial seafloor properties trough the application angula range analysis to multibeam sonar data. Marine Geophysical researches, 28, 119-126.

Freitas R., Silvia S., Quintino V., Rodrigues A.M., Rhynas K., Collins W.T. (2003), Acoustic seabed classification of marine habitats: studies in the western coastal-shelf area of Portugal. ICES Journal of Marine Science 60, 599-608.

Guinan J.C., Grehan A.J., Dolan M.F.J., Brown C. (2008), Quantifying relationships between video observations of cold-water coral cover and seafloor features in Rockall Trough, west of Ireland. Marine Ecology Progress Series, 375, 125-138.

Harris P.T., Baker E.K. (2012), Seafloor geomorphology as benthic habitat. Elsevier, 890 pp.

Huang J.D., Jackson D.W.T., Cooper J.A. (2002), Morphological monitoring of high energy beach system using GPS and total station techniques, Runkerry, Co. Antrim, Northern Ireland. J. of Coastal Research, 36, 390-398.

Hughes Clarke J.E., Danforth W., Valentine P. (1997), Areal seabed classification using backscatter angular response at 95 kHz. SACLANTCEN Conference on High Frequency Acoustics in Shallow Water, Conf. Proc. Ser., 45, 243-250.

IHO-International Hydrografic Organization (2000). IHO Transfer Standard for Digital Hydrographic data, S – 57. International Hydrographic Bureau, 3.1, 114 pp.

Innangi S. (2014). Analisi del segnale di backscatter da Ecoscandaglio Multifascio (EMF) in ambiente marino: applicazioni per lo studio dei fondali e delle risorse ittiche pelagiche in 3D. Università Ca' Foscari Venezia, Tesi di dottorato di ricerca in scienze ambientali BIO/07, ciclo XXVI, 66-105.

Istituto Idrografico della Marina (2012), Porto Isola del Giglio – Bathymetric chart – Costa Concordia Emergency – scale 1:1200.

Istituto Idrografico della Marina (2012), Porto Isola del Giglio – Bathymetric chart – Costa Concordia Emergency – scale 1:1500.

Istituto Idrografico della Marina (2015), Capo Teulada – Porto Scudo – Hydrorecce –– scale 1:2000 – 1:5000 – 1:15000.

Ivaldi R., Demarte M., High North team (2017), High North cruise report, Arctic Marine Geophysical Campaign, Genova Istituto Idrografico della Marina, I.I. 3180, 1-70.

Ivaldi R., Demarte M., Surace L. (2009), Beach morphodynamic parameters in the development of Rapid Environmental Assessment. Geophysical Research Abstracts, Vol. 11, EGU2009-11365-2.

Jackson D., Richardson M. (2007), High Frequency Seafloor Acoustic. Springer, NY, 616 pp.

Kasalos J.G. and Chayes D.N. (1983), A portable system of ocean bottom imaging and charting, Proc. Oceans 83, 649-656.

Kelly C. (2005), Guidelines for rapid environmental impact assessment in disaster. CARE International Benfield Hazard Research Centre, University College London e Cooperative for Assistance and Relief Everywhere, Inc. (CARE), 4.4, 99 pp.

Kinsler L.E., Frey A.R., Coppens A.B., Sanders J.V. (2000), Fundamentals of acoustic, 4th Ed. John Wiley & sons, 560 pp.

Kraus K., Pfeifer N., (1998), Determination of terrain models in wooded areas with airborne laser scanner data. ISPRS Journal of Photogrammetry and Remote Sensing, 53 (4), 193-203.

Kvenvolden K.A., (1993), Gas Hydrates – geological perspective and global change. Reviews of Geophysics, 31 (2), 173-187.

Leblanc E., Foster B. (2015), New algorithm for multibeam imagery processing, Marine Technology: Whitepapers and special reports, 2 pp.

Lurton X. (2010), An introduction to underwater acoustic: principles and applications. 2nd Ed., Springer Praxis Books & Praxis publishing, UK, 346 pp.

Lurton X., Lamarche G. (2015), Introduction to backscatter measurements by seafloor-mapping sonars. In: Backscatter measurements by seafloor- mapping sonars - Guidelines and Recommendations, Lurton X. and Lamarche G. (Eds)., Geohab report, Chapter 1, 11-24.

NATO (2000), Maritime Rapid Environmental Assessment – Concept of Operations – NATO pubs, MCM-051-00, 215 pp.

NATO (2014), Hanbook of Military Oceanographic Information Services – ATP32, 180 pp.

Mazzullo J., Graham G.A. (1988). Handbook for shipboard sedimentologists. Ocean Drilling Program, Texas A&M University, Technical Note 8, 68 pp.

McCarthy E.M., Sabol B.(2000), Acoustic characterization of submerged aquatic vegetation: military and environmental monitoring applications. Proceedings of OCEANS 2000 MTS/IEEE Conference & Exhibition,3, 1957–1961.

Medialdea T., Somoza L., Leon R., Fàrran M., Ercilla G., Maestro A. Casas D., Llave E., Hernandez-Molina F.J., Fernandez-Puga M.C., Alonso B. (2008), Multibeam backscatter as a tool for seafloor characterization and identification of oil-spill in the Galicia Bank. Marine Geology 249, 93-107.

Micallef A., Le Bas T.P., Huvenne V.A.I., Blondel P., Hühnerbach V., Deidun A. (2012), A multi-method approach for benthic habitat mapping of shallow coastal areas with high-resolution multibeam data. Continental Science Research, 39-40, 14-26.

Mitchell G.A., Orange D.L., Gharib J.J., Kennedy P. (2018), Improved detection and mapping of deepwater hydrocarbon seeps: optimizing multibeam echosounder seafloor backscatter acquisition and processing techniques. Marine Geophysical Research, 39 (1-2), 323-347.

Montereale-Gavazzi G., Roche M., Lurton X., Degrendele K., Terseleer N. and Van Lancker V. (2017), Seafloor change detection using multibeam echosounder backscatter: case study on the Belgian part of North Sea. Marine Geophysical Research, 39, 229-247.

Moyle P. B., Cech J.J. (2003), Fishes, an introduction to Ichthyology, Benjamin Cummings, 5th Ed., ISBN 978-0-13-100847-2, 744 pp.

Nardini R. (2017), Use of acoustic backscatter for the mapping of seabed habitats.Thesis of Post Graduate Master Degree on Marine Geomatics: Advanced Technologies Applied on Marine Environment,University of Genoa, 59 pp.

Needham E., Carroll R., (2013), Development and benefits of hydrographic Surveying using Multispectral Imagery. GSI Case Study, Hydro Conference, 5 pp.

Ohlendorf S., Müller A., Heege T., Cerdeira-Estrada S., Kobryn H., (2011), Bathymetry mapping and sea floor classification using multispectral satellite data and standardized physics-based data processing. Proceedings of SPIE - The International Society for Optical Engineering, 11 pp.

Preston J.M., Christney A.C., Beran L.S., Collins W.T. (2004). Statistical seabed segmentation – from images and echoes to objective clustering. Proceeding of 7th European conference on Underwater Acoustic, 813-818.

Preston J., Christney A., Collins W. (2005). Automated acoustic seabed classification for swath images, ifremer/dtmsi/colloques/search04/xlurton/B2_sonar_dataprocessing_1/Preston.pdf, 1-7.

Rebesco M., Ozmaral A., Urgeles R., Accettella D., Lucchi R.G., Ruther D., Winsborrow M., Llopard J.,Caburlotto A., Lantzsch H., Haneburth Till J.J. (2016), Evolution of a high-latitude sediment drift inside a glacially-carved trough based on high-resolution seismic stratigraphy (Kveithola, NW Barents Sea), Quaternary Science Reviews, 147, 178-193.

Richard P., Stump F., Holderied K. (2003), Determination of water depth with high-resolution satellite imagery over variable bottom types. ASLO - Limnology and Oceanography, 48, 547-556.

Rusby J.S.M., Sommer M.L. (1977), the development of the GLORIA, sonar system from 1970 to 1975, A voyage of discovery, Martin Angel ed., Pergamon Press, NY, 611-625.

Schneider von Deimling J., Brockhoff J., Greinert J. (2007), Flare imaging with Multibeam system: data processing for bubble detection at seeps, Geochemistry, Geophysics, Geosystems, 8(6), 1-7.

Sen A., Ondréas H., Gaillot A., Augistin J.M., Karine O. (2016), The use of multibeam backscatter and bathymetry as a means of identifying faunal assemblages in a deep-sea cold seep. Deep Sea Research: Oceanographic Research Papers, 110(Part 1), 33-49.

Short A.D. (1999), Handbook of Beach and Shoreface Morphodynamics, Wiley & Sons LTD, New York, 379 pp.

Spiess F.N. (1980), Some origins and perspectives in deep-ocean instrumentation development. Sears M. and Merriman E., Oceanography: The Past, Springer-Verlag NY, 226-239.

Szlyk T.K., Ciminello M.D. (2002), Rapid Environmental Assessment Methodology (REAM) of coral reef ecosystems at the Atlantic Undersea Test and Evaluation Center (AUTEC) on Andros Island, Bahamas. Naval Undersea Warfare Center Division Newport, Rhode Island (NUWC-NPT) Technical Document, 11 378, 1-14.

Tyce R.C. (1986), Deep seafloor mapping system – a review, MTS Journal, 20, 4-16.

Urban P., Kosen K., Greinert J. (2016), Processing of multibeam water column image data for automated bubble/seep detection and related mapping. Limnology and Oceanography: Methods, 15 (1), 1-21.

Urick R.J. (1983), Principles of underwater sound. 3rd Ed., McGraw-Hill, New York, 423 pp.

Vorren T.O., Laberg J.S., Blaume F., Dowdeswell J.A., Kenyon N.H., Mienert J., Rumohr J., Werner F. (1998), The Norwegian-Greenland sea continental margins: morphology and late quaternary sediment process and environment, Quaternaty Science Review, Elsevier, 17, 273-302.

Weber T.C., Lurton X. (2015), Background and fundamentals. X. Lurton and G. Lamarche (Eds). Backscatter measurements by seafloor- mapping sonars - Guidelines and Recommendations, Chapter 2 - 25-52.

Wernand M.W., Van der Woerd H.J. (2010), Spectral analysis of the Forel-Ule Ocean colour comparator scale. Journal of the European Optical Society Rapid Publications, 5-2010 (10014S), 7 pp.

Wilson M.F.J., O'Connel B., Brown C., Guinanand J.C., Grehan A.J. (2007), Multiscale terrain analysis of multibeam bathymetry data for habitat mapping on the continental slope. Marine Geodesy, 30, 3-35.

Wood S. L. (2009), Autonomous Underwater Gliders, https://www.intechopen.com, DOI: 10.5772/6718, 499-524.

Zakariya R., Abdullah M.A., Hasan R.C., Khalil I.(2018), The use of backscatter classification and bathymetry derivatives from multibeam data for seabed sediment characterization. Engineering applications for new materials and technologies, 579-591.